Study of the anomalous acceleration of Pioneer 10 and 11

John D. Anderson,[*a] Philip A. Laing,[†b] Eunice L. Lau,[‡a]
Anthony S. Liu,[§c] Michael Martin Nieto,[¶d] and Slava G. Turyshev[**a]

[a] *Jet Propulsion Laboratory, California Institute of Technology, Pasadena, CA 91109*
[b] *The Aerospace Corporation, 2350 E. El Segundo Blvd., El Segundo, CA 90245-4691*
[c] *Astrodynamic Sciences, 2393 Silver Ridge Ave., Los Angeles, CA 90039*
[d] *Theoretical Division (MS-B285), Los Alamos National Laboratory,*
University of California, Los Alamos, NM 87545
(Dated: 11 April 2002)

Our previous analyses of radio Doppler and ranging data from distant spacecraft in the solar system indicated that an apparent anomalous acceleration is acting on Pioneer 10 and 11, with a magnitude $a_P \sim 8 \times 10^{-8}$ cm/s^2, directed towards the Sun. Much effort has been expended looking for possible systematic origins of the residuals, but none has been found. A detailed investigation of effects both external to and internal to the spacecraft, as well as those due to modeling and computational techniques, is provided. We also discuss the methods, theoretical models, and experimental techniques used to detect and study small forces acting on interplanetary spacecraft. These include the methods of radio Doppler data collection, data editing, and data reduction.

There is now further data for the Pioneer 10 orbit determination. The extended Pioneer 10 data set spans 3 January 1987 to 22 July 1998. [For Pioneer 11 the shorter span goes from 5 January 1987 to the time of loss of coherent data on 1 October 1990.] With these data sets and more detailed studies of all the systematics, we now give a result, of $a_P = (8.74 \pm 1.33) \times 10^{-8}$ cm/s^2. (Annual/diurnal variations on top of a_P, that leave a_P unchanged, are also reported and discussed.)

PACS numbers: 04.80.-y, 95.10.Eg, 95.55.Pe

I. INTRODUCTION

Some thirty years ago, on 2 March 1972, Pioneer 10 was launched on an Atlas/Centaur rocket from Cape Canaveral. Pioneer 10 was Earth's first space probe to an outer planet. Surviving intense radiation, it successfully encountered Jupiter on 4 December 1973 [1]-[6]. In trail-blazing the exploration of the outer solar system, Pioneer 10 paved the way for, among others, Pioneer 11 (launched on 5 April 1973), the Voyagers, Galileo, Ulysses, and the upcoming Cassini encounter with Saturn. After Jupiter and (for Pioneer 11) Saturn encounters, the two spacecraft followed hyperbolic orbits near the plane of the ecliptic to opposite sides of the solar system. Pioneer 10 was also the first mission to enter the edge of interstellar space. That major event occurred in June 1983, when Pioneer 10 became the first spacecraft to "leave the solar system" as it passed beyond the orbit of the farthest known planet.

The scientific data collected by Pioneer 10/11 has yielded unique information about the outer region of the solar system. This is due in part to the spin-stabilization of the Pioneer spacecraft. At launch they were spinning at approximately 4.28 and 7.8 revolutions per minute (rpm), respectively, with the spin axes running through the centers of the dish antennae. Their spin-stabilizations and great distances from the Earth imply a minimum number of Earth-attitude reorientation maneuvers are required. This permits precise acceleration estimations, to the level of 10^{-8} cm/s^2 (single measurement accuracy averaged over 5 days). Contrariwise, a Voyager-type three-axis stabilized spacecraft is not well suited for a precise celestial mechanics experiment as its numerous attitude-control maneuvers can overwhelm the signal of a small external acceleration.

In summary, Pioneer spacecraft represent an ideal system to perform precision celestial mechanics experiments. It is relatively easy to model the spacecraft's behavior and, therefore, to study small forces affecting its motion in the dynamical environment of the solar system. Indeed, one of the main objectives of the Pioneer extended missions (post Jupiter/Saturn encounters) [5] was to perform accurate celestial mechanics experiments. For instance, an attempt was made to detect the presence of small bodies in the solar system, primarily in the Kuiper belt. It was hoped that a small perturbation of the spacecraft's trajectory would reveal the presence of these objects [7]-[9]. Furthermore, due to extremely precise navigation and a high quality tracking data, the Pioneer 10 scientific program also included a search for low frequency gravitational waves [10, 11].

Beginning in 1980, when at a distance of 20 astronomical units (AU) from the Sun the solar-radiation-pressure acceleration on Pioneer 10 *away* from the Sun had decreased to $< 5 \times 10^{-8}$ cm/s^2, we found that the largest

[*] Electronic address: john.d.anderson@jpl.nasa.gov
[†] Electronic address: Philip.A.Laing@aero.org
[‡] Electronic address: Eunice.L.Lau@jpl.nasa.gov
[§] Deceased (13 November 2000).
[¶] Electronic address: mmn@lanl.gov
[**] turyshev@jpl.nasa.gov

systematic error in the acceleration residuals was a constant bias, a_P, directed *toward* the Sun. Such anomalous data have been continuously received ever since. Jet Propulsion Laboratory (JPL) and The Aerospace Corporation produced independent orbit determination analyses of the Pioneer data extending up to July 1998. We ultimately concluded [12, 13], that there is an unmodeled acceleration, a_P, towards the Sun of $\sim 8 \times 10^{-8}$ cm/s^2 for both Pioneer 10 and Pioneer 11.

The purpose of this paper is to present a detailed explanation of the analysis of the apparent anomalous, weak, long-range acceleration of the Pioneer spacecraft that we detected in the outer regions of the solar system. We attempt to survey all sensible forces and to estimate their contributions to the anomalous acceleration. We will discuss the effects of these small non-gravitational forces (both generated on-board and external to the vehicle) on the motion of the distant spacecraft together with the methods used to collect and process the radio Doppler navigational data.

We begin with descriptions of the spacecraft and other systems and the strategies for obtaining and analyzing information from them. In Section II we describe the Pioneer (and other) spacecraft. We provide the reader with important technical information on the spacecraft, much of which is not easily accessible. In Section III we describe how raw data is obtained and analyzed and in Section IV we discuss the basic elements of a theoretical foundation for spacecraft navigation in the solar system.

The next major part of this manuscript is a description and analysis of the results of this investigation. We first describe how the anomalous acceleration was originally identified from the data of all the spacecraft in Section V [12, 13]. We then give our recent results in Section VI. In the following three sections we discuss possible experimental systematic origins for the signal. These include systematics generated by physical phenomena from sources external to (Section VII) and internal to (Section VIII) the spacecraft. This is followed by Section IX, where the accuracy of the solution for a_P is discussed. In the process we go over possible numerical/calculational errors/systematics. Sections VII-IX are then summarized in the total error budget of Section X.

We end our presentation by first considering possible unexpected physical origins for the anomaly (Section XI). In our conclusion, Section XII, we summarize our results and suggest venues for further study of the discovered anomaly.

II. THE PIONEER AND OTHER SPACECRAFT

In this section we describe in some detail the Pioneer 10 and 11 spacecraft and their missions. We concentrate on those spacecraft systems that play important roles in maintaining the continued function of the vehicles and in determining their dynamical behavior in the solar system. Specifically we present an overview of propulsion

and attitude control systems, as well as thermal and communication systems.

Since our analysis addresses certain results from the Galileo and Ulysses missions, we also give short descriptions of these missions in the final subsection.

A. General description of the Pioneer spacecraft

Although some of the more precise details are often difficult to uncover, the general parameters of the Pioneer spacecraft are known and well documented [1]-[6]. The two spacecraft are identical in design [14]. At launch each had a "weight" (mass) of 259 kg. The "dry weight" of the total module was 223 kg as there were 36 kg of hydrazine propellant [15, 16]. The spacecraft were designed to fit within the three meter diameter shroud of an added third stage to the Atlas/Centaur launch vehicle. Each spacecraft is 2.9 m long from its base to its cone-shaped medium-gain antenna. The high gain antenna (HGA) is made of aluminum honeycomb sandwich material. It is 2.74 m in diameter and 46 cm deep in the shape of a parabolic dish. (See Figures 1 and 2.)
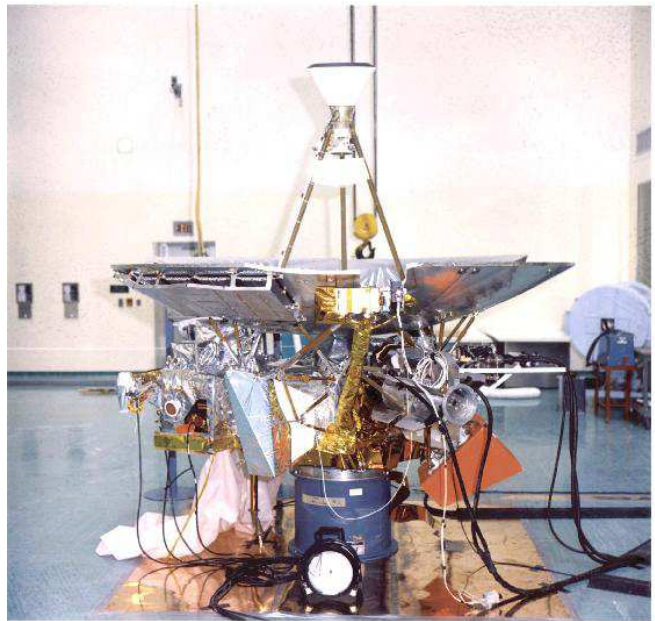

FIG. 1: NASA photo #72HC94, with caption "The Pioneer F spacecraft during a checkout with the launch vehicle third stage at Cape Kennedy." Pioneer F became Pioneer 10.

The main equipment compartment is 36 cm deep. The hexagonal flat top and bottom have 71 cm long sides. The equipment compartment provides a thermally controlled environment for scientific instruments. Two three-rod trusses, 120 degrees apart, project from two sides of the equipment compartment. At their ends, each holds two SNAP-19 (Space Nuclear Auxiliary Power,
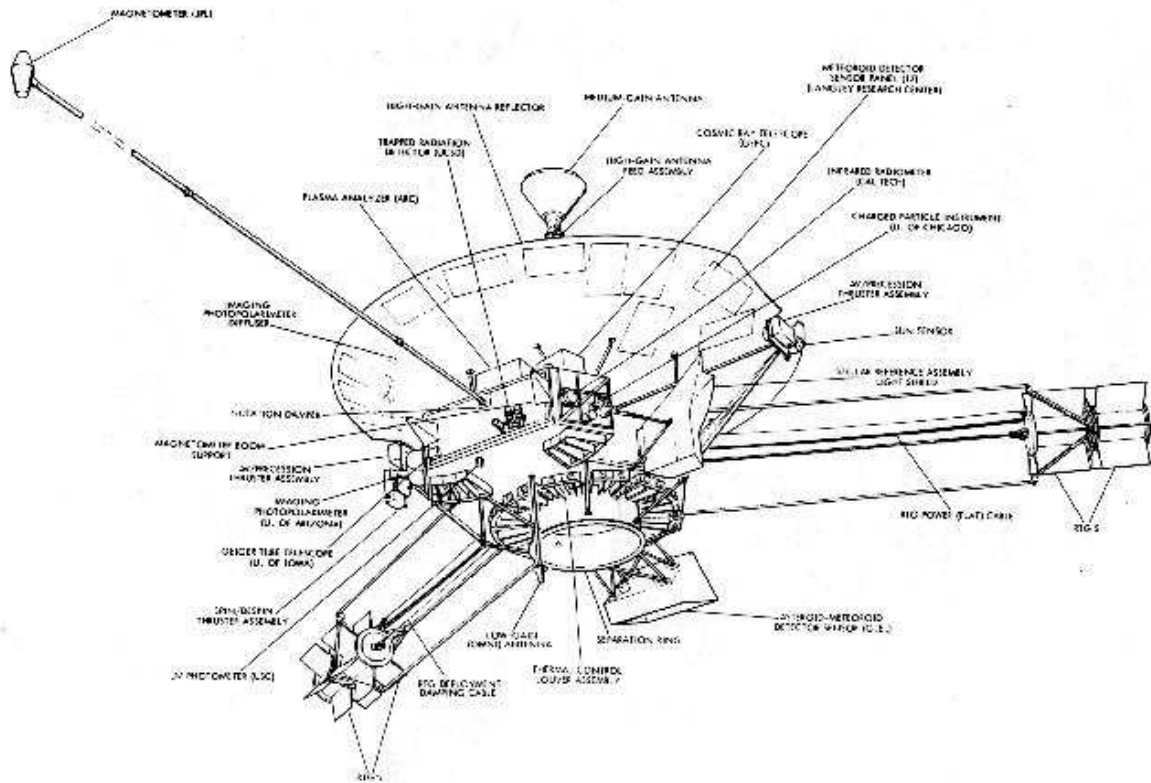
FIG. 2: A drawing of the Pioneer spacecraft.

model 19) RTGs (Radioisotope Thermoelectric Generators) built by Teledyne Isotopes for the Atomic Energy Commission. These RTGs are situated about 3 m from the center of the spacecraft and generate its electric power. [We will go into more detail on the RTGs in Section VIII.] A third single-rod boom, 120 degrees from the other two, positions a magnetometer about 6.6 m from the spacecraft's center. All three booms were extended after launch. With the mass of the magnetometer being 5 kg and the mass of each of the four RTGs being 13.6 kg, this configuration defines the main moment of inertia along the z-spin-axis. It is about $\mathcal{I}_z \approx 588.3$ kg m^2 [17]. [Observe that this all left only about 164 kg for the main bus and superstructure, including the antenna.]

Figures 1 and 2 show the arrangement within the spacecraft equipment compartment. The majority of the spacecraft electrical assemblies are located in the central hexagonal portion of the compartment, surrounding a 16.5-inch-diameter spherical hydrazine tank. Most of the scientific instruments' electronic units and internally-mounted sensors are in an instrument bay ("squashed" hexagon) mounted on one side of the central hexagon. The equipment compartment is in an aluminum honeycomb structure. This provides support and meteoroid protection. It is covered with insulation which, together with louvers under the platform, provides passive thermal control. [An exception is from off-on control by thermal power dissipation of some subsystems. (See Sec. VIII).]

B. Propulsion and attitude control systems

Three pairs of these rocket thrusters near the rim of the HGA provide a threefold function of spin-axis precession, mid-course trajectory correction, and spin control. Each of the three thruster pairs develops its repulsive jet force from a catalytic decomposition of liquid hydrazine in a small rocket thrust chamber attached to the oppositely-directed nozzle. The resulted hot gas is then expended through six individually controlled thruster nozzles to effect spacecraft maneuvers.

The spacecraft is attitude-stabilized by spinning about an axis which is parallel to the axis of the HGA. The nominal spin rate for Pioneer 10 is 4.8 rpm. Pioneer 11 spins at approximately 7.8 rpm because a spin-controlling thruster malfunctioned during the spin-down shortly after launch. [Because of the danger that the thruster's valve would not be able to close again, this particular thruster has not been used since.] During the mission an Earth-pointing attitude is required to illuminate the Earth with the narrow-beam HGA. Periodic attitude adjustments are required throughout the mission to compensate for the variation in the heliocentric longitude of the Earth-spacecraft line. [In addition, correction of launch vehicle injection errors were required to provide the desired Jupiter encounter trajectory and Saturn (for Pioneer 11) encounter trajectory.] These velocity vector adjustments involved reorienting the spacecraft to direct

the thrust in the desired direction.

There were no anomalies in the engineering telemetry from the propulsion system, for either spacecraft, during any mission phase from launch to termination of the Pioneer mission in March 1997. From the viewpoint of mission operations at the NASA/Ames control center, the propulsion system performed as expected, with no catastrophic or long-term pressure drops in the propulsion tank. Except for the above-mentioned Pioneer 11 spin-thruster incident, there was no malfunction of the propulsion nozzles, which were only opened every few months by ground command. The fact that pressure was maintained in the tank has been used to infer that no impacts by Kuiper belt objects occurred, and a limit has been placed on the size and density distribution of such objects [7], another useful scientific result.

For attitude control, a star sensor (referenced to Canopus) and two sunlight sensors provided reference for orientation and roll maneuvers. The star sensor on Pioneer 10 became inoperative at Jupiter encounter, so the sun sensors were used after that. For Pioneer 10, spin calibration was done by the DSN until 17 July 1990. From 1990 to 1993 determinations were made by analysts using data from the Imaging Photo Polarimeter (IPP). After the 6 July 1993 maneuver, there was not enough power left to support the IPP. But approximately every six months analysts still could get a rough determination using information obtained from conscan maneuvers [18] on an uplink signal. When using conscan, the high gain feed is off-set. Thruster firings are used to spiral in to the correct pointing of the spacecraft antenna to give the maximum signal strength. To run this procedure (conscan and attitude) it is now necessary to turn off the traveling-wave-tube (TWT) amplifier. So far, the power and tube life-cycle have worked and the Jet Propulsion Laboratory's (JPL) Deep Space Network (DSN) has been able to reacquire the signal. It takes about 15 minutes or so to do a maneuver. [The magnetometer boom incorporates a hinged, viscous, damping mechanism at its attachment point, for passive nutation control.]

In the extended mission phase, after Jupiter and Saturn encounters, the thrusters have been used for precession maneuvers only. Two pairs of thrusters at opposite sides of the spacecraft have nozzles directed along the spin axis, fore and aft (See Figure 2.) In precession mode, the thrusters are fired by opening one nozzle in each pair. One fires to the front and the other fires to the rear of the spacecraft [19], in brief thrust pulses. Each thrust pulse precesses the spin axis a few tenths of a degree until the desired attitude is reached.

The two nozzles of the third thruster pair, no longer in use, are aligned tangentially to the antenna rim. One points in the direction opposite to its (rotating) velocity vector and the other with it. These were used for spin control.

C. Thermal system and on-board power

Early on the spacecraft instrument compartment is thermally controlled between $\approx$ 0 F and 90 F. This is done with the aid of thermo-responsive louvers located at the bottom of the equipment compartment. These louvers are adjusted by bi-metallic springs. They are completely closed below $\sim$ 40 F and completely open above $\sim$ 85 F. This allows controlled heat to escape in the equipment compartment. Equipment is kept within an operational range of temperatures by multi-layered blankets of insulating aluminum plastic. Heat is provided by electric heaters, the heat from the instruments themselves, and by twelve one-watt radioisotope heaters powered directly by non-fissionable plutonium ($^{238}_{94}$Pu$\rightarrow^{234}_{92}$U+$^4_2$He).

^{238}Pu, with a half life time of 87.74 years, also provides the thermal source for the thermoelectric devices in the RTGs. Before launch, each spacecraft's four RTGs delivered a total of approximately 160 W of electrical power [20, 21]. Each of the four space-proven SNAP-19 RTGs converts 5 to 6 percent of the heat released from plutonium dioxide fuel to electric power. RTG power is greatest at 4.2 Volts; an inverter boosts this to 28 Volts for distribution. RTG life is degraded at low currents; therefore, voltage is regulated by shunt dissipation of excess power.

The power subsystem controls and regulates the RTG power output with shunts, supports the spacecraft load, and performs battery load-sharing. The silver cadmium battery consists of eight cells of 5 ampere-hours capacity each. It supplies pulse loads in excess of RTG capability and may be used for sharing peak loads. The battery voltage is often discharged and charged. This can be seen by telemetry of the battery discharge current and charge current

At launch each RTG supplied about 40 W to the input of the $\sim$ 4.2 V Inverter Assemblies. (The output for other uses includes the DC bus at 28 V and the AC bus at 61 V) Even though electrical power degrades with time (see Section VIII D), at -41 F the essential platform temperature as of the year 2000 is still between the acceptable limits of -63 F to 180 F. The RF power output from the traveling-wave-tube amplifier is still operating normally.

The equipment compartment is insulated from extreme heat influx with aluminized mylar and kapton blankets. Adequate warmth is provided by dissipation of 70 to 120 watts of electrical power by electronic units within the compartment; louvers regulating the release of this heat below the mounting platform maintain temperatures in the vicinity of the spacecraft equipment and scientific instruments within operating limits. External component temperatures are controlled, where necessary, by appropriate coating and, in some cases, by radioisotope or electrical heaters.

The energy production from the radioactive decay obeys an exponential law. Hence, 29 years after launch, the radiation from Pioneer 10's RTGs was about 80 percent of its original intensity. However the electrical power

delivered to the equipment compartment has decayed at a faster rate than the ^{238}Pu decays radioactively. Specifically, the electrical power first decayed very quickly and then slowed to a still fast linear decay [22]. By 1987 the degradation rate was about -2.6 W/yr for Pioneer 10 and even greater for the sister spacecraft.

This fast depletion rate of electrical power from the RTGs is caused by normal deterioration of the thermocouple junctions in the thermoelectric devices.

The spacecraft needs 100 W to power all systems, including 26 W for the science instruments. Previously, when the available electrical power was greater than 100 W, the excess power was either thermally radiated into space by a shunt-resistor radiator or it was used to charge a battery in the equipment compartment.

At present only about 65 W of power is available to Pioneer 10 [23]. Therefore, all the instruments are no longer able to operate simultaneously. But the power subsystem continues to provide sufficient power to support the current spacecraft load: transmitter, receiver, command and data handling, and the Geiger Tube Telescope (GTT) science instrument. As pointed out in Sec. II E, the science package and transmitter are turned off in extended cruise mode to provide enough power to fire the attitude control thrusters.

D. Communication system

The Pioneer 10/11 communication systems use S-band ($\lambda \simeq 13$ cm) Doppler frequencies [24]. The communication uplink from Earth is at approximately 2.11 GHz. The two spacecraft transmit continuously at a power of eight watts. They beam their signals, of approximate frequency 2.29 GHz, to Earth by means of the parabolic 2.74 m high-gain antenna. Phase coherency with the ground transmitters, referenced to H-maser frequency standards, is maintained by means of an S-band transponder with the 240/221 frequency turnaround ratio (as indicated by the values of the above mentioned frequencies).

The communications subsystem provides for: i) uplink and down-link communications; ii) Doppler coherence of the down-link carrier signal; and iii) generation of the conscan [18] signal for closed loop precession of the spacecraft spin axis towards Earth. S-band carrier frequencies, compatible with DSN, are used in conjunction with a telemetry modulation of the down-link signal. The high-gain antenna is used to maximize the telemetry data rate at extreme ranges. The coupled medium-gain/omni-directional antenna with fore and aft elements respectively, provided broad-angle communications at intermediate and short ranges. For DSN acquisition, these three antennae radiate a non-coherent RF signal, and for Doppler tracking, there is a phase coherent mode with a frequency translation ratio of 240/221.

Two frequency-addressable phase-lock receivers are connected to the two antenna systems through a ground-commanded transfer switch and two diplexers, providing access to the spacecraft via either signal path. The receivers and antennae are interchangeable through the transfer switch by ground command or automatically, if needed.

There is a redundancy in the communication systems, with two receivers and two transmitters coupled to two traveling-wave-tube amplifiers. Only one of the two redundant systems has been used for the extended missions, however.

At launch, communication with the spacecraft was at a data rate 256 bps for Pioneer 10 (1024 bps for Pioneer 11). Data rate degradation has been -1.27 mbps/day for Pioneer 10 (-8.78 mbps/day for Pioneer 11). The DSN still continues to provide good data with the received signal strength of about -178 dBm (only a few dB from the receiver threshold). The data signal to noise ratio is still mainly under 0.5 dB. The data deletion rate is often between 0 and 50 percent, at times more. However, during the test of 11 March 2000, the average deletion rate was about 8 percent. So, quality data are still available.

E. Status of the extended mission

The Pioneer 10 mission officially ended on 31 March 1997 when it was at a distance of 67 AU from the Sun. (See Figure 3.) At a now nearly constant velocity relative to the Sun of ~12.2 km/s, Pioneer 10 will continue its motion into interstellar space, heading generally for the red star Aldebaran, which forms the eye of Taurus (The Bull) Constellation. Aldebaran is about 68 light years away and it would be expected to take Pioneer 10 over 2 million years to reach its neighborhood.

FIG. 3: Ecliptic pole view of Pioneer 10, Pioneer 11, and Voyager trajectories. Pioneer 11 is traveling approximately in the direction of the Sun's orbital motion about the galactic center. The galactic center is approximately in the direction of the top of the figure. [Digital artwork by T. Esposito. NASA ARC Image # AC97-0036-3.]

A switch failure in the Pioneer 11 radio system on 1 October 1990 disabled the generation of coherent Doppler signals. So, after that date, when the spacecraft was ~ 30 AU away from the Sun, no useful data have been generated for our scientific investigation. Furthermore, by September 1995, its power source was nearly exhausted. Pioneer 11 could no longer make any scientific observations, and routine mission operations were terminated. The last communication from Pioneer 11 was received in November 1995, when the spacecraft was at distance of ~ 40 AU from the Sun. (The relative Earth motion carried it out of view of the spacecraft antenna.) The spacecraft is headed toward the constellation of Aquila (The Eagle), northwest of the constellation of Sagittarius, with a velocity relative to the Sun of $\sim$11.6 km/s Pioneer 11 should pass close to the nearest star in the constellation Aquila in about 4 million years [6]. (Pioneer 10 and 11 orbital parameters are given in the Appendix.)

However, after mission termination the Pioneer 10 radio system was still operating in the coherent mode when commanded to do so from the Pioneer Mission Operations center at the NASA Ames Research Center (ARC). As a result, after 31 March 1997, JPL's DSN was still able to deliver high-quality coherent data to us on a regular schedule from distances beyond 67 AU.

Recently, support of the Pioneer spacecraft has been on a non-interference basis to other NASA projects. It was used for the purpose of training Lunar Prospector controllers in DSN coordination of tracking activities. Under this training program, ARC has been able to maintain contact with Pioneer 10. This has required careful attention to the DSN's ground system, including the installation of advanced instrumentation, such as low-noise digital receivers. This extended the lifetime of Pioneer 10 to the present. [Note that the DSN's early estimates, based on instrumentation in place in 1976, predicted that radio contact would be lost about 1980.]

At the present time it is mainly the drift of the spacecraft relative to the solar velocity that necessitates maneuvers to continue keeping Pioneer 10 pointed towards the Earth. The latest successful precession maneuver to point the spacecraft to Earth was accomplished on 11 February 2000, when Pioneer 10 was at a distance from the Sun of 75 AU. [The distance from the Earth was ~ 76 AU with a corresponding round-trip light time of about 21 hour.] The signal level increased 0.5-0.75 dBm [25] as a result of the maneuver.

This was the seventh successful maneuver that has been done in the blind since 26 January 1997. At that time it had been determined that the electrical power to the spacecraft had degraded to the point where the spacecraft transmitter had to be turned off to have enough power to perform the maneuver. After 90 minutes in the blind the transmitter was turned back on again. So, despite the continued weakening of Pioneer 10's signal, radio Doppler measurements were still available. The next attempt at a maneuver, on 8 July 2000, turned out in the end to be successful. Signal was tracked on 9 July

2001. Contact was reestablished on the 30th anniversary of launch, 2 March 2002.

F. The Galileo and Ulysses missions and spacecraft

1. The Galileo mission

The Galileo mission to explore the Jovian system [26] was launched 18 October 1989 aboard the Space Shuttle Discovery. Due to insufficient launch power to reach its final destination at 5.2 AU, a trajectory was chosen with planetary flybys to gain gravity assists. The spacecraft flew by Venus on 10 February 1990 and twice by the Earth, on 8 December 1990 and on 8 December 1992. The current Galileo Millennium Mission continues to study Jupiter and its moons, and coordinated observations with the Cassini flyby in December 2000.

The dynamical properties of the Galileo spacecraft are very well known. At launch the orbiter had a mass of 2,223 kg. This included 925 kg of usable propellant, meaning over 40% of the orbiter's mass at launch was for propellant! The science payload was 118 kg and the probe's total mass was 339 kg. Of this latter, the probe descent module was 121 kg, including a 30 kg science payload. The tensor of inertia of the spacecraft had the following components at launch: $J_{xx} = 4454.7, J_{yy} = 4061.2, J_{zz} = 5967.6, J_{xy} = -52.9, J_{xz} = 3.21, J_{yz} = -15.94$ in units of kg m^2. Based on the area of the sun-shade plus the booms and the RTGs we obtained a maximal cross-sectional area of 19.5 m^2. Each of the two of the Galileo's RTGs at launch delivered of 285 W of electric power to the subsystems.

Unlike previous planetary spacecraft, Galileo featured an innovative "dual spin" design: part of the orbiter would rotate constantly at about three rpm and part of the spacecraft would remain fixed in (solar system) inertial space. This means that the orbiter could easily accommodate magnetospheric experiments (which need to made while the spacecraft is sweeping) while also providing stability and a fixed orientation for cameras and other sensors. The spin rate could be increased to 10 revolutions per minute for additional stability during major propulsive maneuvers.

Apparently there was a mechanical problem between the spinning and non-spinning sections. Because of this, the project decided to often use an all-spinning mode, of about 3.15 rpm. This was especially true close to the Jupiter Orbit Insertion (JOI), when the entire spacecraft was spinning (with a slower rate, of course).

Galileo's original design called for a deployable high-gain antenna (HGA) to unfurl. It would provide approximately 34 dB of gain at X-band (10 GHz) for a 134 kbps downlink of science and priority engineering data. However, the X-band HGA failed to unfurl on 11 April 1991. When it again did not deploy following the Earth flyby in 1992, the spacecraft was reconfigured to utilize the S-band, 8 dB, omni-directional low-gain antenna (LGA)

for downlink.

The S-band frequencies are 2.113 GHz - up and 2.295 GHz - down, a conversion factor of 240/221 at the Doppler frequency transponder. This configuration yielded much lower data rates than originally scheduled, 8-16 bps through JOI [27]. Enhancements at the DSN and reprogramming the flight computers on Galileo increased telemetry bit rate to 8-160 bps, starting in the spring of 1996.

Currently, two types of Galileo navigation data are available, namely Doppler and range measurements. As mentioned before, an instantaneous comparison between the ranging signal that goes up with the ranging signal that comes down would yield an "instantaneous" two-way range delay. Unfortunately, an instantaneous comparison was not possible in this case. The reason is that the signal-to-noise ratio on the incoming ranging signal is small and a long integration time (typically minutes) must be used (for correlation purposes). During such long integration times, the range to the spacecraft is constantly changing. It is therefore necessary to "electronically freeze" the range delay long enough to permit an integration to be performed. The result represents the range at the moment of freezing [28, 29].

2. The Ulysses mission

Ulysses was launched on 6 October 1990, also from the Space Shuttle Discovery, as a cooperative project of NASA and the European Space Agency (ESA). JPL manages the US portion of the mission for NASA's Office of Space Science. Ulysses' objective was to characterize the heliosphere as a function of solar latitude [30]. To reach high solar latitudes, its voyage took it to Jupiter on 8 February 1992. As a result, its orbit plane was rotated about 80 degrees out of the ecliptic plane.

Ulysses explored the heliosphere over the Sun's south pole between June and November, 1994, reaching maximum Southern latitude of 80.2 degrees on 13 September 1994. It continued in its orbit out of the plane of the ecliptic, passing perihelion in March 1995 and over the north solar pole between June and September 1995. It returned again to the Sun's south polar region in late 2000.

The total mass at launch was the sum of two parts: a dry mass of 333.5 kg plus a propellant mass of 33.5 kg. The tensor of inertia is given by its principal components $J_{xx} = 371.62, J_{yy} = 205.51, J_{zz} = 534.98$ in units kg m^2. The maximal cross section is estimated to be 10.056 m^2. This estimation is based on the radius of the antenna 1.65 m (8.556 m^2) plus the areas of the RTGs and part of the science compartment (yielding an additional ≈ 1.5 m^2). The spacecraft was spin-stabilized at 4.996 rpm. The electrical power is generated by modern RTGs, which are located much closer to the main bus than are those of the Pioneers. The power generated at launch was 285 W.

Communications with the spacecraft are performed at X-band (for downlink at 20 W with a conversion factor of 880/221) and S-band (both for uplink 2111.607 MHz and downlink 2293.148 MHz, at 5 W with a conversion factor of 240/221). Currently both Doppler and range data are available for both frequency bands. While the main communication link is S-up/X-down, the S-down link was used only for radio-science purposes.

Because of Ulysses' closeness to the Sun and also because of its construction, any hope to model Ulysses for small forces might appear to be doomed by solar radiation pressure and internal heat radiation from the RTGs. However, because the Doppler signal direction is towards the Earth while the radiation pressure varies with distance and has a direction parallel the Sun-Ulysses line, in principle these effects could be separated. And again, there was range data. This all would make it easier to model non-gravitational acceleration components normal to the line of sight, which usually are poorly and not significantly determined.

The Ulysses spacecraft spins at ~ 5 rpm around its antenna axis (4.996 rpm initially). The angle of the spin axis with respect to the spacecraft-Sun line varies from near zero at Jupiter to near 50 degrees at perihelion. Any on-board forces that could perturb the spacecraft trajectory are restricted to a direction along the spin axis. [The other two components are canceled out by the spin.]

As the spacecraft and the Earth travel around the Sun, the direction from the spacecraft to the Earth changes continuously. Regular changes of the attitude of the spacecraft are performed throughout the mission to keep the Earth within the narrow beam of about one degree full width of the spacecraft–fixed parabolic antenna.

III. DATA ACQUISITION AND PREPARATION

Discussions of radio-science experiments with spacecraft in the solar system requires at least a general knowledge of the sophisticated experimental techniques used at the DSN complex. Since its beginning in 1958 the DSN complex has undergone a number of major upgrades and additions. This was necessitated by the needs of particular space missions. [The last such upgrade was conducted for the Cassini mission when the DSN capabilities were extended to cover the Ka radio frequency bandwidth. For more information on DSN methods, techniques, and present capabilities, see [31].] For the purposes of the present analysis one will need a general knowledge of the methods and techniques implemented in the radio-science subsystem of the DSN complex.

This section reviews the techniques that are used to obtain the radio tracking data from which, after analysis, results are generated. Here we will briefly discuss the DSN hardware that plays a pivotal role for our study of the anomalous acceleration.

A. Data acquisition

The Deep Space Network (DSN) is the network of ground stations that are employed to track interplanetary spacecraft [31, 32]. There are three ground DSN complexes, at Goldstone, California, at Robledo de Chavela, outside Madrid, Spain, and at Tidbinbilla, outside Canberra, Australia.

There are many antennae, both existing and decommissioned, that have been used by the DSN for spacecraft navigation. For our four spacecraft (Pioneer 10, 11, Galileo, and Ulysses), depending on the time period involved, the following Deep Space Station (DSS) antennae were among those used: (DSS 12, 14, 24) at the California antenna complex; (DSS 42, 43, 45, 46) at the Australia complex; and (DSS 54, 61, 62, 63) at the Spain complex. Specifically, the Pioneers used (DSS 12, 14, 42, 43, 62, 63), Galileo used (DSS 12, 14, 42, 43, 63), and Ulysses used (DSS 12, 14, 24, 42, 43, 46, 54, 61, 63).

The DSN tracking system is a phase coherent system. By this we mean that an "exact" ratio exists between the transmission and reception frequencies; i.e., 240/221 for S-band or 880/221 for X-band [24]. (This is in distinction to the usual concept of coherent radiation used in atomic and astrophysics.)

Frequency is an average frequency, defined as the number of cycles per unit time. Thus, accumulated phase is the integral of frequency. High measurement precision is attained by maintaining the frequency accuracy to 1 part per 10^{12} or better (This is in agreement with the expected Allan deviation for the S-band signals.)

The DSN Frequency and Timing System (FTS): The DSN's FTS is the source for the high accuracy just mentioned (see Figure 4). At its center is an hydrogen maser that produces a precise and stable reference frequency [33, 34]. These devices have Allan deviations [35] of approximately 3×10^{-15} to 1×10^{-15} for integration times of 10^2 to 10^3 seconds, respectively.
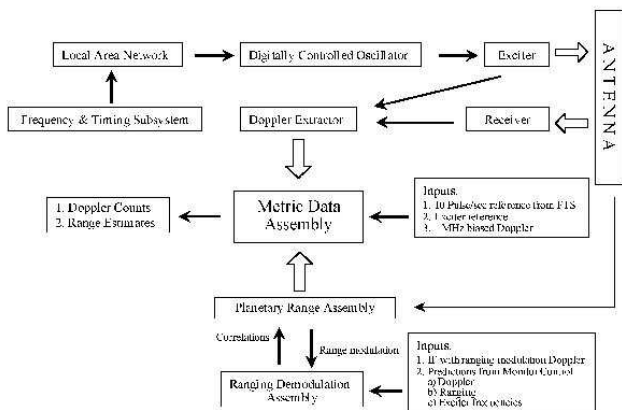
FIG. 4: Block-diagram of the DSN complex as used for radio Doppler tracking of an interplanetary spacecraft. For more detailed drawings and technical specifications see Ref. [31].

These masers are good enough so that the quality of Doppler-measurement data is limited by thermal or plasma noise, and not by the inherent instability of the frequency references. Due to the extreme accuracy of the hydrogen masers, one can very precisely characterize the spacecraft's dynamical variables using Doppler and range techniques. The FTS generates a 5 MHz and 10 MHz reference frequency which is sent through the local area network to the Digitally Controlled Oscillator (DCO).

The Digitally Controlled Oscillator (DCO) and Exciter: Using the highly stable output from the FTS, the DCO, through digitally controlled frequency multipliers, generates the Track Synthesizer Frequency (TSF) of ~ 22 MHz. This is then sent to the Exciter Assembly. The Exciter Assembly multiplies the TSF by 96 to produce the S-band carrier signal at ~ 2.2 GHz. The signal power is amplified by Traveling Wave Tubes (TWT) for transmission. If ranging data are required, the Exciter Assembly adds the ranging modulation to the carrier. [The DSN tracking system has undergone many upgrades during the 29 years of tracking Pioneer 10. During this period internal frequencies have changed.]

This S-band frequency is sent to the antenna where it is amplified and transmitted to the spacecraft. The onboard receiver tracks the up-link carrier using a phase lock loop. To ensure that the reception signal does not interfere with the transmission, the spacecraft (e.g., Pioneer) has a turnaround transponder with a ratio of 240/221. The spacecraft transmitter's local oscillator is phase locked to the up-link carrier. It multiplies the received frequency by the above ratio and then re-transmits the signal to Earth.

Receiver and Doppler Extractor: When the two-way [36] signal reaches the ground, the receiver locks on to the signal and tunes the Voltage Control Oscillator (VCO) to null out the phase error. The signal is sent to the Doppler Extractor. At the Doppler Extractor the current transmitter signal from the Exciter is multiplied by 240/221 (or 880/241 for X-band)) and a bias, of 1 MHz for S-band or 5 MHz for X-band [24], is added to the Doppler. The Doppler data is no longer modulated at S-band but has been reduced as a consequence of the bias to an intermediate frequency of 1 or 5 MHz

Since the light travel time to and from Pioneer 10 is long (more than 20 hours), the transmitted frequency and the current transmitted frequency can be different. The difference in frequencies are recorded separately and are accounted for in the orbit determination programs we discuss in Section V.

Metric Data Assembly (MDA): The MDA consists of computers and Doppler counters where continuous count Doppler data are generated. The intermediate frequency (IF) of 1 or 5 MHz with a Doppler modulation is sent to the Metric Data Assembly (MDA). From the FTS a 10 pulse per second signal is also sent to the MDA for timing. At the MDA, the IF and the resulting Doppler pulses are counted at a rate of 10 pulses per second. At

each tenth of a second, the number of Doppler pulses are counted. A second counter begins at the instant the first counter stops. The result is continuously-counted Doppler data. (The Doppler data is a biased Doppler of 1 MHz, the bias later being removed by the analyst to obtain the true Doppler counts.) The Range data (if present) together with the Doppler data is sent separately to the Ranging Demodulation Assembly. The accompanying Doppler data is used to rate aid (i.e., to "freeze" the range signal) for demodulation and cross correlation.

Data Communication: The total set of tracking data is sent by local area network to the communication center. From there it is transmitted to the Goddard Communication Facility via commercial phone lines or by government leased lines. It then goes to JPL's Ground Communication Facility where it is received and recorded by the Data Records Subsystem.

B. Radio Doppler and range techniques

Various radio tracking strategies are available for determining the trajectory parameters of interplanetary spacecraft. However, radio tracking Doppler and range techniques are the most commonly used methods for navigational purposes. The position and velocities of the DSN tracking stations must be known to high accuracy. The transformation from a Earth fixed coordinate system to the International Earth Rotation Service (IERS) Celestial System is a complex series of rotations that includes precession, nutation, variations in the Earth's rotation (UT1-UTC) and polar motion.

Calculations of the motion of a spacecraft are made on the basis of the range time-delay and/or the Doppler shift in the signals. This type of data was used to determine the positions, the velocities, and the magnitudes of the orientation maneuvers for the Pioneer, Galileo, and Ulysses spacecraft considered in this study.

Theoretical modeling of the group delays and phase delay rates are done with the orbit determination software we describe in the next section.

Data types: Our data describes the observations that are the basis of the results of this paper. We receive our data from DSN in closed-loop mode, i.e., data that has been tracked with phase lock loop hardware. (Open loop data is tape recorded but not tracked by phase lock loop hardware.) The closed-loop data constitutes our Archival Tracking Data File (ATDF), which we copy [37] to the National Space Science Data Center (NSSDC) on magnetic tape. The ATDF files are stored on hard disk in the RMDC (Radio Metric Data Conditioning group) of JPL's Navigation and Mission Design Section. We access these files and run standard software to produce an Orbit Data File for input into the orbit determination programs which we use. (See Section V.)

The data types are two-way and three-way [36] Doppler and two-way range. (Doppler and range are defined in the following two subsections.) Due to unknown clock offsets between the stations, three-way range is generally not taken or used.

The Pioneer spacecraft only have two- and three-way S-band [24] Doppler. Galileo also has S-band range data near the Earth. Ulysses has two- and three-way S-band up-link and X-band [24] down-link Doppler and range as well as S-band up-link and S-band down-link, although we have only processed the Ulysses S-band up-link and X-band down-link Doppler and range.

1. Doppler experimental techniques and strategy

In Doppler experiments a radio signal transmitted from the Earth to the spacecraft is coherently transponded and sent back to the Earth. Its frequency change is measured with great precision, using the hydrogen masers at the DSN stations. The observable is the DSN frequency shift [38]

$$\Delta\nu(t) = \nu_0 \, \frac{1}{c} \frac{d\ell}{dt}, \qquad (1)$$

where ℓ is the overall optical distance (including diffraction effects) traversed by a photon in both directions. [In the Pioneer Doppler experiments, the stability of the fractional drift at the S-band is on the order of $\Delta\nu/\nu_0 \simeq 10^{-12}$, for integration times on the order of 10^3 s.] Doppler measurements provide the "range rate" of the spacecraft and therefore are affected by all the dynamical phenomena in the volume between the Earth and the spacecraft.

Expanding upon what was discussed in Section III A, the received signal and the transmitter frequency (both are at S-band) as well as a 10 pulse per second timing reference from the FTS are fed to the Metric Data Assembly (MDA). There the Doppler phase (difference between transmitted and received phases plus an added bias) is counted. That is, digital counters at the MDA record the zero crossings of the difference (i.e., Doppler, or alternatively the beat frequency of the received frequency and the exciter frequency). After counting, the bias is removed so that the true phase is produced.

The system produces "continuous count Doppler" and it uses two counters. Every tenth of a second, a Doppler phase count is recorded from one of the counters. The other counter continues the counts. The recording alternates between the two counters to maintain a continuous unbroken count. The Doppler counts are at 1 MHz for S-band or 5 MHz for X-band. The wavelength of each S-band cycle is about 13 cm. Dividers or "time resolvers" further subdivide the cycle into 256 parts, so that fractional cycles are measured with a resolution of 0.5 mm. This accuracy can only be maintained if the Doppler is continuously counted (no breaks in the count) and coherent frequency standards are kept throughout the pass. It should be noted that no error is accumulated in the phase count as long as lock is not lost. The only errors are the

stability of the hydrogen maser and the resolution of the "resolver."

Consequently, the JPL Doppler records are not frequency measurements. Rather, they are digitally counted measurements of the Doppler phase difference between the transmitted and received S-band frequencies, divided by the count time.

Therefore, the Doppler observables, we will refer to, have units of cycles per second or Hz. Since total count phase observables are Doppler observables multiplied by the count interval T_c, they have units of cycles. The Doppler integration time refers to the total counting of the elapsed periods of the wave with the reference frequency of the hydrogen maser. The usual Doppler integrating times for the Pioneer Doppler signals refers to the data sampled over intervals of 10 s, 60 s, 600 s, or 1980 s.

2. Range measurements

A range measurement is made by phase modulating a signal onto the up-link carrier and having it echoed by the transponder. The transponder demodulates this ranging signal, filters it, and then re-modulates it back onto the down-link carrier. At the ground station, this returned ranging signal is demodulated and filtered. An instantaneous comparison between the outbound ranging signal and the returning ranging signal that comes down would yield the two-way delay. Cross correlating the returned phase modulated signal with a ground duplicate yields the time delay. (See [28] and references therein.) As the range code is repeated over and over, an ambiguity can exist. The orbit determination programs are then used to infer (some times with great difficulty) the number of range codes that exist between a particular transmitted code and its own corresponding received code.

Thus, the ranging data are independent of the Doppler data, which represents a frequency shift of the radio carrier wave without modulation. For example, solar plasma introduces a group delay in the ranging data but a phase advance in the Doppler data.

Ranging data can also be used to distinguish an actual range change from a fictitious range change seen in Doppler data that is caused by a frequency error [39]. The Doppler frequency integrated over time (the accumulated phase) should equal the range change except for the difference introduced by charged particles

3. Inferring position information from Doppler

It is also possible to infer the position in the sky of a spacecraft from the Doppler data. This is accomplished by examining the diurnal variation imparted to the Doppler shift by the Earth's rotation. As the ground station rotates underneath a spacecraft, the Doppler shift is modulated by a sinusoid. The sinusoid's amplitude depends on the declination angle of the spacecraft and its phase depends upon the right ascension. These angles can therefore be estimated from a record of the Doppler shift that is (at least) of several days duration. This allows for a determination of the distance to the spacecraft through the dynamics of spacecraft motion using standard orbit theory contained in the orbit determination programs.

C. Data preparation

In an ideal system, all scheduled observations would be used in determining parameters of physical interest. However, there are inevitable problems that occur in data collection and processing that corrupt the data. So, at various stages of the signal processing one must remove or "edit" corrupted data. Thus, the need arises for objective editing criteria. Procedures have been developed which attempt to excise corrupted data on the basis of objective criteria. There is always a temptation to eliminate data that is not well explained by existing models, to thereby "improve" the agreement between theory and experiment. Such an approach may, of course, eliminate the very data that would indicate deficiencies in the *a priori* model. This would preclude the discovery of improved models.

In the processing stage that fits the Doppler samples, checks are made to ensure that there are no integer cycle slips in the data stream that would corrupt the phase. This is done by considering the difference of the phase observations taken at a high rate (10 times a second) to produce Doppler. Cycle slips often are dependent on tracking loop bandwidths, the signal to noise ratios, and predictions of frequencies. Blunders due to out-of-lock can be determined by looking at the original tracking data. In particular, cycle slips due to loss-of-lock stand out as a 1 Hz blunder point for each cycle slipped.

If a blunder point is observed, the count is stopped and a Doppler point is generated by summing the preceding points. Otherwise the count is continued until a specified maximum duration is reached. Cases where this procedure detected the need for cycle corrections were flagged in the database and often individually examined by an analyst. Sometimes the data was corrected, but nominally the blunder point was just eliminated. This ensures that the data is consistent over a pass. However, it does not guarantee that the pass is good, because other errors can affect the whole pass and remain undetected until the orbit determination is done.

To produce an input data file for an orbit determination program, JPL has a software package known as the Radio Metric Data Selection, Translation, Revision, Intercalation, Processing and Performance Evaluation Reporting (RMD-STRIPPER) Program. As we discussed in Section III B 1, this input file has data that can be integrated over intervals with different durations: 10 s, 60

s, 600 s and 1980 s. This input Orbit Determination File (ODFILE) obtained from the RMDC group is the initial data set with which both the JPL and The Aerospace Corporation groups started their analyses. Therefore, the initial data file already contained some common data editing that the RMDC group had implemented through program flags, etc. The data set we started with had already been compressed to 60 s. So, perhaps there were some blunders that had already been removed using the initial STRIPPER program.

The orbit analyst manually edits the remaining corrupted data points. Editing is done either by plotting the data residuals and deleting them from the fit or plotting weighted data residuals. That is, the residuals are divided by the standard deviation assigned to each data point and plotted. This gives the analyst a realistic view of the data noise during those times when the data was obtained while looking through the solar plasma. Applying an "N-σ" (σ is the standard deviation) test, where N is the choice of the analyst (usually 4-10) the analyst can delete those points that lie outside the N-σ rejection criterion without being biased in his selection. The N-σ test, implemented in CHASMP, is very useful for data taken near solar conjunction since the solar plasma adds considerable noise to the data. This criterion later was changed to a similar criteria that rejects all data with residuals in the fit extending for more than ± 0.025 Hz from the mean. Contrariwise, the JPL analysis edits only very corrupted data; e.g., a blunder due to a phase lock loss, data with bad spin calibration, etc. Essentially the Aerospace procedure eliminates data in the tails of the Gaussian probability frequency distribution whereas the JPL procedure accepts this data.

If needed or desired, the orbit analyst can choose to perform an additional data compression of the original navigation data. The JPL analysis does not apply any additional data compression and uses all the original data from the ODFILE as opposed to Aerospace's approach. Aerospace makes an additional compression of data within CHASMP. It uses the longest available data integration times which can be composed from either summing up adjacent data intervals or by using data spans with duration $\geq$ 600 s. (Effectively Aerospace prefers 600 and 1980 second data intervals and applies a low-pass filter.)

The total count of corrupted data points is about 10% of the total raw data points. The analysts' judgments play an important role here and is one of the main reasons that JPL and Aerospace have slightly different results. (See Sections V and VI.) In Section V we will show a typical plot (Figure 8 below) with outliers present in the data. Many more outliers are off the plot. One would expect that the two different strategies of data compression used by the two teams would result in significantly different numbers of total data points used in the two independent analyses. The influence of this fact on the solution estimation accuracy will be addressed in Section VI below.

D. Data weighting

Considerable effort has gone into accurately estimating measurement errors in the observations. These errors provide the data weights necessary to accurately estimate the parameter adjustments and their associated uncertainties. To the extent that measurement errors are accurately modeled, the parameters extracted from the data will be unbiased and will have accurate sigmas assigned to them. Both JPL and Aerospace assign a standard uncertainty of 1 mm/s over a 60 second count time for the S–band Pioneer Doppler data. (Originally the JPL team was weighting the data by 2 mm/s uncertainty.)

A change in the DSN antenna elevation angle also directly affects the Doppler observables due to tropospheric refraction. Therefore, to correct for the influence of the Earth's troposphere the data can also be deweighted for low elevation angles. The phenomenological range correction is given as

$$\sigma = \sigma_{\texttt{nominal}} \left(1 + \frac{18}{(1 + \theta_E)^2} \right), \qquad (2)$$

where $\sigma_{\texttt{nominal}}$ is the basic standard deviation (in Hz) and θ_E is the elevation angle in degrees [40]. Each leg is computed separately and summed. For Doppler the same procedure is used. First, Eq. (2) is multiplied by $\sqrt{60\,\text{s}/T_c}$, where T_c is the count time. Then a numerical time differentiation of Eq. (2) is performed. That is, Eq. (2) is differenced and divided by the count time, T_c. (For more details on this standard technique see Refs. [41]-[44].)

There is also the problem of data weighting for data influenced by the solar corona. This will be discussed in Section IV D.

E. Spin calibration of the data

The radio signals used by DSN to communicate with spacecraft are circularly polarized. When these signals are reflected from spinning spacecraft antennae a Doppler bias is introduced that is a function of the spacecraft spin rate. Each revolution of the spacecraft adds one cycle of phase to the up-link and the down-link. The up-link cycle is multiplied by the turn around ratio 240/221 so that the bias equals (1+240/221) cycles per revolution of the spacecraft.

High-rate spin data is available for Pioneer 10 only up to July 17, 1990, when the DSN ceased doing spin calibrations. (See Section II B.) After this date, in order to reconstruct the spin behavior for the entire data span and thereby account for the spin bias in the Doppler signal, both analyses modeled the spin by performing interpolations between the data points. The JPL interpolation was non-linear with a high-order polynomial fit of the data. (The polynomial was from second up to sixth order, depending on the data quality.) The CHASMP interpolation was linear between the spin data points.

After a maneuver in mid-1993, there was not enough power left to support the IPP. But analysts still could get a rough determination approximately every six months using information obtained from the conscan maneuvers. No spin determinations were made after 1995. However, the archived conscan data could still yield spin data at every maneuver time if such work was approved. Further, as the phase center of the main antenna is slightly offset from the spin axis, a very small (but detectable) sine-wave signal appears in the high-rate Doppler data. In principle, this could be used to determine the spin rate for passes taken after 1993, but it has not been attempted. Also, the failure of one of the spin-down thrusters prevented precise spin calibration of the Pioneer 11 data.

Because the spin rate of the Pioneers was changing over the data span, the calibrations also provide an indication of gas leaks that affect the acceleration of the spacecraft. A careful look at the records shows how this can be a problem. This will be discussed in Sections VI A and VIII F.

IV. BASIC THEORY OF SPACECRAFT NAVIGATION

Accuracy of modern radio tracking techniques has provided the means necessary to explore the gravitational environment in the solar system up to a limit never before possible [45]. The major role in this quest belongs to relativistic celestial mechanics experiments with planets (e.g., passive radar ranging) and interplanetary spacecraft (both Doppler and range experiments). Celestial mechanics experiments with spacecraft have been carried out by JPL since the early 1960's [46, 47]. The motivation was to improve both the ephemerides of solar system bodies and also the knowledge of the solar system's dynamical environment. This has become possible due to major improvements in the accuracy of spacecraft navigation, which is still a critical element for a number of space missions. The main objective of spacecraft navigation is to determine the present position and velocity of a spacecraft and to predict its future trajectory. This is usually done by measuring changes in the spacecraft's position and then, using those measurements, correcting (fitting and adjusting) the predicted spacecraft trajectory.

In this section we will discuss the theoretical foundation that is used for the analysis of tracking data from interplanetary spacecraft. We describe the basic physical models used to determine a trajectory, given the data.

A. Relativistic equations of motion

The spacecraft ephemeris, generated by a numerical integration program, is a file of spacecraft positions and velocities as functions of ephemeris (or coordinate) time (ET). The integrator requires the input of various parameters. These include adopted constants (c, G, planetary mass ratios, etc.) and parameters that are estimated from fits to observational data (e.g., corrections to planetary orbital elements).

The ephemeris programs use equations for point-mass relativistic gravitational accelerations. They are derived from the variation of a time-dependent, Lagrangian-action integral that is referenced to a non-rotating, solar-system, barycentric, coordinate frame. In addition to modeling point-mass interactions, the ephemeris programs contain equations of motion that model terrestrial and lunar figure effects, Earth tides, and lunar physical librations [48]-[50]. The programs treat the Sun, the Moon, and the nine planets as point masses in the isotropic, parameterized post-Newtonian, N-body metric with Newtonian gravitational perturbations from large, main-belt asteroids.

Responding to the increasing demand of the navigational accuracy, the gravitational field in the solar system is modeled to include a number of relativistic effects that are predicted by the different metric theories of gravity. Thus, within the accuracy of modern experimental techniques, the parameterized post-Newtonian (PPN) approximation of modern theories of gravity provides a useful starting point not only for testing these predictions, but also for describing the motion of self-gravitating bodies and test particles. As discussed in detail in [51], the accuracy of the PPN limit (which is slow motion and weak field) is adequate for all foreseeable solar system tests of general relativity and a number of other metric theories of gravity. (For the most general formulation of the PPN formalism, see the works of Will and Nordtvedt [51, 52].)

For each body i (a planet or spacecraft anywhere in the solar system), the point-mass acceleration is written as [41, 42, 48, 53, 54]

$$\ddot{\mathbf{r}}_i = \sum_{j \neq i} \frac{\mu_j(\mathbf{r}_j - \mathbf{r}_i)}{r_{ij}^3} \left(1 - \frac{2(\beta+\gamma)}{c^2} \sum_{k \neq i} \frac{\mu_k}{r_{ik}} - \frac{2\beta-1}{c^2} \sum_{k \neq j} \frac{\mu_k}{r_{jk}} - \frac{3}{2c^2}\left[\frac{(\mathbf{r}_j - \mathbf{r}_i)\dot{\mathbf{r}}_j}{r_{ij}}\right]^2 + \frac{1}{2c^2}(\mathbf{r}_j - \mathbf{r}_i)\ddot{\mathbf{r}}_j - \frac{2(1+\gamma)}{c^2}\dot{\mathbf{r}}_i\dot{\mathbf{r}}_j + \right.$$

$$\left. + \gamma\left(\frac{v_i}{c}\right)^2 + (1+\gamma)\left(\frac{v_j}{c}\right)^2 \right) + \frac{1}{c^2} \sum_{j \neq i} \frac{\mu_j}{r_{ij}^3}\Big([\mathbf{r}_i - \mathbf{r}_j)] \cdot [(2+2\gamma)\dot{\mathbf{r}}_i - (1+2\gamma)\dot{\mathbf{r}}_j]\Big)(\dot{\mathbf{r}}_i - \dot{\mathbf{r}}_j) + \frac{3+4\gamma}{2c^2} \sum_{j \neq i} \frac{\mu_j\ddot{\mathbf{r}}_j}{r_{ij}} \quad (3)$$

where μ_i is the "gravitational constant" of body i. It actually is its mass times the Newtonian constant: $\mu_i = Gm_i$. Also, $\mathbf{r}_i(t)$ is the barycentric position of body i, $r_{ij} = |\mathbf{r}_j - \mathbf{r}_i|$ and $v_i = |\dot{\mathbf{r}}_i|$. For planetary motion, each of these equations depends on the others. So they must be iterated in each step of the integration of the equations of motion.

The barycentric acceleration of each body j due to Newtonian effects of the remaining bodies and the asteroids is denoted by $\ddot{\mathbf{r}}_j$. In Eq. (3), β and γ are the PPN parameters [51, 52]. General relativity corresponds to $\beta = \gamma = 1$, which we choose for our study. The Brans-Dicke theory is the most famous among the alternative theories of gravity. It contains, besides the metric tensor, a scalar field φ and an arbitrary coupling constant ω, related to the two PPN parameters as $\gamma = \frac{1+\omega}{2+\omega}$, $\beta = 1$. Equation (3) allows the consideration of any problem in celestial mechanics within the PPN framework.

B. Light time solution and time scales

In addition to planetary equations of motion Eq. (3), one needs to solve the relativistic light propagation equation in order to get the solution for the total light time travel. In the solar system, barycentric, space-time frame of reference this equation is given by:

$$
\begin{aligned}
t_2 - t_1 &= \frac{r_{21}}{c} + \frac{(1+\gamma)\mu_\odot}{c^3} \ln\left[\frac{r_1^\odot + r_2^\odot + r_{12}^\odot}{r_1^\odot + r_2^\odot - r_{12}^\odot}\right] + \\
&+ \sum_i \frac{(1+\gamma)\mu_i}{c^3} \ln\left[\frac{r_1^i + r_2^i + r_{12}^i}{r_1^i + r_2^i - r_{12}^i}\right],
\end{aligned} \tag{4}
$$

where $\mu_\odot$ is the gravitational constant of the Sun and μ_i is the gravitational constant of a planet, an outer planetary system, or the Moon. $r_1^\odot, r_2^\odot$ and $r_{12}^\odot$ are the heliocentric distances to the point of RF signal emission on Earth, to the point of signal reflection at the spacecraft, and the relative distance between these two points. Correspondingly, r_1^i, r_2^i, and r_{12}^i are similar distances relative to a particular i-th body in the solar system. In the spacecraft light time solution, t_1 refers to the transmission time at a tracking station on Earth, and t_2 refers to the reflection time at the spacecraft or, for one-way [36] data, the transmission time at the spacecraft. The reception time at the tracking station on Earth or at an Earth satellite is denoted by t_3. Hence, Eq. (4) is the up-leg light time equation. The corresponding down-leg light time equation is obtained by replacing subscripts as follows: $1 \to 2$ and $2 \to 3$. (See the details in [42].)

The spacecraft equations of motion relative to the solar system barycenter are essentially the same as given by Eq. (3). The gravitational constants of the Sun, planets and the planetary systems are the values associated with the solar system barycentric frame of reference, which are obtained from the planetary ephemeris [54]. We treat a distant spacecraft as a point-mass particle. The spacecraft acceleration is integrated numerically to produce

the spacecraft ephemeris. The ephemeris is interpolated at the ephemeris time (ET) value of the interpolation epoch. This is the time coordinate t in Eqs. (3) and (4), i.e., $t \equiv$ ET. As such, ephemeris time means coordinate time in the chosen celestial reference frame. It is an independent variable for the motion of celestial bodies, spacecraft, and light rays. The scale of ET depends upon which reference frame is selected and one may use a number of time scales depending on the practical applications. It is convenient to express ET in terms of International Atomic Time (TAI). TAI is based upon the second in the International System of Units (SI). This second is defined to be the duration of 9,192,631,770 periods of the radiation corresponding to the transition between two hyperfine levels of the ground state of the cesium-133 atom [55].

The differential equation relating ephemeris time (ET) in the solar system barycentric reference frame to TAI at a tracking station on Earth or on Earth satellite can be obtained directly from the Newtonian approximation to the N-body metric [54]. This expression has the form

$$
\frac{d\,\text{TAI}}{d\,\text{ET}} = 1 - \frac{1}{c^2}\left(U - \langle U \rangle + \frac{1}{2}v^2 - \frac{1}{2}\langle v^2 \rangle\right) + \mathcal{O}(\frac{1}{c^4}), \tag{5}
$$

where U is the solar system gravitational potential evaluated at the tracking station and v is the solar system barycentric velocity of the tracking station. The brackets $\langle\ \rangle$ on the right side of Eq. (5) denote long-time average of the quantity contained within them. This averaging amounts to integrating out periodic variations in the gravitational potential, U, and the barycentric velocity, v^2, at the location of a tracking station. The desired time scale transformation is then obtained by using the planetary ephemeris to calculate the terms in Eq. (5).

The vector expression for the ephemeris/coordinate time (ET) in the solar system barycentric frame of reference minus the TAI obtained from an atomic clock at a tracking station on Earth has the form [54]

$$
\begin{aligned}
\text{ET} - \text{TAI} &= 32.184\,\text{s} + \frac{2}{c^2}(\dot{\mathbf{r}}_B^\odot \cdot \mathbf{r}_B^\odot) + \frac{1}{c^2}(\dot{\mathbf{r}}_B^{\text{SSB}} \cdot \mathbf{r}_E^B) + \\
&+ \frac{1}{c^2}(\dot{\mathbf{r}}_E^{\text{SSB}} \cdot \mathbf{r}_A^E) + \frac{\mu_J}{c^2(\mu_\odot + \mu_J)}(\dot{\mathbf{r}}_J^\odot \cdot \mathbf{r}_J^\odot) + \\
&+ \frac{\mu_{Sa}}{c^2(\mu_\odot + \mu_{Sa})}(\dot{\mathbf{r}}_{Sa}^\odot \cdot \mathbf{r}_{Sa}^\odot) + \frac{1}{c^2}(\dot{\mathbf{r}}_\odot^{\text{SSB}} \cdot \mathbf{r}_B^\odot), \tag{6}
\end{aligned}
$$

where $\mathbf{r}_i^j$ and $\dot{\mathbf{r}}_i^j$ position and velocity vectors of point i relative to point j (they are functions of ET); superscript or subscript SSB denotes solar system barycenter; $\odot$ stands for the Sun; B for the Earth-Moon barycenter; E, J, Sa denote the Earth, Jupiter, and Saturn correspondingly, and A is for the location of the atomic clock on Earth which reads TAI. This approximated analytic result contains the clock synchronization term which depends upon the location of the atomic clock and five location-independent periodic terms. There are several alternate expressions that have up to several hundred additional periodic terms which provide greater accuracies than Eq. (6). The use of these extended expressions

provide transformations of `ET` – `TAI` to accuracies of 1 ns [42].

For the purposes of our study the Station Time (`ST`) is especially significant. This time is the atomic time `TAI` at a DSN tracking station on Earth, `ST=TAI`$_{\text{station}}$. This atomic time scale departs by a small amount from the "reference time scale." The reference time scale for a DSN tracking station on Earth is the Coordinated Universal Time (`UTC`). This last is standard time for 0° longitude. (For more details see [42, 55].)

All the vectors in Eq. (6) except the geocentric position vector of the tracking station on Earth can be interpolated from the planetary ephemeris or computed from these quantities. Universal Time (`UT`) is the measure of time which is the basis for all civil time keeping. It is an observed time scale. The specific version used in JPL's Orbit Determination Program (ODP) is `UT1`. This is used to calculate mean sidereal time, which is the Greenwich hour angle of the mean equinox of date measured in the true equator of date. Observed `UT1` contains 41 short-term terms with periods between 5 and 35 days. They are caused by long-period solid Earth tides. When the sum of these terms, Δ`UT1`, is subtracted from `UT1` the result is called `UT1R`, where `R` means regularized.

Time in any scale is represented as seconds past 1 January 2000, 12$^{\text{h}}$, in that time scale. This epoch is J2000.0, which is the start of the Julian year 2000. The Julian Date for this epoch is JD 245,1545.0. Our analyses used the standard space-fixed J2000 coordinate system, which is provided by the International Celestial Reference Frame (ICRF). This is a quasi-inertial reference frame defined from the radio positions of 212 extragalactic sources distributed over the entire sky [56].

The variability of the earth-rotation vector relative to the body of the planet or in inertial space is caused by the gravitational torque exerted by the Moon, Sun and planets, displacements of matter in different parts of the planet and other excitation mechanisms. The observed oscillations can be interpreted in terms of mantle elasticity, earth flattening, structure and properties of the core-mantle boundary, rheology of the core, underground water, oceanic variability, and atmospheric variability on time scales of weather or climate.

Several space geodesy techniques contribute to the continuous monitoring of the Earth's rotation by the International Earth Rotation Service (IERS). Measurements of the Earth's rotation presented in the form of time developments of the so-called Earth Orientation Parameters (`EOP`). Universal time (`UT1`), polar motion, and the celestial motion of the pole (precession/nutation) are determined by Very Long-Baseline Interferometry (VLBI). Satellite geodesy techniques, such as satellite laser ranging (SLR) and using the Global Positioning System (GPS), determine polar motion and rapid variations of universal time. The satellite geodesy programs used in the IERS allow determination of the time variation of the Earth's gravity field. This variation reflects the evolutions of the Earth's shape and of the distribution

of mass in the planet. The programs have also detected changes in the location of the center of mass of the Earth relative to the crust. It is possible to investigate other global phenomena such as the mass redistributions of the atmosphere, oceans, and solid Earth.

Using the above experimental techniques, Universal time and polar motion are available daily with an accuracy of about 50 picoseconds (ps). They are determined from VLBI astrometric observations with an accuracy of 0.5 milliarcseconds (mas). Celestial pole motion is available every five to seven days at the same level of accuracy. These estimations of accuracy include both short term and long term noise. Sub-daily variations in Universal time and polar motion are also measured on a campaign basis.

In summary, this dynamical model accounts for a number of post-Newtonian perturbations in the motions of the planets, the Moon, and spacecraft. Light propagation is correct to order c^{-2}. The equations of motion of extended celestial bodies are valid to order c^{-4}. Indeed, this dynamical model has been good enough to perform tests of general relativity [28, 51, 52].

C. Standard modeling of small, non-gravitational forces

In addition to the mutual gravitational interactions of the various bodies in the solar system and the gravitational forces acting on a spacecraft as a result of presence of those bodies, it is also important to consider a number of non-gravitational forces which are important for the motion of a spacecraft. (Books and lengthy reports have been written about practically all of them. Consult Ref. [57, 58] for a general introduction.)

The Jet Propulsion Laboratory's ODP accounts for many sources of non-gravitational accelerations. Among them, the most relevant to this study, are: i) solar radiation pressure, ii) solar wind pressure, iii) attitude-control maneuvers together with a model for unintentional spacecraft mass expulsion due to gas leakage of the propulsion system. We can also account for possible influence of the interplanetary media and DSN antennae contributions to the spacecraft radio tracking data and consider the torques produced by above mentioned forces. The Aerospace CHASMP code uses a model for gas leaks that can be adjusted to include the effects of the recoil force due to emitted radio power and anisotropic thermal radiation of the spacecraft.

In principle, one could set up complicated engineering models to predict at least some of the effects. However, their residual uncertainties might be unacceptable for the experiment, in spite of the significant effort required. In fact, a constant acceleration produces a linear frequency drift that can be accounted for in the data analysis by a single unknown parameter.

The figure against which we compare the effects of non-gravitational accelerations on the Pioneers' trajectories is

the expected error in the acceleration error estimations. This is on the order of

$$\sigma_0 \sim 2 \times 10^{-8} \ \ \text{cm/s}^2, \tag{7}$$

where σ_0 is a single determination accuracy related to acceleration measurements averaged over number of days. This would contribute to our result as $\sigma_N \sim \sigma_0/\sqrt{N}$. Thus, if no systematics are involved then σ_N will just tend to zero as time progresses.

Therefore, the important thing is to know that these effects (systematics) are not too large, thereby overwhelming any possibly important signal (such as our anomalous acceleration). This will be demonstrated in Sections VII and VIII.

D. Solar corona model and weighting

The electron density and density gradient in the solar atmosphere influence the propagation of radio waves through the medium. So, both range and Doppler observations at S-band are affected by the electron density in the interplanetary medium and outer solar corona. Since, throughout the experiment, the closest approach to the center of the Sun of a radio ray path was greater than 3.5 $R_\odot$, the medium may be regarded as collisionless. The *one way* time delay associated with a plane wave passing through the solar corona is obtained [44, 46, 59] by integrating the group velocity of propagation along the ray's path, ℓ:

$$\Delta t = \pm \frac{1}{2c\, n_{\text{crit}}(\nu)} \int_\oplus^{SC} d\ell \ n_e(t, \mathbf{r}),$$

$$n_{\text{crit}}(\nu) = 1.240 \times 10^4 \left(\frac{\nu}{1 \ \text{MHz}}\right)^2 \ \text{cm}^{-3}, \tag{8}$$

where $n_e(t, \mathbf{r})$ is the free electron density in the solar plasma, c is the speed of light, and $n_{\text{crit}}(\nu)$ is the critical plasma density for the radio carrier frequency ν. The plus sign is applied for ranging data and the minus sign for Doppler data [60].

Therefore, in order to calibrate the plasma contribution, one should know the electron density along the path. One usually decomposes the electron density, n_e, into a static, steady-state part, $\overline{n}_e(\mathbf{r})$, plus a fluctuation $\delta n_e(t, \mathbf{r})$, i.e., $n_e(t, \mathbf{r}) = \overline{n}_e(\mathbf{r}) + \delta n_e(t, \mathbf{r})$. The physical properties of the second term are hard to quantify. But luckily, its effect on Doppler observables and, therefore, on our results is small. (We will address this issue in Sec. VII B.) On the contrary, the steady-state corona behavior is reasonably well known and several plasma models can be found in the literature [59]-[62].

Consequently, while studying the effect of a systematic error from propagation of the S-band carrier wave through the solar plasma, both analyses adopted the following model for the electron density profile [44]:

$$n_e(t, \mathbf{r}) = A\left(\frac{R_\odot}{r}\right)^2 + B\left(\frac{R_\odot}{r}\right)^{2.7} e^{-\left[\frac{\phi}{\phi_0}\right]^2} + C\left(\frac{R_\odot}{r}\right)^6. \tag{9}$$

r is the heliocentric distance to the immediate ray trajectory and ϕ is the helio-latitude normalized by the reference latitude of $\phi_0 = 10°$. The parameters r and ϕ are determined from the trajectory coordinates on the tracking link being modeled. The parameters A, B, C are parameters chosen to describe the solar electron density. (They are commonly given in two sets of units, meters or cm^{-3} [63].) They can be treated as stochastic parameters, to be determined from the fit. But in both analyses we ultimately chose to use the values determined from the recent solar corona studies done for the Cassini mission. These newly obtained values are: $A = 6.0 \times 10^3, B = 2.0 \times 10^4, C = 0.6 \times 10^6$, all in meters [64]. [This is what we will refer to as the "Cassini corona model."]

Substitution of Eq. (9) into Eq. (8) results in the following steady-state solar corona contribution to the range model that we used in our analysis:

$$\Delta_{\text{sc}}\text{range} = \pm\left(\frac{\nu_0}{\nu}\right)^2 \left[A\left(\frac{R_\odot}{\rho}\right)F + \right.$$
$$\left. + \ B\left(\frac{R_\odot}{\rho}\right)^{1.7} e^{-\left[\frac{\phi}{\phi_0}\right]^2} + C\left(\frac{R_\odot}{\rho}\right)^5\right]. \tag{10}$$

ν_0 and ν are a reference frequency and the actual frequency of radio-wave [for Pioneer 10 analysis $\nu_0 = 2295$ MHz], ρ is the impact parameter with respect to the Sun and F is a light-time correction factor. For distant spacecraft this function is given as follows:

$$F = F(\rho, r_T, r_E) = \tag{11}$$
$$= \frac{1}{\pi}\left\{\text{ArcTan}\left[\frac{\sqrt{r_T^2 - \rho^2}}{\rho}\right] + \text{ArcTan}\left[\frac{\sqrt{r_E^2 - \rho^2}}{\rho}\right]\right\},$$

where r_T and r_E are the heliocentric radial distances to the target and to the Earth, respectively. Note that the sign of the solar corona range correction is negative for Doppler and positive for range. The Doppler correction is obtained from Eq. (10) by simple time differentiation. Both analyses use the same physical model, Eq. (10), for the steady-state solar corona effect on the radio-wave propagation through the solar plasma. Although the actual implementation of the model in the two codes is different, this turns out not to be significant. (See Section IX B.)

CHASMP can also consider the effect of temporal variation in the solar corona by using the recorded history of solar activity. The change in solar activity is linked to the variation of the total number of sun spots per year as observed at a particular wavelength of the solar radiation, λ=10.7 cm. The actual data corresponding to this variation is given in Ref. [65]. CHASMP averages this data over 81 days and normalizes the value of the flux by 150. Then it is used as a time-varying scaling factor in Eq. (10). The result is referred to as the "F10.7 model."

Next we come to corona data weighting. JPL's ODP does not apply corona weighting. On the other hand, Aerospace's CHASMP can apply corona weighting if desired. Aerospace uses a standard weight augmented by

a weight function that accounts for noise introduced by solar plasma and low elevation. The weight values are adjusted so that i) the post-fit weighted sum of the squares is close to unity and ii) approximately uniform noise in the residuals is observed throughout the fit span.

Thus, the corresponding solar-corona weight function is:

$$\sigma_r = \frac{k}{2}\left(\frac{\nu_0}{\nu}\right)^2\left(\frac{R_\odot}{\rho}\right)^{\frac{3}{2}}, \tag{12}$$

where, for range data, k is an input constant nominally equal to 0.005 light seconds, ν_0 and ν are a reference frequency and the actual frequency, ρ is the trajectory's impact parameter with respect to the Sun in km, and $R_\odot$ is the solar radius in km [66]. The solar-corona weight function for Doppler is essentially the same, but obtained by numerical time differentiation of Eq. (12).

E.   Modeling of maneuvers

There were 28 Pioneer 10 maneuvers during our data interval from 3 January 1987 to 22 July 1998. Imperfect coupling of the hydrazine thrusters used for the spin orientation maneuvers produced integrated velocity changes of a few millimeters per second. The times and durations of each maneuver were provided by NASA/Ames. JPL used this data as input to ODP. The Aerospace team used a slightly different approach. In addition to the original data, CHASMP used the spin-rate data file to help determine the times and duration of maneuvers. The CHASMP determination mainly agreed with the data used by JPL. [There were minor variations in some of the times, one maneuver was split in two, and one extraneous maneuver was added to Interval II to account for data not analyzed (see below).]

Because the effect on the spacecraft acceleration could not be determined well enough from the engineering telemetry, JPL included a single unknown parameter in the fitting model for each maneuver. In JPL's ODP analysis, the maneuvers were modeled by instantaneous velocity increments at the beginning time of each maneuver (instantaneous burn model). [Analyses of individual maneuver fits show the residuals to be small.] In the CHASMP analysis, a constant acceleration acting over the duration of the maneuver was included as a parameter in the fitting model (finite burn model). Analyses of individual maneuver fits show the residuals are small. Because of the Pioneer spin, these accelerations are important only along the Earth-spacecraft line, with the other two components averaging out over about 50 revolutions of the spacecraft over a typical maneuver duration of 10 minutes.

By the time Pioneer 11 reached Saturn, the pattern of the thruster firings was understood. Each maneuver caused a change in spacecraft spin and a velocity increment in the spacecraft trajectory, immediately followed by two to three days of gas leakage, large enough to be observable in the Doppler data [67].

Typically the Doppler data is time averaged over 10 to 33 minutes, which significantly reduces the high-frequency Doppler noise. The residuals represent our fit. They are converted from units of Hz to Doppler velocity by the formula [38]

$$[\Delta v]_{\text{DSN}} = \frac{c}{2}\frac{[\Delta \nu]_{\text{DSN}}}{\nu_0}, \tag{13}$$

where ν_0 is the downlink carrier frequency, ~ 2.29 GHz, $\Delta \nu$ is the Doppler residual in Hz from the fit, and c is the speed of light.

As an illustration, consider the fit to one of the Pioneer 10 maneuvers, # 17, on 22 December 1993, given in Figure 5. This was particularly well covered by low-noise
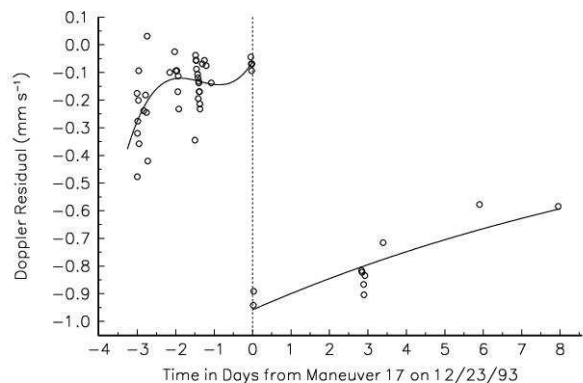
FIG. 5: The Doppler residuals after a fit for maneuver # 17 on 23 December 1993.

Doppler data near solar opposition. Before the start of the maneuver, there is a systematic trend in the residuals which is represented by a cubic polynomial in time. The standard error in the residuals is 0.095 mm/s. After the maneuver, there is a relatively small velocity discontinuity of -0.90 ± 0.07 mm/s. The discontinuity arises because the model fits the entire data interval. In fact, the residuals increase after the maneuver. By 11 January 1994, 19 days after the maneuver, the residuals are scattered about their pre-maneuver mean of -0.15 mm/s.

For purposes of characterizing the gas leak immediately after the maneuver, we fit the post-maneuver residuals by a two-parameter exponential curve,

$$\Delta v = -v_0 \exp\left[-\frac{t}{\tau}\right] - 0.15 \quad \text{mm/s}. \tag{14}$$

The best fit yields $v_0 = 0.808$ mm/s and the time constant τ is 13.3 days, a reasonable result. The time derivative of the exponential curve yields a residual acceleration immediately after the maneuver of 7.03×10^{-8} cm/s^2. This is close to the magnitude of the anomalous acceleration inferred from the Doppler data, but in the *opposite*

direction. However the gas leak rapidly decays and becomes negligible after 20 days or so.

F. Orbit determination procedure

Our orbit determination procedure first determines the spacecraft's initial position and velocity in a data interval. For each data interval, we then estimate the magnitudes of the orientation maneuvers, if any. The analyses are modeled to include the effects of planetary perturbations, radiation pressure, the interplanetary media, general relativity, and bias and drift in the Doppler and range (if available). Planetary coordinates and solar system masses are obtained using JPL's Export Planetary Ephemeris DE405, where DE stands for the Development Ephemeris. [Earlier in the study, DE200 was used. See Section V A.]

We include models of precession, nutation, sidereal rotation, polar motion, tidal effects, and tectonic plates drift. Model values of the tidal deceleration, nonuniformity of rotation, polar motion, Love numbers, and Chandler wobble are obtained observationally, by means of Lunar and Satellite Laser Ranging (LLR and SLR) techniques and VLBI. Previously they were combined into a common publication by either the International Earth Rotation Service (IERS) or by the United States Naval Observatory (USNO). Currently this information is provided by the ICRF. JPL's Earth Orientation Parameters (EOP) is a major source contributor to the ICRF.

The implementation of the J2000.0 reference coordinate system in CHASMP involves only rotation from the Earth-fixed to the J2000.0 reference frame and the use of JPL's   DE200   planetary ephemeris [68]. The rotation from   J2000.0   to Earth-fixed is computed from a series of rotations which include precession, nutation, the Greenwich hour angle, and pole wander. Each of these general categories is also a multiple rotation and is treated separately by most software. Each separate rotation matrix is chain multiplied to produce the final rotation matrix.

CHASMP, however, does not separate precession and nutation. Rather, it combines them into a single matrix operation. This is achieved by using a different set of angles to describe precession than is used in the ODP. (See a description of the standard set of angles in [69].) These angles separate luni-solar precession from planetary precession. Luni-solar precession, being the linear term of the nutation series for the nutation in longitude, is combined with the nutation in longitude from the DE200 ephemeris tape [70].

Both JPL's ODP and The Aerospace Corporation's CHASMP use the JPL/Earth Orientation Parameters (EOP) values. This could be a source of common error. However the comparisons between EOP and IERS show an insignificant difference. Also, only secular terms, such as precession, can contribute errors to the anomalous acceleration. Errors in short period terms are not correlated with the anomalous acceleration.

G. Parameter estimation strategies

During the last few decades, the algorithms of orbital analysis have been extended to incorporate Kalman-filter estimation procedure that is based on the concept of "process noise" (i.e., random, non-systematic forces, or random-walk effects). This was motivated by the need to respond to the significant improvement in observational accuracy and, therefore, to the increasing sensitivity to numerous small perturbing factors of a stochastic nature that are responsible for observational noise. This approach is well justified when one needs to make accurate predictions of the spacecraft's future behavior using only the spacecraft's past hardware and electronics state history as well as the dynamic environment conditions in the distant craft's vicinity. Modern navigational software often uses Kalman filter estimation since it more easily allows determination of the temporal noise history than does the weighted least-squares estimation.

To take advantage of this while obtaining JPL's original results [12, 13] discussed in Section V, JPL used batch-sequential methods with variable batch sizes and process noise characteristics. That is, a batch-sequential filtering and smoothing algorithm with process noise was used with ODP. In this approach any small anomalous forces may be treated as stochastic parameters affecting the spacecraft trajectory. As such, these parameters are also responsible for the stochastic noise in the observational data. To better characterize these noise sources, one splits the data interval into a number of constant or variable size batches and makes assumptions on possible statistical properties of these noise factors. One then estimates the mean values of the unknown parameters within the batch and also their second statistical moments.

Using batches has the advantage of dealing with a smaller number of experimental data segments. We experimented with a number of different constant batch sizes; namely, 0, 5, 30, and 200 day batch sizes. (Later we also used 1 and 10 day batch sizes.) In each batch one estimates the same number of desired parameters. So, one expects that the smaller the batch size the larger the resulting statistical errors. This is because a smaller number of data points is used to estimate the same number of parameters. Using the entire data interval as a single batch while changing the process noise *a priori* values is expected in principle (see below) to yield a result identical to the least-squares estimation. In the single batch case, it would produce only one solution for the anomalous acceleration.

There is another important parameter that was taken into account in the statistical data analysis reported here. This is the expected correlation time for the underlying stochastic processes (as well as the process noise) that may be responsible for the anomalous acceleration. For example, using a zero correlation time is useful in

searches for an a_P that is generated by a random process. One therefore expects that an a_P estimated from one batch is statistically independent (uncorrelated) from those estimated from other batches. Also, the use of finite correlation times indicates one is considering an a_P that may show a temporal variation within the data interval. We experimented with a number of possible correlation times and will discuss the corresponding assumptions when needed.

In each batch one estimates solutions for the set of desired parameters at a specified epoch within the batch. One usually chooses to report solutions corresponding to the beginning, middle, or end of the batch. General coordinate and time transformations (discussed in Section IV B) are then used to report the solution in the epoch chosen for the entire data interval. One may also adjust the solutions among adjacent batches by accounting for possible correlations. This process produces a smoothed solution for the set of solved-for parameters. More details on this so called "batch–sequential algorithm with smoothing filter" are available in Refs. [41]-[43].

Even without process noise, the inversion algorithms of the Kalman formulation and the weighted least-squares method seem radically different. But as shown in [71], if one uses a single batch for all the data and if one uses certain assumptions about, for instance, the process noise and the smoothing algorithms, then the two methods are mathematically identical. When introducing process noise, an additional process noise matrix is also added into the solution algorithm. The elements of this matrix are chosen by the user as prescribed by standard statistical techniques used for navigational data processing.

For the recent results reported in Section VI, JPL used both the batch-sequential and the weighted least-squares estimation approaches. JPL originally implemented only the batch-sequential method, which yielded the detection (at a level smaller than could be detected with any other spacecraft) of an annual oscillatory term smaller in size than the anomalous acceleration [13]. (This term is discussed in Section IX C.) The recent studies included weighted least-squares estimation to see if this annual term was a calculational anomaly.

The Aerospace Corporation uses only the weighted least-squares approach with its CHASMP software. A χ^2 test is used as an indicator of the quality of the fit. In this case, the anomalous acceleration is treated as a constant parameter over the entire data interval. To solve for a_P one estimates the statistical weights for the data points and then uses these in a general weighted least-squares fashion. Note that the weighted least-squares method can obtain a result similar to that from a batch-sequential approach (with smoothing filter, zero correlation time and without process noise) by cutting the data interval into smaller pieces and then looking at the temporal variation among the individual solutions.

As one will see in the following, in the end, both programs yielded very similar results. The differences between them can be mainly attributed to (other) systematics. This gives us confidence that both programs and their implemented estimation algorithms are correct to the accuracy of this investigation.

V. ORIGINAL DETECTION OF THE ANOMALOUS ACCELERATION

A. Early JPL studies of the anomalous Pioneer Doppler residuals

As mentioned in the introduction, by 1980 Pioneer 10 was at 20 AU, so the solar radiation pressure acceleration had decreased to $< 5 \times 10^{-8}$ cm/s^2. Therefore, a search for unmodeled accelerations (at first with the further out Pioneer 10) could begin at this level. With the acceptance of a proposal of two of us (JDA and ELL) to participate in the Heliospheric Mission on Pioneer 10 and 11, such a search began in earnest [72].

The JPL analysis of unmodeled accelerations used the JPL's Orbit Determination Program (ODP) [41]-[42]. Over the years the data continually indicated that the largest systematic error in the acceleration residuals is a constant bias of $a_P \sim (8 \pm 3) \times 10^{-8}$ cm/s^2, directed *toward* the Sun (to within the beam-width of the Pioneers' antennae [73]).

As stated previously, the analyses were modeled to include the effects of planetary perturbations, radiation pressure, the interplanetary media, general relativity, together with bias and drift in the Doppler signal. Planetary coordinates and the solar system masses were taken from JPL's Export Planetary Ephemeris DE405, referenced to ICRF. The analyses used the standard space-fixed J2000 coordinate system with its associated JPL planetary ephemeris DE405 (or earlier, DE200). The time-varying Earth orientation in J2000 coordinates is defined by a 1998 version of JPL's EOP file, which accounts for the inertial precession and nutation of the Earth's spin axis, the geophysical motion of the Earth's pole with respect to its spin axis, and the Earth's time varying spin rate. The three-dimensional locations of the tracking stations in the Earth's body-fixed coordinate system (geocentric radius, latitude, longitude) were taken from a set recommended by ICRF for JPL's DE405.

Consider $\nu_{\texttt{obs}}$, the frequency of the re-transmitted signal observed by a DSN antennae, and $\nu_{\texttt{model}}$, the predicted frequency of that signal. The observed, two-way anomalous effect can be expressed to first order in v/c as [38]

$$[\nu_{\texttt{obs}}(t) - \nu_{\texttt{model}}(t)]_{\texttt{DSN}} = -\nu_0 \frac{2a_P\,t}{c},$$
$$\nu_{\texttt{model}} = \nu_0 \left[1 - \frac{2v_{\texttt{model}}(t)}{c}\right]. \qquad (15)$$

Here, ν_0 is the reference frequency, the factor 2 is because we use two- and three-way data [36]. $v_{\texttt{model}}$ is the modeled velocity of the spacecraft due to the gravitational

and other large forces discussed in Section IV. (This velocity is outwards and hence produces a red shift.) We have already included the sign showing that a_P is inward. (Therefore, a_P produces a slight blue shift on top of the larger red shift.) By DSN convention [38], the first of Eqs. (15) is $[\Delta\nu_{\text{obs}} - \Delta\nu_{\text{model}}]_{\text{usual}} = -[\Delta\nu_{\text{obs}} - \Delta\nu_{\text{model}}]_{\text{DSN}}$.

Over the years the anomaly remained in the data of both Pioneer 10 and Pioneer 11 [74]. (See Figure 6.)
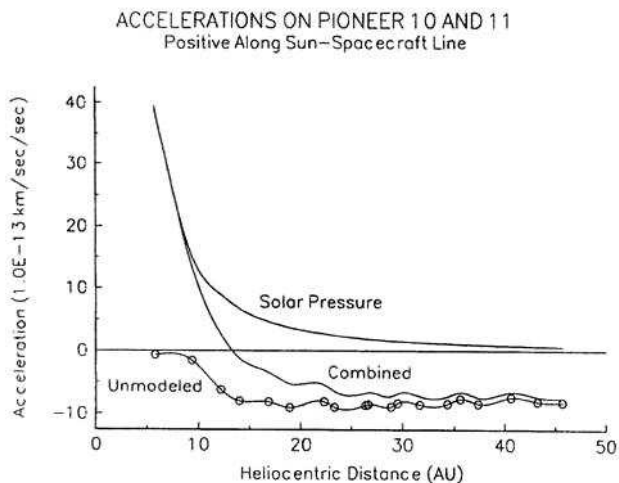
FIG. 6: ODP plots, as a function of distance from the Sun, of accelerations on Pioneers 10/11. The accelerations are a) the calculated solar radiation acceleration (top line), b) the unmodeled acceleration (bottom line), and c) the sum of the two above (middle line) [75].

In order to model any unknown forces acting on Pioneer 10, the JPL group introduced a stochastic acceleration, exponentially correlated in time, with a time constant that can be varied. This stochastic variable is sampled in ten-day batches of data. We found that a correlation time of one year produces good results. We did, however, experiment with other time constants as well, including a zero correlation time (white noise). The result of applying this technique to 6.5 years of Pioneer 10 and 11 data is shown in Figure 7. The plotted points represent our determination of the stochastic variable at ten-day sample intervals. We plot the stochastic variable as a function of heliocentric distance, not time, because that is more fundamental in searches for trans-Neptunian sources of gravitation.

As possible "perturbative forces" to explain this bias, we considered gravity from the Kuiper belt, gravity from the galaxy, spacecraft "gas leaks," errors in the planetary ephemeris, and errors in the accepted values of the Earth's orientation, precession, and nutation. We found that none of these mechanisms could explain the apparent acceleration, and some were three orders of magnitude or more too small. [We also ruled out a number
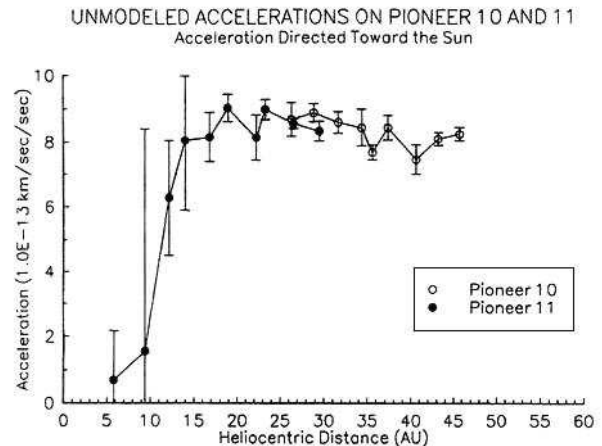
FIG. 7: An ODP plot of the early unmodeled accelerations of Pioneer 10 and Pioneer 11, from about 1981 to 1989 and 1977 to 1989, respectively [75].

of specific mechanisms involving heat radiation or "gas leaks," even though we feel these are candidates for the cause of the anomaly. We will return to this in Sections VII and VIII.]

We concluded [12], from the JPL-ODP analysis, that there is an unmodeled acceleration, a_P, towards the Sun of $(8.09 \pm 0.20) \times 10^{-8}$ cm/s^2 for Pioneer 10 and of $(8.56 \pm 0.15) \times 10^{-8}$ cm/s^2 for Pioneer 11. The error was determined by use of a five-day batch sequential filter with radial acceleration as a stochastic parameter subject to white Gaussian noise (~ 500 independent five-day samples of radial acceleration) [76]. No magnitude variation of a_P with distance was found, within a sensitivity of $\sigma_0 = 2 \times 10^{-8}$ cm/s^2 over a range of 40 to 60 AU. All our errors are taken from the covariance matrices associated with the least–squares data analysis. The assumed data errors are larger than the standard error on the post–fit residuals. [For example, the Pioneer S–band Doppler error was set at 1 mm/s at a Doppler integration time of 60 s, as opposed to a characteristic χ^2 value of 0.3 mm/s.] Consequently, the quoted errors are realistic, not formal, and represent our attempt to include systematics and a reddening of the noise spectrum by solar plasma. Any spectral peaks in the post-fit Pioneer Doppler residuals were not significant at a 90% confidence level [12].

B. First Aerospace study of the apparent Pioneer acceleration

With no explanation of this data in hand, our attention focused on the possibility that there was some error in JPL's ODP. To investigate this, an analysis of the raw

data was performed using an independent program, The Aerospace Corporation's Compact High Accuracy Satellite Motion Program (CHASMP) [77] – one of the standard Aerospace orbit analysis programs. CHASMP's orbit determination module is a development of a program called POEAS (Planetary Orbiter Error Analysis Study program) that was developed at JPL in the early 1970's independently of JPL's ODP. As far as we know, not a single line of code is common to the two programs [78].

Although, by necessity, both ODP and CHASMP use the same physical principles, planetary ephemeris, and timing and polar motion inputs, the algorithms are otherwise quite different. If there were an error in either program, they would not agree.

Aerospace analyzed a Pioneer 10 data arc that was initialized on 1 January 1987 at 16 hr (the data itself started on 3 January) and ended at 14 December 1994, 0 hr. The raw data set was averaged to 7560 data points of which 6534 points were used. This CHASMP analysis of Pioneer 10 data also showed an unmodeled acceleration in a direction along the radial toward the Sun [79]. The value is $(8.65 \pm 0.03) \times 10^{-8}$ cm/s^2, agreeing with JPL's result. The smaller error here is because the CHASMP analysis used a batch least-squares fit over the whole orbit [76, 77], not looking for a variation of the magnitude of a_P with distance.

Without using the apparent acceleration, CHASMP shows a steady frequency drift [38] of about -6×10^{-9} Hz/s, or 1.5 Hz over 8 years (one-way only). (See Figure 8.) This equates to a clock acceleration, $-a_t$, of -2.8×10^{-18} s/s^2. The identity with the apparent Pioneer acceleration is

$$a_t \equiv a_P/c. \qquad (16)$$

The drift in the Doppler residuals (observed minus computed data) is seen in Figure 9.

The drift is clear, definite, and cannot be removed without either the added acceleration, a_P, or the inclusion in the data itself of a frequency drift, i.e., a "clock acceleration" a_t. If there were a systematic drift in the atomic clocks of the DSN or in the time-reference standard signals, this would appear like a non-uniformity of time; i.e., all clocks would be changing with a constant acceleration. We now have been able to rule out this possibility. (See Section XI D.)

Continuing our search for an explanation, we considered the possibilities: i) that the Pioneer 10/11 spacecraft had internal systematic properties, undiscovered because they are of identical design, and ii) that the acceleration was due to some not-understood viscous drag force (proportional to the approximately constant velocity of the Pioneers). Both these possibilities could be investigated by studying spin-stabilized spacecraft whose spin axes are not directed towards the Sun, and whose orbital velocity vectors are far from being radially directed.

Two candidates were Galileo in its Earth-Jupiter mission phase and Ulysses in Jupiter-perihelion cruise out of the plane of the ecliptic. As well as Doppler, these
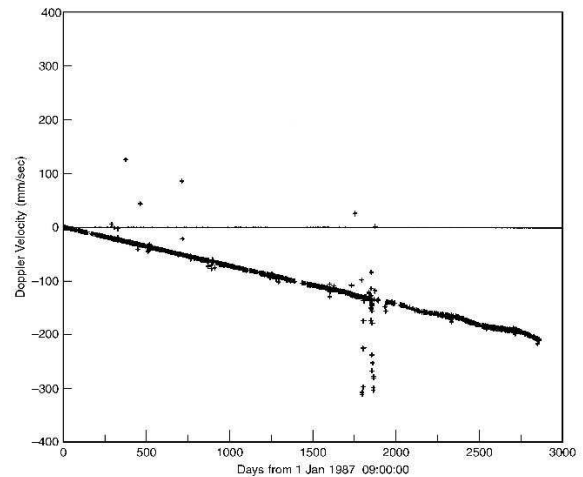
FIG. 8: CHASMP two-way Doppler residuals (observed Doppler velocity minus model Doppler velocity) for Pioneer 10 vs. time. 1 Hz is equal to 65 mm/s range change per second. The model is fully-relativistic. The solar system's gravitational field is represented by the Sun and its planetary systems [49].
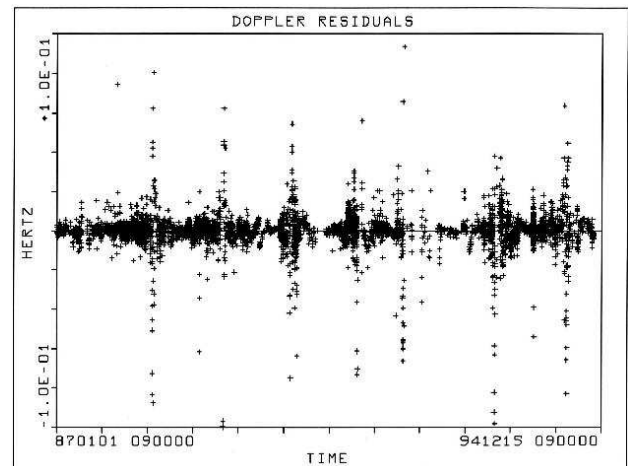
FIG. 9: CHASMP best fit for the Pioneer 10 Doppler residuals with the anomalous acceleration taken out. After adding one more parameter to the model (a constant radial acceleration) the residuals are distributed about zero Doppler velocity with a systematic variation ~ 3.0 mm/s on a time scale of ~ 3 months. The outliers on the plot were rejected from the fit. [The quality of the fit may be determined by the ratio of residuals to the downlink carrier frequency, $\nu_0 \approx 2.29$ GHz.]

spacecraft also yielded a considerable quantity of range data. By having range data one can tell if a spacecraft is accumulating a range effect due to a spacecraft acceleration or if the orbit determination process is fooled by a Doppler frequency rate bias.

C. Galileo measurement analysis

We considered the dynamical behavior of Galileo's trajectory during its cruise flight from second Earth encounter (on 8 December 1992) to arrival at Jupiter. [This period ends just before the Galileo probe release on 13 July 1995. The probe reached Jupiter on 7 December 1995.] During this time the spacecraft traversed a distance of about 5 AU with an approximately constant velocity of 7.19(4) km/s.

A quick JPL look at limited Galileo data (241 days from 8 January 1994 to 6 September 1994) demonstrated that it was impossible to separate solar radiation effects from an anomalous constant acceleration. The Sun was simply too close and the radiation cross-section too large. The nominal value obtained was $\sim 8 \times 10^{-8}$ cm/s^2.

The Aerospace's analysis of the Galileo data covered the same arc as JPL and a second arc from 2 December 1992 to 24 March 1993. The analysis of Doppler data from the first arc resulted in a determination for a_P of $\sim (8 \pm 3) \times 10^{-8}$ cm/s^2, a value similar to that from Pioneer 10. But the correlation with solar pressure was so high (0.99) that it is impossible to decide whether solar pressure is a contributing factor [80].

The second data arc was 113 days long, starting six days prior to the second Earth encounter. This solution was also too highly correlated with solar pressure, and the data analysis was complicated by many mid-course maneuvers in the orbit. The uncertainties in the maneuvers were so great, a standard null result could not be ruled out.

However, there was an additional result from the data of this second arc. This arc was chosen for study because of the availability of ranging data. It had 11596 Doppler points of which 10111 were used and 5643 range points of which 4863 used. The two-way range change and time integrated Doppler are consistent (see Figure 10) to $\sim$ 4 m over a time interval of one day. For comparison, note that for a time of $t = 1$ day, $(a_P t^2/2) \sim 3$ m. For the apparent acceleration to be the result of hardware problems at the tracking stations, one would need a linear frequency drift at all the DSN stations, a drift that is not observed.

D. Ulysses measurement analysis

1. JPL's analysis

An analysis of the radiation pressure on Ulysses, in its out-of-the-ecliptic journey from 5.4 AU near Jupiter in February 1992 to the perihelion at 1.3 AU in February 1995, found a varying profile with distance [81]. The orbit solution requires a periodic updating of the solar radiation pressure. The radio Doppler and ranging data can be fit to the noise level with a time-varying solar constant in the fitting model [82]. We obtained values for the time-varying solar constant determined by Ulysses
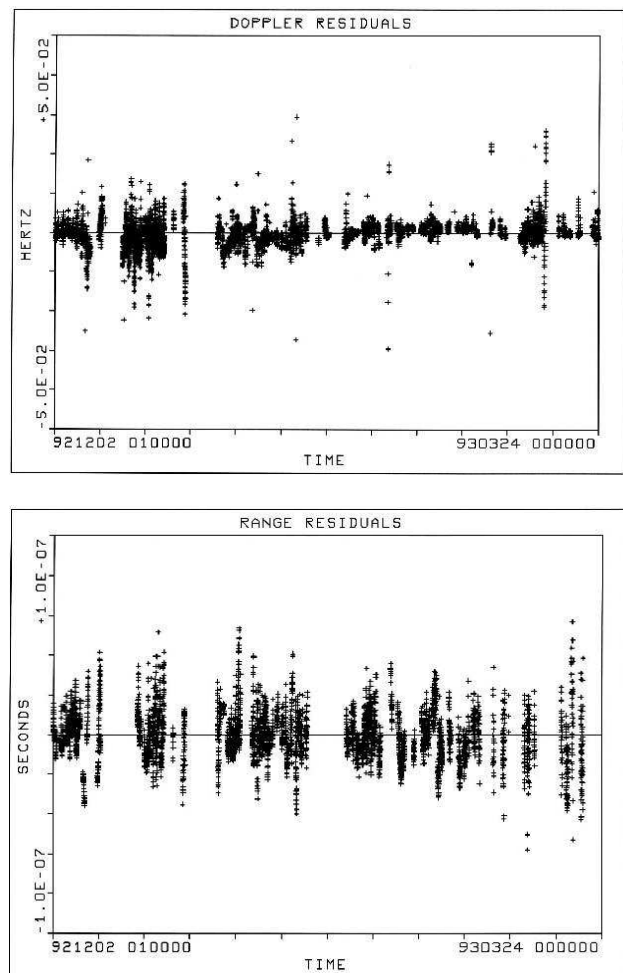
FIG. 10: Galileo best fit Doppler and range residuals using CHASMP.

navigational data during this south polar pass [81]. The inferred solar constant is about 40 percent larger at perihelion (1.3 AU) than at Jupiter (5.2 AU), a physical impossibility!

We sought an alternative explanation. Using physical parameters of the Ulysses spacecraft, we first converted the time-varying values of the solar constant to a positive (i.e., outward) radial spacecraft acceleration, a_r, as a function of heliocentric radius. Then we fit the values of a_r with the following model:

$$a_r = \frac{\mathcal{K} f_\odot A}{cM} \frac{\cos \theta(r)}{r^2} - a_{P(U)}, \qquad (17)$$

where r is the heliocentric distance in AU, M is the total mass of the spacecraft, $f_\odot = 1367$ W/m^2(AU)^2 is the (effective-temperature Stefan-Boltzmann) "solar radiation constant" at 1 AU, A is the cross-sectional area of the spacecraft and $\theta(r)$ is the angle between the direction to the Sun at distance r and orientation of the antennae. [For the period analyzed $\theta(r)$ was almost a constant. Therefore its average value was used which corresponded to $\langle \cos \theta(r) \rangle \approx 0.82$.] Optical parameters

defining the reflectivity and emissivity of the spacecraft's surface were taken to yield $\mathcal{K} \approx 1.8$. (See Section VII A for a discussion on solar radiation pressure.) Finally, the parameter $a_{P(U)}$ was determined by linear least squares. The best–fit value was obtained

$$a_{P(U)} = (12 \pm 3) \times 10^{-8} \text{ cm/s}^2, \qquad (18)$$

where both random and systematic errors are included.

So, by interpreting this time variation as a true r^{-2} solar pressure plus a constant radial acceleration, we found that Ulysses was subjected to an unmodeled acceleration towards the Sun of $(12 \pm 3) \times 10^{-8}$ cm/s^2.

Note, however, that the determined constant $a_{P(U)}$ is highly correlated with solar radiation pressure (0.888). This shows that the constant acceleration and the solar-radiation acceleration are not independently determined, even over a heliocentric distance variation from 5.4 to 1.3 AU.

2. Aerospace's analysis

The next step was to perform a detailed calculation of the Ulysses orbit from near Jupiter encounter to Sun perihelion, using CHASMP to evaluate Doppler and ranging data. The data from 30 March 1992 to 11 August 1994 was processed. It consisted of 50213 Doppler points of which 46514 were used and 9851 range points of which 8465 were used.

Such a calculation would in principle allow a more precise and believable differentiation between an anomalous constant acceleration towards the Sun and systematics. Solar radiation pressure and radiant heat systematics are both larger on Ulysses than on the Pioneers.

However, this calculation turned out to be a much more difficult than imagined. Because of a failed nutation damper, an inordinate number of spacecraft maneuvers were required (257). Even so, the analysis was completed. But even though the Doppler and range residuals were consistent as for Galileo, the results were disheartening. For an unexpected reason, any fit is not significant. The anomaly is dominated by (what appear to be) gas leaks [83]. That is, after each maneuver the measured anomaly changes. The measured anomalies randomly change sign and magnitude. The values go up to about an order of magnitude larger than a_P. So, although the Ulysses data was useful for range/Doppler checks to test models (see Section XI D), like Galileo it could not provide a good number to compare to a_P.

VI. RECENT RESULTS

Recent changes to our strategies and orbit determination programs, leading to new results, are threefold. First, we have added a longer data arc for Pioneer 10, extending the data studied up to July 1998. The entire data set used (3 Jan. 1987 to 22 July 1998) covers a heliocentric distance interval from 40 AU to 70.5 AU [84]. [Pioneer 11 was much closer in (22.42 to 31.7 AU) than Pioneer 10 during its data interval (5 January 1987 to 1 October 1990).] For later use in discussing systematics, we here note that in the ODP calculations, masses used for the Pioneers were $M_{Pio\ 10} = 251.883$ kg and $M_{Pio\ 11} = 239.73$ kg. CHASMP used 251.883 kg for both [16]. As the majority of our results are from Pioneer 10, we will make $M_0 = 251.883$ kg to be our nominal working mass.

Second, and as we discuss in the next subsection, we have studied the spin histories of the craft. In particular, the Pioneer 10 history exhibited a very large anomaly in the period 1990.5 to 1992.5. This led us to take a closer look at any possible variation of a_P among the three time intervals: The JPL analysis defined the intervals as I (3 Jan. 1987 to 17 July 1990); II (17 July 1990 to 12 July 1992) bounded by 49.5 to 54.8 AU; and III (12 July 1992 to 22 July 1998). (CHASMP used slightly different intervals [85]) The total updated data set now consists of 20,055 data points for Pioneer 10. (10,616 data points were used for Pioneer 11.) This helped us to better understand the systematic due to gas leaks, which is taken up in Section VIII F.

Third, in looking at the detailed measurements of a_P as a function of time using ODP, we found an anomalous oscillatory annual term, smaller in size than the anomalous acceleration [13]. As mentioned in Section IV G, and as will be discussed in detail in Section IX C, we wanted to make sure this annual term was not an artifact of our computational method. For the latest results, JPL used both the batch-sequential and the least-squares methods.

All our recent results obtained with both the JPL and The Aerospace Corporation software have given us a better understanding of systematic error sources. At the same time they have increased our confidence in the determination of the anomalous acceleration. We present a description and summary of the new results in the rest of this section.

A. Analysis of the Pioneer spin history

Both Pioneers 10 and 11 were spinning down during the respective data intervals that determined their a_P values. Because any changes in spacecraft spin must be associated with spacecraft torques (which for lack of a plausible external mechanism we assume are internally generated), there is also a possibility of a related internally generated translational force along the spin axis. Therefore, it is important to understand the effects of the spin anomalies on the anomalous acceleration. In Figures 11 and 12 we show the spin histories of the two craft during the periods of analysis.

Consider Pioneer 10 in detail. In time Interval I there is a slow spin down at an average rate (slope) of $\sim (-0.0181 \pm 0.0001)$ rpm/yr. Indeed, a closer look at the
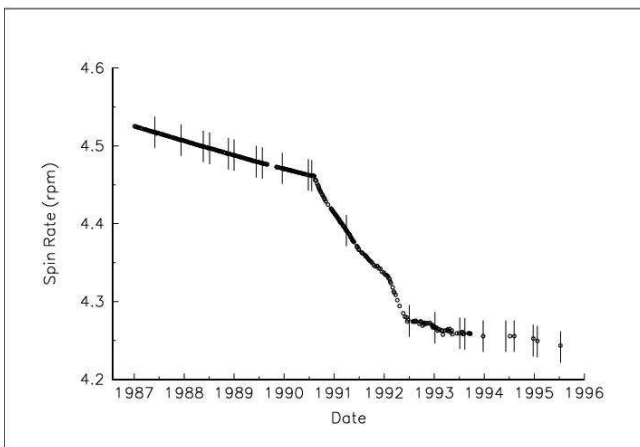
FIG. 11: The spin history of Pioneer 10. The vertical lines indicate the times when precession maneuvers were made. How this spin data was obtained is described in Section III E. The final data points were obtained at the times of maneuvers, the last being in 1995.
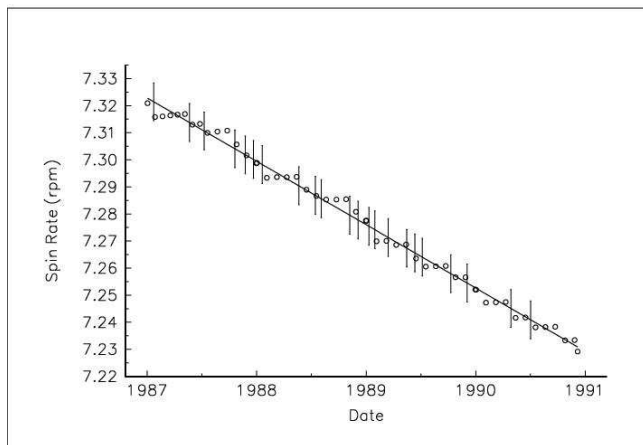

FIG. 12: The spin history of Pioneer 11 over the period of analysis. The vertical lines indicate the times when precession maneuvers were made. This spin calibration was done by the DSN until 17 July 1990. At that time the DSN ceased doing spin calibrations. From 1990 until the loss of coherent Doppler, orbit analysts made estimates of the spin rate.

curve (either by eye or from an expanded graph) shows that the spin down is actually slowing with time (the curve is flattening). This last feature will be discussed in Sections VIII B and VIII D.

Every time thrusters are used, there tends to be a short-term leakage of gas until the valves set (perhaps a few days later). But there can also be long-term leakages due to some mechanism which does not quickly correct itself. The major Pioneer 10 spin anomaly that marks the boundary of Intervals I and II, is a case in point. During this interval there was a major factor of ~ 4.5 increase in the average spin-rate change to $\sim (-0.0861 \pm 0.0009)$ rpm/yr. One also notices kinks during the interval.

Few values of the Pioneer 10 spin rate were obtained

after mid-1993, so the long-term spin-rate change is not well-determined in Interval III. But from what was measured, there was first a short-term transition region of about a year where the spin-rate change was ~ -0.0160 rpm/yr. Then things settled down to a spin-rate change of about $\sim (-0.0073 \pm 0.0015)$ rpm/yr, which is small and less than that of interval I.

The effects of the maneuvers on the values of a_P will allow an estimation of the gas leak systematic in Section VIII F. Note, however, that in the time periods studied, only orientation maneuvers were made, not trajectory maneuvers.

Shortly after Pioneer 11 was launched on 5 April 1973, the spin period was 4.845 s. A spin precession maneuver on 18 May 1973 reduced the period to 4.78 s and afterwards, because of a series of precession maneuvers, the period lengthened until it reached 5.045 s at encounter with Jupiter in December 1974. The period was fairly constant until 18 December 1976, when a mid-course maneuver placed the spacecraft on a Saturn-encounter trajectory. Before the maneuver the period was 5.455 s, while after the maneuver it was 7.658 s. At Saturn encounter in December 1979 the period was 7.644 s, little changed over the three-year post maneuver cruise phase. At the start of our data interval on 5 January 1987, the period was 7.321 s, while at the end of the data interval in October 1990 it was 7.238 s.

Although the linear fit to the Pioneer 11 spin rate shown in Figure 12 is similar to that for Pioneer 10 in Interval I, $\sim (-0.0234 \pm 0.0003)$ rpm/yr, the causes appear to be very different. (Remember, although identical in design, Pioneers 10 and 11 were not identical in quality [14].) Unlike Pioneer 10, the spin period for Pioneer 11 was primarily affected at the time of spin precession maneuvers. One sees that at maneuvers the spin period decreases very quickly, while in between maneuvers the spin rate actually tends to *increase* at a rate of $\sim (+0.0073 \pm 0.0003)$ rpm/yr (perhaps due to a gas leak in the opposite direction).

All the above observations aid us in the interpretation of systematics in the following three sections.

B. Recent results using JPL software

The latest results from JPL are based on an upgrade, *Sigma*, to JPL's ODP software [86]. *Sigma*, developed for NASA's Cassini Mission to Saturn, eliminates structural restrictions on memory and architecture that were imposed 30 years ago when JPL space navigation depended solely on a Univac 1108 mainframe computer. Five ODP programs and their interconnecting files have been replaced by the single program *Sigma* to support filtering, smoothing, and mapping functions.

We used *Sigma* to reduce the Pioneer 10 (in three time intervals) and 11 Doppler of the unmodeled acceleration, a_P, along the spacecraft spin axis. As mentioned, the Pioneer 10 data interval was extended to cover the to-

TABLE I: Determinations of a_P in units of 10^{-8} cm/s^2 from the three time intervals of Pioneer 10 data and from Pioneer 11. As described in the text, results from various ODP/$Sigma$ and CHASMP calculations are listed. For ODP/$Sigma$, "WLS" signifies a weighted least-squares calculation, which was used with i) no solar corona model and ii) the 'Cassini' solar corona model. Also for ODP/$Sigma$, "BSF" signifies a batch-sequential filter calculation, which was done with iii) the 'Cassini' solar corona model. Further (see Section IX C), a 1-day batch-sequential estimation for the entire data interval of 11.5 years for Pioneer 10 yielded a result $a_P = (7.77 \pm 0.16) \times 10^{-8}$ cm/s^2. The CHASMP calculations were all WLS. These calculations were done with i) no solar corona model, ii) the 'Cassini' solar corona model, iii) the 'Cassini' solar corona model with corona data weighting and F10.7 time variation calibration. Note that the errors given are only formal calculational errors. The much larger deviations of the results from each other indicate the sizes of the systematics that are involved.

Program/Estimation method	Pio 10 (I)	Pio 10 (II)	Pio 10 (III)	Pio 11
$Sigma$, WLS, no solar corona model	8.02 ± 0.01	8.65 ± 0.01	7.83 ± 0.01	8.46 ± 0.04
$Sigma$, WLS, with solar corona model	8.00 ± 0.01	8.66 ± 0.01	7.84 ± 0.01	8.44 ± 0.04
$Sigma$, BSF, 1-day batch, with solar corona model	7.82 ± 0.29	8.16 ± 0.40	7.59 ± 0.22	8.49 ± 0.33
CHASMP, WLS, no solar corona model	8.25 ± 0.02	8.86 ± 0.02	7.85 ± 0.01	8.71 ± 0.03
CHASMP, WLS, with solar corona model	8.22 ± 0.02	8.89 ± 0.02	7.92 ± 0.01	8.69 ± 0.03
CHASMP, WLS, with corona, weighting, and F10.7	8.25 ± 0.03	8.90 ± 0.03	7.91 ± 0.01	8.91 ± 0.04

tal time interval 3 January 1987 to 22 July 1998. Of the total data set of 20,055 Pioneer 10 Doppler points, JPL used ∼19,403, depending on the initial conditions and editing for a particular run. Of the available 10,616 (mainly shorter time-averaged) Pioneer 11 data points, 10,252 were used (4919 two-way and 5333 three-way).

We wanted to produce independent (i.e., uncorrelated) solutions for a_P in the three Pioneer 10 segments of data. The word independent solution in our approach means only the fact that data from any of the three segments must not have any information (in any form) passed onto it from the other two intervals while estimating the anomaly. We moved the epoch from the beginning of one data interval to the next by numerically integrating the equations of motion and not iterating on the data to obtain a better initial conditions for this consequent segment. Note that this numerical iteration provided us only with an *a priori* estimate for the initial conditions for the data interval in question.

Other parameters included in the fitting model were the six spacecraft heliocentric position and velocity coordinates at the 1987 epoch of 1 January 1987, 01:00:00 ET, and 84 (i.e., 28×3) instantaneous velocity increments along the three spacecraft axes for 28 spacecraft attitude (or spin orientation) maneuvers. If these orientation maneuvers had been performed at exactly six month intervals, there would have been 23 maneuvers over our 11.5 year data interval. But in fact, five more maneuvers were performed than expected over this 11.5 year interval giving a total of 28 maneuvers in all.

As noted previously, in fitting the Pioneer 10 data over 11.5 years we used the standard space-fixed J2000 coordinate system with planetary ephemeris DE405, referenced to ICRF. The three-dimensional locations of the tracking stations in the Earth's body-fixed coordinate system (geocentric radius, latitude, longitude) were taken from a set recommended by ICRF for JPL's DE405. The time-varying Earth orientation in J2000 coordinates was defined by a 1998 version of JPL's EOP file. This accounted for the geophysical motion of the Earth's pole with respect to its spin axis and the Earth's time varying spin rate.

JPL used both the weighted least-squares (WLS) and the batch-sequential filter (BSF) algorithms for the final calculations. In the first three rows of Table I are shown the ODP results for i) WLS with no corona, ii) WLS with the Cassini corona model, and iii) BSF with the Cassini corona model.

Observe that the WLS acceleration values for Pioneer 10 in Intervals I, II, and III are larger or smaller, respectively, just as the spin-rate changes in these intervals are larger or smaller, respectively. This indicates that the small deviations may be due to a correlation with the large gas leak/spin anomaly. We will argue this quantitatively in Section VIII F. For now we just note that we therefore expect the number from Interval III, $a_P = 7.83 \times 10^{-8}$cm/s^2, to be close to our basic (least perturbed) JPL result for Pioneer 10. We also note that the statistical errors and the effect of the solar corona are both small for WLS, and will be handled in our error budget.

In Figure 13 we show ODP/$Sigma$ WLS Doppler residuals for the entire Pioneer 10 data set. The residuals were obtained by first solving for a_P with no corona in each of the three Now look at the batch-sequential results in row 3 of Table I. First, note that the statistical Intervals in-

dependently and then subtracting these solutions (given in Table I) from the fits within the corresponding data intervals.
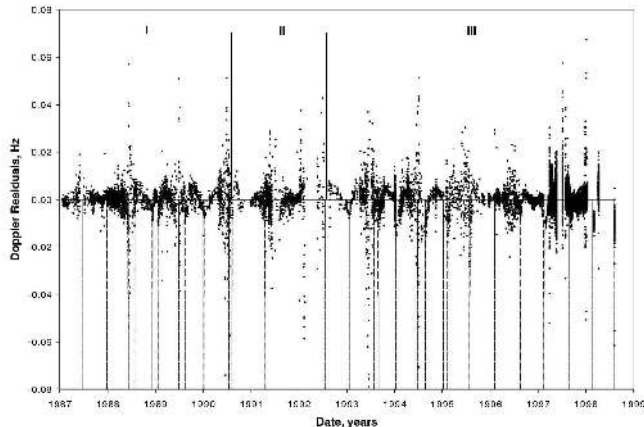

FIG. 13: ODP Doppler residuals in Hz for the entire Pioneer 10 data span. The two solid vertical lines in the upper part of the plot indicate the boundaries between data Intervals I/II and II/III, respectively. Maneuver times are indicated by the vertical dashed lines in the lower part of the plot.

One can easily see the very close agreement with the CHASMP residuals of Figure 9, which go up to 14 December 1994.

The Pioneer 11 number is significantly higher. A deviation is not totally unexpected since the data was relatively noisy, was from much closer in to the Sun, and was taken during a period of high solar activity. We also do not have the same handle on spin-rate change effects as we did for Pioneer 10. We must simply take the number for what it is, and give the basic JPL result for Pioneer 11 as $a_P = 8.46 \times 10^{-8}$ cm/s^2.

Now look at the batch-sequential results in row 3 of Table I. First, note that the statistical errors are an order of magnitude larger than for WLS. This is not surprising since: i) the process noise significantly affects the precision, ii) BSF smoothes the data and the data from the various intervals is more correlated than in WLS. The effects of all this are that all four numbers change so as to make them all closer to each other, but yet all the numbers vary by less than 2σ from their WLS counterparts.

Finally, there is the annual term. It remains in the data (for both Pioneers 10 and 11). A representation of it can be seen in a 1-day batch-sequential averaged over all 11.5 years. It yielded a result $a_P = (7.77\pm0.16)\times10^{-8}$ cm/s^2, consistent with the other numbers/errors, but with an added annual oscillation. In the following subsection we will compare JPL results showing the annual term with the counterpart Aerospace results.

We will argue in Section IX C that this annual term is due to the inability to model the angles of the Pioneers' orbits accurately enough. [Note that this annual term is not to be confused with a small oscillation seen in Figure 8 that can be caused by mispointing towards the spacecraft by the fit programs.]

C. Recent results using The Aerospace Corporation software

As part of an ongoing upgrade to CHASMP's accuracy, Aerospace has used Pioneer 10 and 11 as a test bed to confirm the revision's improvement. In accordance with the JPL results of Section VI B, we used the new version of CHASMP to concentrate on the Pioneer 10 and 11 data. The physical models are basically the same ones that JPL used, but the techniques and methods used are largely different. (See Section IX B.)

The new results from the Aerospace Corporation's software are based on first improving the Planetary Ephemeris and Earth orientation and spacecraft spin models required by the program. That is: i) the spin data file has been included with full detail; ii) a newer JPL Earth Orientation Parameters file was used; iii) all IERS tidal terms were included; iv) plate tectonics were included; v) DE405 was used; vi) no *a priori* information on the solved for parameters was included in the fit; vii) Pioneer 11 was considered, viii) the Pioneer 10 data set used was extended to 14 Feb. 1998. Then the Doppler data was refitted.

Beginning with this last point: CHASMP uses the same original data file, but it performs an additional data compression. This compression combines the longest contiguous data composed of adjacent data intervals or data spans with duration ≥ 600 s (effectively it prefers 600 and 1980 second data intervals). It ignores short-time data points. Also, Aerospace uses an N-σ/fixed boundary rejection criteria that rejects all data in the fit with a residual greater than ±0.025 Hz. These rejection criteria resulted in the loss of about 10 % of the original data for both Pioneers 10 and 11. In particular, the last five months of Pioneer 10 data, which was all of data-lengths less than 600 s, was ignored. Once these data compression/cuts were made, CHASMP used 10,499 of its 11,610 data points for Pioneer 10 and 4,380 of its 5,137 data points for Pioneer 11.

Because of the spin-anomaly in the Pioneer 10 data, the data arc was also divided into three time intervals (although the I/II boundary was taken as 31 August 1990 [85]). In what was especially useful, the Aerospace analysis uses direct propagation of the trajectory data and solves for the parameter of interest only for the data within a particular data interval. That means the three interval results were truly independent. Pioneer 11 was fit as a single arc.

Three types of runs are listed, with: i) no corona; ii) with Cassini corona model of Sections IV D and VII C; and iii) with the Cassini corona model, but added are corona data weighting (Section IV D) and the time-variation called "F10.7" [65]. (The number 10.7 labels the wavelength of solar radiation, λ=10.7 cm, that, in our analysis, is averaged over 81 days.)

The results are given in rows 4-6 of Table I. The no corona results (row 4) are in good agreement with the *Sigma* results of the first row. This is especially true

for the extended-time Interval III values for Pioneer 10, which interval had clean data. However there is more disagreement with the values for Pioneer 10 in Intervals I and II and for Pioneer 11. These three data sets all were noisy and underwent more data-editing. Therefore, it is significant that the deviations between *Sigma* and CHASMP in these arcs are all similar, but small, between 0.20 to 0.25 of our units. As before, the effect of the solar corona is small, even with the various model variations. But most important, the numbers from *Sigma* and CHASMP for Pioneer 10 Interval III are in excellent agreement.

Further, CHASMP also found the annual term. (Recall that CHASMP can also look for a temporal variation by calculating short time averages.) Results on the time variation in a_P can be seen in Figure 14. Although there could possibly be a_P variations of $\pm 2 \times 10^{-8}$ cm/s^2 on a 200-day time scale, a comparison of the variations with the error limits shown in Figure 14 indicate that our measurements of these variations are not statistically significant. The 5-day averages of a_P from ODP (using the batch-sequential method) are not reliable at solar conjunction in the middle (June) of each year, and hence should be ignored there. The CHASMP 200-day averages suppress the solar conjunction bias inherent in the ODP 5-day averages, and they reliably indicate a constant value of a_P. Most encouraging, these results clearly indicate that the obtained solution is consistent, stable, and its mean value does not strongly depend on the estimation procedure used. The presence of the small annual term on top of the obtained solution is apparent.

D. Our solution, before systematics, for the anomalous acceleration

From Table I we can intuitively draw a number of conclusions:

A) The effect of the corona is small. This systematic will be analyzed in Section VII B.

B) The numerical error is small. This systematic will be analyzed in Section IX A.

C) The differences between the *Sigma* and CHASMP Pioneer 10 results for Interval I and Interval II, respectively, we attribute to two main causes: especially i) the different data rejection techniques of the two analyses but also ii) the different maneuver simulations. Both of these effects were especially significant in Interval II, where the data arc was small and a large amount of noisy data was present. Also, to account for the discontinuity in the spin data that occurred on 28 January 1992 (see Figure 11), Aerospace introduced a fictitious maneuver for this interval. Even so, the deviation in the two values of a_P was relatively small, namely 0.23 and 0.21, respectively, $\times 10^{-8}$ cm/s^2.

D) The changes in a_P in the different Intervals, correlated with the changes in spin-rate change, are likely (at least partially) due to gas leakage. This will be discussed
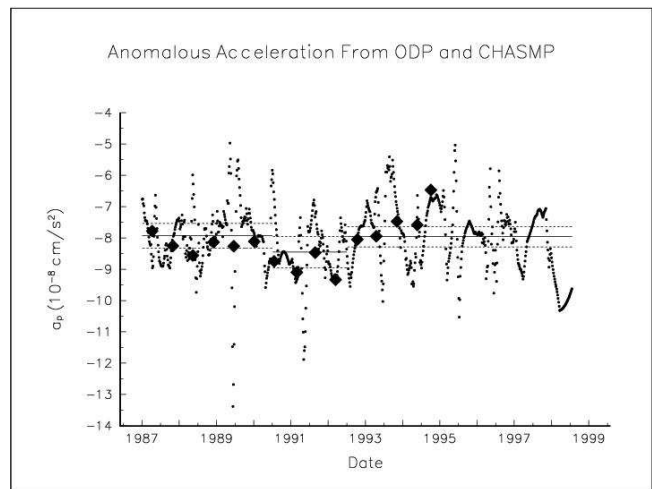
FIG. 14: Consistency of the ODP/*Sigma* and CHASMP time-variation signals. The dots show 5-day sample averages of the anomalous acceleration of Pioneer 10 from ODP/*Sigma* using `BSF` with a 200-day correlation time. From this data, the solid lines show the mean values of a_P in the three intervals corresponding to the three separate spin down histories. The dashed lines represent the large batch-sequential computational error bounds on the three values of a_P. The 200-day acceleration values using CHASMP are the solid squares. At the time positions where there are CHASMP results, the agreement between the CHASMP and the ODP/*Sigma* results is clear.

in Section VIII F.

But independent of the origin, this last correlation between shifts in a_P and changes in spin rate actually allows us to calculate the best "experimental" base number for Pioneer 10. To do this, assume that the spin-rate change is directly contributing to an anomalous acceleration offset. Mathematically, this is saying that in any interval $i = $ I, II, III, for which the spin-rate change is an approximate constant, one has

$$a_P(\ddot{\theta}) = a_{P(0)} - \kappa\, \ddot{\theta}, \tag{19}$$

where κ is a constant with units of length and $a_{P(0)} \equiv a_P(\ddot{\theta} = 0)$ is the Pioneer acceleration without any spin-rate change.

One now can fit the data to Eq. (19) to obtain solutions for κ and $a_{P(0)}$. The three intervals $i = $ I, II, III provide three data combinations $\{a_{P(i)}(\ddot{\theta}), \ddot{\theta}_i\}$. We take our base number, with which to reference systematics, to be the weighted average of the *Sigma* and CHASMP results for $a_{P(0)}$ when no corona model was used. Start first with the *Sigma* Pioneer 10 solutions in row one of Table I and the Pioneer 10 spin-down rates given in Section VI B and Figure 11: $a_{P(i)}^{\texttt{Sigma}} = (8.02 \pm 0.01,\ 8.65 \pm 0.01,\ 7.83 \pm 0.01)$ in units of 10^{-8} cm/s^2 and $\ddot{\theta}_i = -(0.0181 \pm 0.0001,\ 0.0861 \pm 0.0009,\ 0.0073 \pm 0.0015)$ in units of rpm/yr, where

$$\begin{aligned} 1 \text{ rpm/year} &= 5.281 \times 10^{-10} \text{ rev/s}^2 \\ &= 3.318 \times 10^{-9} \text{ radians/s}^2. \end{aligned} \tag{20}$$

With these data we use the maximum likelihood and minimum variance approach to find the optimally weighted least-squares solution for $a_{P(0)}$:

$$a_{P(0)}^{\texttt{Sigma}} = (7.82 \pm 0.01) \times 10^{-8} \text{ cm/s}^2, \qquad (21)$$

with solution for the parameter κ obtained as $\kappa^{\texttt{Sigma}} = (29.2 \pm 0.7)$ cm. Similarly, for CHASMP one takes the values for a_P from row four of Table I: $a_{P(i)}^{\texttt{CHASMP}} = (8.25 \pm 0.02,\ 8.86 \pm 0.02,\ 7.85 \pm 0.01)$ and uses them with the same $\ddot{\theta}_i$ as above. The solution for $a_{P(0)}$ in this case is

$$a_{P(0)}^{\texttt{CHASMP}} = (7.89 \pm 0.02) \times 10^{-8} \text{ cm/s}^2, \qquad (22)$$

together with $\kappa^{\texttt{CHASMP}} = (34.7 \pm 1.1)$ cm. The solutions for *Sigma* and CHASMP are similar, 7.82 and 7.89 in our units. We take the weighted average of these two to yield our base line "experimental" number for a_P:

$$a_{P(\texttt{exper})}^{\texttt{Pio10}} = (7.84 \pm 0.01) \times 10^{-8} \text{ cm/s}^2. \quad (23)$$

[The weighted average constant κ is $\kappa_0 = (30.7 \pm 0.6)$ cm.]

For Pioneer 11, we only have the one $3\frac{3}{4}$ year data arc. The weighted average of the two programs' no corona results is $(8.62 \pm 0.02) \times 10^{-8}$ cm/s^2. We observed in Section VI A that between maneuvers (which are accounted for - see Section IV E) there is actually a spin rate *increase* of $\sim (+0.0073 \pm 0.0003)$ rpm/yr. If one uses this spin-up rate and the Pioneer 10 value for $\kappa_0 = 30.7$ cm given above, one obtains a spin-rate change corrected value for a_P. We take this as the experimental value for Pioneer 11:

$$a_{P(\texttt{exper})}^{\texttt{Pio11}} = (8.55 \pm 0.02) \times 10^{-8} \text{ cm/s}^2. \qquad (24)$$

VII. SOURCES OF SYSTEMATIC ERROR EXTERNAL TO THE SPACECRAFT

We are concerned with possible systematic acceleration errors that could account for the unexplained anomalous acceleration directed toward the Sun. There exist detailed publications describing analytic recipes developed to account for non-gravitational accelerations acting on spacecraft. (For a summary see Milani et al. [57].) With regard to the specific Pioneer spacecraft, possible sources of systematic acceleration have been discussed before for Pioneer 10 and 11 at Jupiter [87] and Pioneer 11 at Saturn [67].

External forces can produce three vector components of spacecraft acceleration, unlike forces generated on board the spacecraft, where the two non-radial components (i.e., those that are effectively perpendicular to the spacecraft spin) are canceled out by spacecraft rotation. However, non-radial spacecraft accelerations are difficult to observe by the Doppler technique, which measures spacecraft velocity along the Earth-spacecraft line of sight. But with several years of Doppler data, it is in principle possible to detect systematic non-radial acceleration components [73].

With our present analysis [73] we find that the Doppler data yields only one significant component of unmodeled acceleration, and that any acceleration components perpendicular to the spin axis are small. This is because in the fitting we tried including three unmodeled acceleration constants along the three spacecraft axes (spin axis and two orthogonal axes perpendicular to the spin axis). The components perpendicular to the spin axis had values consistent with zero to a 1-σ accuracy of 2 $\times$ 10^{-8} cm/s^2 and the radial component was equal to the reported anomalous acceleration. Further, the radial acceleration was not correlated with the other two unmodeled acceleration components.

Although one could in principle set up complicated engineering models to predict all or each of the systematics, often the uncertainty of the models is too large to make them useful, despite the significant effort required. A different approach is to accept our ignorance about a non-gravitational acceleration and assess to what extent these can be assumed a constant bias over the time scale of all or part of the mission. (In fact, a constant acceleration produces a linear frequency drift that can be accounted for in the data analysis by a single unknown parameter.) In fact, we will use both approaches.

In most orbit determination programs some effects, like the solar radiation pressure, are included in the set of routinely estimated parameters. Nevertheless we want to demonstrate their influence on Pioneer's navigation from the general physics standpoint. This is not only to validate our results, but also to be a model as to how to study the influence of the other physical phenomena that are not yet included in the standard navigational packages for future more demanding missions. Such missions will involve either spacecraft that will be distant or spacecraft at shorter distances where high-precision spacecraft navigation will be required.

In this section we will discuss possible systematics (including forces) generated external to the spacecraft which might significantly affect our results. These start with true forces due to (1) solar-radiation pressure and (2) solar wind pressure. We go on to discuss (3) the effect of the solar corona and its mismodeling, (4) electro-magnetic Lorentz forces, (5) the influence of the Kuiper belt, (6) the phase stability of the reference atomic clocks, and (7) the mechanical and phase stability of the DSN antennae, together with influence of the station locations and troposphere and ionosphere contributions.

A. Direct solar radiation pressure and mass

There is an exchange of momentum when solar photons impact the spacecraft and are either absorbed or reflected. Models for this solar pressure effect were developed before either Pioneer 10 or 11 were launched [88]

and have been refined since then. The models take into account various parts of the spacecraft exposed to solar radiation, primarily the high-gain antenna. It computes an acceleration directed away from the Sun as a function of spacecraft orientation and solar distance.

The models for the acceleration due to solar radiation can be formulated as

$$a_{\mathsf{s.p.}}(r) = \frac{\mathcal{K} f_\odot A}{c\, M} \frac{\cos\theta(r)}{r^2}. \qquad (25)$$

$f_\odot = 1367$ W/m^2(AU)^2 is the (effective-temperature Stefan-Boltzmann) "solar radiation constant" at 1 AU from the Sun and A is the effective size of the craft as seen by the Sun [89]. (For Pioneer the area was taken to be the antenna dish of radius 1.73 m.) θ is the angle between the axis of the antenna and the direction of the Sun, c is the speed of light, M is the mass of the spacecraft (taken to be 251.883 for Pioneer 10), and r is the distance from the Sun to the spacecraft in AU. $\mathcal{K}$ [90] is the *effective* [91] absorption/reflection coefficient. For Pioneer 10 the simplest approximately correct model yields $\mathcal{K}_0 = 1.71$ [91]. Eq. (25) provides a good model for analysis of the effect of solar radiation pressure on the motion of distant spacecraft and is accounted for by most of the programs used for orbit determination.

However, in reality the absorptivities, emissivities, and effective areas of spacecraft parts parameters which, although modeled by design, are determined by calibration early in the mission [92]. One determines the magnitude of the solar-pressure acceleration at various orientations using Doppler data. (The solar pressure effect can be distinguished from gravity's $1/r^2$ law because $\cos\theta$ varies [45].) The complicated set of program input parameters that yield the parameters in Eq. (25) are then set for later use [92]. Such a determination of the parameters for Pioneer 10 was done, soon after launch and later. When applied to the solar radiation acceleration in the region of Jupiter, this yields (from a 5 % uncertainty in $a_{\mathsf{s.p.}}$ [87])

$$a_{\mathsf{s.p.}}(r = \mathsf{5.2AU}) = (70.0 \pm 3.5) \times 10^{-8} \text{ cm/s}^2,$$
$$\mathcal{K}_{\mathsf{5.2}} = 1.77. \qquad (26)$$

The second of Eqs. (26) comes from putting the first into Eq. (25). Note, specifically, that in a fit a too high input mass will be compensated for by a higher effective $\mathcal{K}$.

Because of the $1/r^2$ law, by the time the craft reached 10 AU the solar radiation acceleration was 18.9×10^{-8} cm/s^2 going down to 0.39 of those units by 70 AU. Since this systematic falls off as r^{-2}, it can bias the Doppler determination of a constant acceleration at some level, even though most of the systematic is correctly modeled by the program itself. By taking the average of the r^{-2} acceleration curves over the Pioneer distance intervals, we estimate that the systematic error from solar-radiation pressure in units of 10^{-8} cm/s^2 is 0.001 for Pioneer 10 over an interval from 40 to 70 AU, and 0.006 for Pioneer 11 over an interval from 22 to 32 AU.

However, this small uncertainty is not our main problem. In actuality, since the parameters were fit the mass has decreased with the consumption of propellant. Effectively, the $1/r^2$ systematic has changed its normalization with time. If not corrected for, the difference between the original $1/r^2$ and the corrected $1/r^2$ will be interpreted as a bias in a_P. Unfortunately, exact information on gas usage is unavailable [16]. Therefore, in dealing with the effect of the temporal mass variation during the entire data span (i.e. nominal input mass vs. actual mass history [15, 16]) we have to address two effects on the solutions for the anomalous acceleration a_P. They are i) the effect of mass variation from gas consumption and ii) the effect of an incorrect input mass [15, 16].

To resolve the issue of mass variation uncertainty we performed a sensitivity analysis of our solutions to different spacecraft input masses. We simply re-did the no-corona, WLS runs of Table I with a range of different masses. The initial wet weight of the package was 259 kg with about 36 kg of consumable propellant. For Pioneer 10, the input mass in the program fit was 251.883 kg, roughly corresponding to the mass after spin-down. By our data period, roughly half the fuel (18 kg) was gone so we take 241 kg as our nominal Pioneer 10 mass. Thus, the effect of going from 251.883 kg to 241 kg we take to be our bias correction for Pioneer 10. We take the uncertainty to be given by one half the effect of going from plus to minus 9 kg (plus or minus a quarter tank) from the nominal mass of 241 kg.

For the three intervals of Pioneer 10 data, using ODP/$Sigma$ yields the following changes in the accelerations:

$$\delta a_P^{\mathsf{mass}} = [(0.040 \pm 0.035),\ (0.029 \pm 0.025),$$
$$(0.020 \pm 0.017)] \times 10^{-8} \text{ cm/s}^2.$$

As expected, these results make a_P larger. For our systematic bias we take the weighted average of $\delta a_P^{\mathsf{mass}}$ for the three intervals of Pioneer 10. The end result is

$$a_{\mathsf{s.p.}} = (0.03 \pm 0.01) \times 10^{-8} \text{ cm/s}^2. \qquad (27)$$

For Pioneer 11 we did the same except our bias point was 3/4 of the fuel gone (232 kg). Therefore the bias results by going from the input mass of 239.73 to 232 kg. The uncertainty is again defined by $\pm$ 9 kg. The result for Pioneer 11 is more sensitive to mass changes, and we find using ODP/$Sigma$

$$a_{\mathsf{s.p.}} = (0.09 \pm 0.21) \times 10^{-8} \text{ cm/s}^2. \qquad (28)$$

The bias number is three times larger than the similar number for Pioneer 10, and the uncertainty much larger. We return to this difference in Section VIII G.

The previous analysis also allowed us to perform consistency checks on the effective values of $\mathcal{K}$ which the programs were using. By taking $[r_{\min} r_{\max}]^{-1} = [\int (dr/r^2)/\int dr]$ for the inverse distance squared of a data set, varying the masses, and determining the shifts in a_P

we could determine the values of $\mathcal{K}$ implied, We found: $\mathcal{K}^{\texttt{ODP}}_{\texttt{Pio}-10(\texttt{I})} \approx 1.72$; $\mathcal{K}^{\texttt{ODP}}_{\texttt{Pio}-11} \approx 1.82$; $\mathcal{K}^{\texttt{CHASMP}}_{\texttt{Pio}-10(\texttt{I})} \approx 1.74$; and $\hat{\mathcal{K}}^{\texttt{CHASMP}}_{\texttt{Pio}-11)} \approx 1.84$. [The hat over the last $\mathcal{K}$ indicates it was multiplied by (237.73/251.883) because CHASMP uses 259.883 kg instead of 239.73 kg for the input mass.] All these values of $\mathcal{K}$ are in the region expected and are clustered around the value $\mathcal{K}_{5.2}$ in Eq. (26).

Finally, if you take the average values of $\mathcal{K}$ for Pioneers 10 and 11 (1.73, 1.83), multiply these numbers by the input masses (251.883, 239.73) kg, and divide them by our nominal masses (241, 232) kg, you obtain (1.87, 1.89), indicating our choice of nominal masses was well motivated.

B. The solar wind

The acceleration caused by the solar wind has the same form as Eq. (25), with $f_\odot$ replaced by $m_p v^3 n$, where $n \approx 5$ cm^{-3} is the proton density at 1 AU and $v \approx 400$ km/s is the speed of the wind. Thus,

$$
\begin{aligned}
\sigma_{\text{s.w.}}(r) &= \mathcal{K}_{\text{s.w.}} \frac{m_p v^3\, n\, A\cos\theta}{cM\, r^2}\\
&\approx 1.24 \times 10^{-13} \left(\frac{20 \text{ AU}}{r}\right)^2 \text{ cm/s}^2. \quad (29)
\end{aligned}
$$

Because the density can change by as much as 100%, the exact acceleration is unpredictable. But there are measurements [89] showing that it is about 10^{-5} times smaller than the direct solar radiation pressure. Even if we make the very conservative assumption that the solar wind contributes only 100 times less force than the solar radiation, its smaller contribution is completely negligible.

C. The effects of the solar corona and models of it

As we saw in the previous Section VII B, the effect of the solar wind pressure is negligible for distant spacecraft motion in the solar system. However, the solar corona effect on propagation of radio waves between the Earth and the spacecraft needs to be analyzed in more detail.

Initially, to study the sensitivity of a_P to the solar corona model, we were also solving for the solar corona parameters A, B, and C of Eq. (9) in addition to a_P. However, we realized that the Pioneer Doppler data is not precise enough to produce credible results for these physical parameters. In particular, we found that solutions could yield a value of a_P which was changed by of order 10 % even though it gave unphysical values of the parameters (especially B, which previously had been poorly defined even by the Ulysses mission [62]). [By "unphysical" we mean electron densities that were either negative or positive with values that are vastly different from what would be expected.]

Therefore, as noted in Section IV D, we decided to use the newly obtained values for A, B, and C from the Cassini mission and use them as inputs for our analyses: $A = 6.0 \times 10^3, B = 2.0 \times 10^4, C = 0.6 \times 10^6$, all in meters [64]. This is the "Cassini corona model."

The effect of the solar corona is expected to be small for Doppler and large for range. Indeed it is small for $Sigma$. For ODP/$Sigma$, the time-averaged effect of the corona was small, of order

$$
\sigma_{\texttt{corona}} = \pm 0.02 \times 10^{-8} \text{ cm/s}^2, \quad (30)
$$

as might be expected. We take this number to be the error due to the corona.

What about the results from CHASMP. Both analyses use the same physical model for the effect of the steady-state solar corona on radio-wave propagation through the solar plasma (that is given by Eq. (10)). However, there is a slight difference in the actual implementation of the model in the two codes.

ODP calculates the corona effect only when the Sun-spacecraft separation angle as seen from the Earth (or Sun-Earth-spacecraft angle) is less then $\pi/2$. It sets the corona contribution to zero in all other cases. Earlier CHASMP used the same model and got a small corona effect. Presently CHASMP calculates an approximate corona contribution for all the trajectory. Specific attention is given to the region when the spacecraft is at opposition from the Sun and the Sun-Earth-spacecraft angle $\sim \pi$. There CHASMP's implementation truncates the code approximation to the scaling factor F in Eq. (10). This is specifically done to remove the fictitious divergence in the region where "impact parameter" is small, $\rho \to 0$.

However, both this and also the more complicated corona models (with data-weighting and/or "F10.7" time variation) used by CHASMP produce small deviations from the no-corona results. Our decision was to incorporate these small deviations between the two results due to corona modeling into our overall error budget as a separate item:

$$
\sigma_{\texttt{corona\_model}} = \pm 0.02 \times 10^{-8} \text{ cm/s}^2. \quad (31)
$$

This number could be discussed in Section IX, on computational systematics. Indeed, that is where it will be listed in our error budget.

D. Electro-magnetic Lorentz forces

The possibility that the spacecraft could hold a charge, and be deflected in its trajectory by Lorentz forces, was a concern for the magnetic field strengths at Jupiter and Saturn. However, the magnetic field strength in the outer solar system is on the order of $< 1\ \gamma$ ($\gamma = 10^{-5}$ Gauss). This is about a factor of 10^5 times smaller than the magnetic field strengths measured by the Pioneers at their nearest approaches to Jupiter: 0.185 Gauss for Pioneer 10 and 1.135 Gauss for the closer in Pioneer 11 [93].

Also, there is an upper limit to the charge that a spacecraft can hold. For the Pioneers that limit produced an upper bound on the Lorentz acceleration at closest approach to Jupiter of 20×10^{-8} cm/s^2 [87]. With the interplanetary field being so much lower than at Jupiter, we conclude that the electro-magnetic force on the Pioneer spacecraft in the outer solar system is at worst on the order of 10^{-12} cm/s^2, completely negligible [94].

Similarly, the magnetic torques acting on the spacecraft were about a factor of 10^{-5} times smaller than those acting on Earth satellites, where they are a concern. Therefore, for the Pioneers any observed changes in spacecraft spin cannot be caused by magnetic torques.

E.   The Kuiper belt's gravity

From the study of the resonance effect of Neptune upon Pluto, two primary mass concentration resonances of 3:2 and 2:1 were discovered [95], corresponding to 39.4 AU and 47.8 AU, respectively. Previously, Boss and Peale had derived a model for a non-uniform density distribution in the form of an infinitesimally thin disc extending from 30 AU to 100 AU in the ecliptic plane [96]. We combined the results of Refs. [95] and [96] to determine if the matter in the Kuiper belt could be the source of the anomalous acceleration of Pioneer 10 [97].

We specifically studied three distributions, namely: i) a uniform distribution, ii) a 2:1 resonance distribution with a peak at 47.8 AU, and iii) a 3:2 resonance distribution with a peak at 39.4 AU. Figure 15 exhibits the resulting acceleration felt by Pioneer 10, from 30 to 65 AU which encompassed our data set at the time.
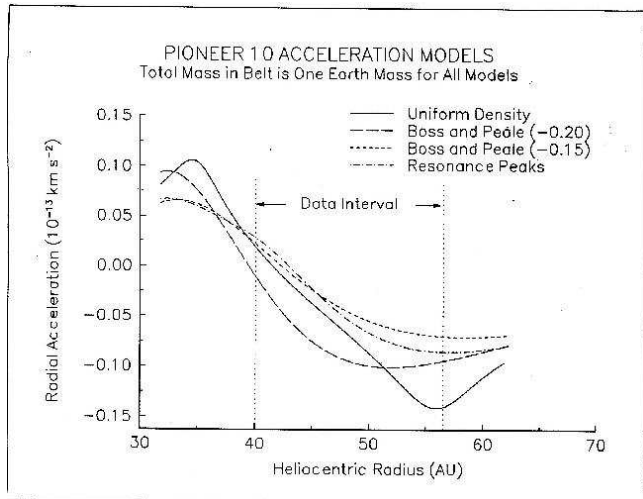
FIG. 15: Possible acceleration caused by dust in the Kuiper belt.

We assumed a total mass of one Earth mass, which is significantly larger than standard estimates. Even so, the accelerations are only on the order of 10^{-9} cm/s^2, which is two orders of magnitude smaller than the observed effect. (See Figure 15.) Further, the accelerations are not constant across the data range. Rather, they show an increasing effect as Pioneer 10 approaches the belt and a decreasing effect as Pioneer 10 recedes from the belt, even with a uniform density model. For these two reasons, we excluded the dust belt as a source for the Pioneer effect.

More recent infrared observations have ruled out more than 0.3 Earth mass of Kuiper Belt dust in the trans-Neptunian region [98, 99]. Therefore, we can now place a limit of $\pm 3 \times 10^{-10}$ cm/s^2 for the contribution of the Kuiper belt.

Finally, we note that searches for gravitational encounters of Pioneer with large Kuiper-belt objects have so far not been successful [100].

F.   Phase and frequency stability of clocks

After traversing the mechanical components of the antenna, the radio signal enters the DSN antenna feed and passes through a series of amplifiers, filters, and cables. Averaged over many experiments, the net effect of this on the calculated dynamical parameters of a spacecraft should be very small. We expect instrumental calibration instabilities to contribute 0.2×10^{-8} cm/s^2 to the anomalous acceleration on a 60 s time interval. Thus, in order for the atomic clocks [101] to have caused the Pioneer effect, all the atomic clocks used for signal referencing clocks would have had to have drifted in the same manner as the local DSN clocks.

In Section V we observed that without using the apparent anomalous acceleration, the CHASMP residuals show a steady frequency drift [38] of about -6×10^{-9} Hz/s, or 1.5 Hz over 8 years (one-way only). This equates to a clock acceleration, $-a_t$, of -2.8×10^{-18} s/s^2. (See Eq. (16) and Figure 8.) To verify that it is actually not the clocks that are drifting, we analyzed the calibration of the frequency standards used in the DSN complex.

The calibration system itself is referenced to Hydrogen maser atomic clocks. Instabilities in these clocks are another source of instrumental error which needs to be addressed. The local reference is synchronized to the frequency standards generated either at the National Institute of Standards and Technology (NIST), located in Boulder, Colorado or at the U. S. Naval Observatory (USNO), Washington, DC. These standards are presently distributed to local stations by the Global Positioning System (GPS) satellites. [During the pre-GPS era, the station clocks used signals from WWV to set the Cesium or Hydrogen masers. WWV, the radio station which broadcasts time and frequency services, is located in Fort Collins, CO.] While on a track, the station is "free-running," i.e., the frequency and timing data are generated locally at the station. The Allan variances are about 10^{-13} for Cesium and 10^{-15} for Hydrogen masers. Therefore, over the data-pass time interval, the data accuracy is on the order of one part in 1000 GHz or better.

Long-term frequency stability tests are conducted with the exciter/transmitter subsystems and the DSN's radio-science open-loop subsystem. An uplink signal generated by the exciter is translated at the antenna by a test translator to a downlink frequency. (See Section III.) The downlink signal is then passed through the RF-IF downconverter present at the antenna and into the radio science receiver chain [31]. This technique allows the processes to be synchronized in the DSN complex based on the frequency standards whose Allan variances are of the order of $\sigma_y \sim 10^{-14} - 10^{-15}$ for integration time in the range from 10 s to 10^3 s. For the S-band frequencies of the Pioneers, the corresponding Allan variances are 1.3×10^{-12} and 1.0×10^{-12}, respectively, for a 10^3 s Doppler integration time.

Phase-stability testing characterizes stability over very short integration times; that is, spurious signals whose frequencies are very close to the carrier (frequency). The phase noise region is defined to be frequencies within 100 kHz of the carrier. Both amplitude and phase variations appear as phase noise. Phase noise is quoted in dB relative to the carrier, in a 1 Hz band at a specified deviation from the carrier; for example, dBc-Hz at 10 Hz. Thus, for the frequency 1 Hz, the noise level is at -51 dBc and 10 Hz corresponds to -60 dBc. This was not significant for our study.

Finally, the influence of the clock stability on the detected acceleration, a_P, may be estimated based on the reported Allan variances for the clocks, σ_y. Thus, the standard 'single measurement' error on acceleration as derived by the time derivative of the Doppler frequency data is $(c\sigma_y)/\tau$, where the Allan variance, σ_y, is calculated for 1000 s Doppler integration time, and τ is the signal averaging time. This formula provides a good rule of thumb when the Doppler power spectral density function obeys a $1/f$ flicker-noise law, which is approximately the case when plasma noise dominates the Doppler error budget. Assume a worst case scenario, where only one clock was used for the whole 11 years study. (In reality each DSN station has its own atomic clock.) To estimate the influence of that one clock on the reported accuracy of the detected anomaly a_P, combine $\sigma_y = \Delta\nu/\nu_0$, the fractional Doppler frequency shift from the reference frequency of $\nu_0 = \sim 2.29$ GHz, with the estimate for the Allan variance, $\sigma_y = 1.3 \times 10^{-12}$. This yields a number that characterizes the upper limit for a frequency uncertainty introduced in a single measurement by the instabilities in the atomic clock: $\sigma_\nu = \nu_0 \sigma_y = 2.98 \times 10^{-3}$ Hz for a 10^3 Doppler integration time.

In order to derive an estimate for the total effect, recall that the Doppler observation technique is essentially a continuous count of the total number of complete frequency circles during observational time. Within a year one can have as many as $N \approx 3.156 \times 10^3$ independent single measurements of the clock with duration 10^3 seconds. This yields an upper limit for the contribution of atomic clock instability on the frequency drift of $\sigma_{\texttt{clock}} = \sigma_\nu/\sqrt{N} \approx 5.3 \times 10^{-5}$ Hz/year. But in Section

V B we noted that the observed a_P corresponds to a frequency drift of about 0.2 Hz/year, so the error in a_P is about 0.0003×10^{-8} cm/s^2. Since all data is not integrated over 1,000 seconds and is data is not available for all time, we increase the numerical factor to 0.001, which is still negligible to us. [But further, this upper limit for the error becomes even smaller if one accounts for the number of DSN stations and corresponding atomic clocks that were used for the study.]

Therefore, we conclude that the clocks are not a contributing factor to the anomalous acceleration at a meaningfully level. We will return to this issue in Section XI D where we will discuss a number of phenomenological time models that were used to fit the data.

G. DSN antennae complex

The mechanical structures which support the reflecting surfaces of the antenna are not perfectly stable. Among the numerous effects influencing the DSN antennae performance, we are only interested in those whose behavior might contribute to the estimated solutions for a_P. The largest systematic instability over a long period is due to gravity loads and the aging of the structure. As discussed in [102], antenna deformations due to gravity loads should be absorbed almost entirely into biases of the estimated station locations and clock offsets. Therefore, they will have little effect on the derived solutions for the purposes of spacecraft navigation.

One can also consider ocean loading, wind loading, thermal expansion, and aging of the structure. We found none of these can produce the constant drift in the Doppler frequency on a time scale comparable to the Pioneer data. Also, routine tests are performed by DSN personnel on a regular basis to access all the effects that may contribute to the overall performance of the DSN complex. The information is available and it shows all parameters are in the required ranges. Detailed assessments of all these effect on the astrometric VLBI solutions were published in [35, 102]. The results for the astrometric errors introduced by the above factors may be directly translated to the error budget for the Pioneers, scaled by the number of years. It yields a negligible contribution.

Our analyses also estimated errors introduced by a number of station-specific parameters. These include the error due to imperfect knowledge in a DSN station location, errors due to troposphere and ionosphere models for different stations, and errors due to the Faraday rotation effects in the Earth's atmosphere. Our analysis indicates that at most these effects would produce a distance-and/or time-dependent drifts that would be easily noticeable in the radio Doppler data. What is more important is that none of the effects would be able to produce a constant drift in the Doppler residuals of Pioneers over such a long time scale. The updated version of the ODP, *Sigma*, routinely accounts for these error factors. Thus, we run covariance analysis for the whole set of these parameters

using both *Sigma* and CHASMP. Based on these studies we conclude that mechanical and phase stability of the DSN antennae together with geographical locations of the antennae, geophysical and atmospheric conditions on the antennae site have negligible effects on our solutions for a_P. At most their contributions are at the level of $\sigma_{\text{DSN}} \leq 10^{-5} a_P$.

VIII. SOURCES OF SYSTEMATIC ERROR INTERNAL TO THE SPACECRAFT

In this section we will discuss the forces that may be generated by spacecraft systems. The mechanisms we consider that may contribute to the found constant acceleration, a_P, and that may be caused by the on-board mechanisms include: (1) the radio beam reaction force, (2) RTG heat reflecting off the spacecraft, (3) differential emissivity of the RTGs, (4) non-isotropic radiative cooling of the spacecraft, (5) expelled Helium produced within the RTG, (6) thruster gas leakage, and (7) the difference in experimental results from the two spacecraft.

A. Radio beam reaction force

The Pioneer navigation does not require that the spacecraft constantly beam its radio signal, but instead it does so only when it is requested to do so from the ground control. Nevertheless, the recoil force due to the emitted radio-power must also be analyzed.

The Pioneers have a total nominal emitted radio power of eight Watts. It is parameterized as

$$P_{\text{rp}} = \int_0^{\theta_{\max}} d\theta \ \sin \theta \ \mathcal{P}(\theta), \tag{32}$$

$\mathcal{P}(\theta)$ being the antenna power distribution. The radiated power has been kept constant in time, independent of the coverage from ground stations. That is, the radio transmitter is always on, even when not received by a ground station.

The recoil from this emitted radiation produces an acceleration bias, b_{rp}, on the spacecraft away from the Earth of

$$b_{\text{rp}} = \frac{\beta \, P_{\text{rp}}}{Mc}. \tag{33}$$

M is taken to be the Pioneer mass when half the fuel is gone [15]. β is the fractional component of the radiation momentum that is going in a direction opposite to a_P:

$$\beta = \frac{1}{P_{\text{rp}}} \int_0^{\theta_{\max}} d\theta \ \sin \theta \ \cos \theta \ \mathcal{P}(\theta). \tag{34}$$

Ref [4] describes the HGA and shows its downlink antenna pattern in Fig. 3.6-13. (Thermal antenna expansion mismodeling is thought to be negligible.) The gain is given as (33.3 ± 0.4) dB at zero (peak) degrees. The intensity is down by a factor of two (-3 dB) at 1.8 degrees. It is down a factor of 10 (-10 dB) at 2.7 degrees and down by a factor of 100 (-20 dB) at 3.75 degrees. [The first diffraction minimum is at a little over four degrees.] Therefore, the pattern is a very good conical beam. Further, since $\cos[3.75°] = 0.9978$, we can take $\beta = (0.99 \pm 0.01)$, yielding $b_{\text{rp}} = 1.10$.

Finally, taking the error for the nominal 8 Watts power to be given by the 0.4 dB antenna error (0.10) and the error due to the uncertainty in our nominal mass (0.04), we arrive at the result

$$a_{\text{rp}} = b_{\text{rp}} \pm \sigma_{\text{rp}} = (1.10 \pm 0.11) \times 10^{-8} \ \text{cm/s}^2. \tag{35}$$

B. RTG heat reflecting off the spacecraft

It has been argued that the anomalous acceleration seen in the Pioneer spacecraft is due to anisotropic heat reflection off of the back of the spacecraft high-gain antennae, the heat coming from the RTGs [103]. Before launch, the four RTGs had a total thermal fuel inventory of 2580 W (now ~ 2070 W). They produced a total electrical power of 160 W (now ~ 65 W). Presently ~ 2000 W of RTG heat must be dissipated. Only ~ 63 W of directed power could explain the anomaly. Therefore, in principle there is enough power to explain the anomaly this way. However, there are two reasons that preclude such a mechanism, namely:

i) The spacecraft geometry: The RTGs are located at the end of booms, and rotate about the spacecraft in a plane that contains the approximate base of the antenna. From the closest axial center point of the RTGs, the antenna is seen nearly "edge on" (the longitudinal angular width is 24.5^o). The total solid angle subtended is $\sim$ 1-2% of 4π steradians [104]. Even though a more detailed calculation yields a value of 1.5% [105], even taking the higher bound of 2% means this proposal could provide at most ~ 40 W. But there is more [106].

ii) The RTGs' radiation pattern: The above estimate was based on the assumption that the RTGs are spherical black bodies. But they are not. The main bodies of the RTGs are cylinders and they are grouped in two packages of two. Each package has the two cylinders end to end extending away from the antenna. Every RTG has six fins separated by equal angles of 60 degrees that go radially out from the cylinder. Presumably this results in a symmetrical radiation of thermal power into space.

Thus, the fins are "edge on" to the antenna (the fins point perpendicular to the cylinder axes). The largest opening angle of the fins is seen only by the narrow-angle parts of the antenna's outer edges. Ignoring these edge effects, only $\sim$2.5% of the surface area of the RTGs is facing the antenna. This is a factor 10 less than that from integrating the directional intensity from a hemisphere: $[(\int^{\text{h.sph.}} d\Omega \cos \theta)/(4\pi)] = 1/4$. So, one has only 4 W of directed power. This suggests a systematic bias of

$\sim 0.55 \times 10^{-8}$ cm/s^2. Even adding an uncertainty of the same size yields a systematic for heat reflection of

$$a_{\mathrm{h.r.}} = (-0.55 \pm 0.55) \times 10^{-8} \text{ cm/s}^2. \qquad (36)$$

But there are reasons to consider this an upper bound. The Pioneer SNAP 19 RTGs have larger fins than the earlier test models and the packages were insulated so that the end caps have lower temperatures. This results in lower radiation from the end caps than from the cylinder/fins [20, 21]. As a result, even though this is not exact, we can argue that the vast majority of the heat radiated by the RTGs is symmetrically directed to space unobscured by the antenna. Further, for this mechanism to work one still has to assume that the energy hitting the antenna is completely reradiated in the direction of the spin axis [106].

Finally, if this mechanism were the cause, ultimately an unambiguous decrease in the size of a_P should be seen because the RTGs' radioactively produced radiant heat is decreasing. As noted previously, the heat produced is now about 80% of the original magnitude. In fact, one would similarly expect a decrease of about 0.75×10^{-8} cm/s^2 in a_P over the 11.5 year Pioneer 10 data interval if this mechanism were the origin of a_P.

So, even though a complete thermal/physical model of the spacecraft might be able to ascertain if there are any other unsuspected heat systematics, we conclude that this particular mechanism does not provide enough power to explain the Pioneer anomaly [107].

In addition to the observed constancy of the anomalous acceleration, any explanation involving thermal radiation must also discuss the absence of a disturbance to the spin of the spacecraft. There may be a small correlation of the spin angular acceleration with the anomalous linear acceleration. However, as described in Section VI, the linear acceleration is much more constant than the spin. This suggests that most of the linear acceleration is not caused by whatever disturbs the spin, thermal or not.

However, a careful look at the Interval I results of Figure 11 shows that the nearly steady, background spin-rate change of about 6×10^{-5} rpm/day is slowly decreasing.

In principle this could be caused by heat.

The spin-rate change produced by the torque of radiant power directed against the rotation with a lever arm d is

$$\ddot{\theta} = \frac{P\, d}{c\, \mathcal{I}_{\mathbf{z}}}, \qquad (37)$$

where $\mathcal{I}_{\mathbf{z}}$ is the moment of inertia, 588.3 kg m^2 [17]. We take a base unit of $\ddot{\theta}_0$ for a power of one Watt and a lever arm of one meter. This is

$$\begin{aligned}
\ddot{\theta}_0 &= 5.63 \times 10^{-12} \text{ rad/s}^2 = 4.65 \times 10^{-6} \text{ rpm/day} = \\
&= 1.71 \times 10^{-3} \text{ rpm/yr}. \qquad (38)
\end{aligned}$$

So, about 13 Watt-meters of directed power could cause the base spin-rate change.

It turns out that such sources could, in principle, be available. There are $3 \times 3 = 9$ radioisotope heater units (RHUs) with one Watt power to heat the Thruster Cluster Assembly (TCA). (See pages 3.4-4 and 3.8-1–3.8-17 of Ref. [4].) The units are on the edge of the antenna of radius 1.37 m, in the housings of the TCAs which are approximately 180° apart from each other. At one position there are six RHUs and at the other position there are three. An additional RHU is near the sun sensor which is located near the second assembly. The final RHU is located at the magnetometer, 6.6 meters out from the center of the spacecraft.

The placement gives an "ideal" rotational asymmetry of two Watts. But note, the real asymmetry should be less, since these RHUs do not radiate only in one direction. Even one Watt unidirected at the magnetometer, is not enough to cause the baseline spin rate decrease. Further, since the base line is decreasing faster than what would come from the change cause by radioactive decay decrease, one cannot look for this effect or some complicated RTG source as the entire origin of the baseline change. One would suspect a very small gas leak or a combination of this and heat from the powered bus. (See Section VIII D.) Indeed, the factor $1/c$ in Eq. (37) is a manifestation of the energy-momentum conservation power needed to produce $\ddot{\theta}$ by heat vs. massive particles.

But in any event, this baseline spin-rate change is not significantly correlated with the anomalous acceleration, so we do not have to pursue it further.

C. Differential emissivity of the RTGs

Another suggestion related to the RTGs is the following [108]: during the early parts of the missions, there might have been a differential change of the radiant emissivity of the solar-pointing sides of the RTGs with respect to the deep-space facing sides. Note that, especially closer in the Sun, the inner sides were subjected to the solar wind. Contrariwise, the outer sides were sweeping through the solar-system dust cloud. Therefore, it can be argued that these two processes could have caused the effect. However, other information seems to make it difficult for this explanation to work.

The six fins of each RTG, designed to "provide the bulk of the heat rejection capacity," were fabricated of HM21A-T8 magnesium alloy plate [20]. The metal, after being specially prepared, was coated with two to three mils of zirconia in a sodium silicate binder to provide a high emissivity (~ 0.9) and low absorptivity (~ 0.2). Depending on how symmetrically fore-and-aft they radiated, the relative fore-and-aft emissivity of the alloy would have had to have changed by $\sim 10\%$ to account for a_P (see below). Given our knowledge of the solar wind and the interplanetary dust (see Section XI A), we find that this amount of a radiant change would be difficult to explain, even if it were of the right sign. (In fact, even the brace bars holding the RTGs were built such

that radiation is roughly fore/aft symmetric,)

We also have "visual" evidence from the Voyager spacecraft. As mentioned, the Voyagers are not spin-stabilized. They have imaging video cameras attached [109]. The cameras are mounted on a scan platform that is pointed under both celestial and inertial attitude control modes [110]. The cameras *do not* have lens covers [111]. During the outward cruise calibrations, the cameras were sometimes pointed towards an imaging target plate mounted at the rear of the spacecraft. But most often they were pointed all over the sky at specific star fields in support of ultraviolet spectrometer observations. Meanwhile, the spacecraft antennae were pointed towards Earth. Therefore, at an angle, the lenses were sometimes hit by the solar wind and sometimes by the interplanetary dust. Even so, there was no noticeable deterioration of the images received, even when Voyager 2 reached Neptune [112]. We infer, therefore, that this mechanism can not explain the Pioneer effect.

It turned out that the greatest radiation damage occurred during the flybys. The peak Pioneer 10 radiation flux near Jupiter was about 10,000 times that of Earth for electrons (1,000 times for protons). Pioneer 11 experienced an even higher radiation flux and also went by Saturn [3]. (We return to this in Section VIII G.) Therefore, if radiation damage was a problem, one should have seen an approximately uniform change in emissivity during flyby. Since the total heat flux, $\mathcal{F}$, from the RTGs was a constant over a flyby, there would have been a change in the RTG surface temperature manifested by the radiation formula $\mathcal{F} \propto \epsilon_1 T_1^4 = \epsilon_2 T_2^4$, the ϵ_i being the emissivities of the fin material. There are several temperature sensors mounted at RTG fin bases. They measured average temperatures of approximately 330 F, roughly 440 K. Therefore, a 10% change in the *total average* emissivity would have produced a temperature change of $\sim$12.2 K = 22 F. Such a change would have been noticed. (Measurements would be compared from, say, 30 days before and after flyby to eliminate the flyby power/thermal distortions.) Since (see below) a 10% *differential* fore/aft emissivity could cause the Pioneer effect, the lack of observation of a 10% *total average* emissivity change limits the size of the differential emissivity systematic.

To obtain a reasonable estimate of the uncertainty, consider if one side (fore or aft) of the RTGs had its emissivity changed by 1% with respect to the other side. In a simple cylindrical model of the RTGs, with 2000 W power (here we presume only radial emission with no loss out the sides), the ratio of power emitted by the two sides would be 0.99 = 995/1005, or a differential emission between the half cylinders of 10 W. Therefore, the fore/aft asymmetry towards the normal would be $[10 \text{ W}] \times \int_0^\pi [\sin\phi] d\phi/\pi \approx 6.37$ W. If one does a more sophisticated fin model, with 4 of the 12 fins facing the normal (two flat and two at 30°), one gets a number of 6.12 W. We take this to yield our uncertainty,

$$\sigma_{\text{d.e.}} = 0.85 \times 10^{-8} \text{ cm/s}^2. \qquad (39)$$

Note that 10 $\sigma_{\text{d.e.}}$ almost equals our final a_P. This is the origin of our previous statement that $\sim 10\%$ differential emissivity (in the correct direction) would be needed to explain a_P.

Finally, we want to comment on the significance of radioactive decay for this mechanism. Even acknowledging the Interval jumps due to gas leaks (see below), we reported a one-day batch-sequential value (before systematics) for a_P, averaged over the entire 11.5 year interval, of $a_P = (7.77 \pm 0.16) \times 10^{-8}$ cm/s^2. From radioactive decay, the value of a_P should have decreased by 0.75 of these units over 11.5 years. This is 5 times the above variance, which is very large with batch sequential. Even more stringently, this bound is good for *all* radioactive heat sources. So, what if one were to argue that emissivity changes occurring before 1987 were the cause of the Pioneer effect? There still should have been a decrease in a_P with time since then, which has not been observed.

We will return to these points in Section VIII G.

D. Non-isotropic radiative cooling of the spacecraft

It has also been suggested that the anomalous acceleration seen in the Pioneer 10/11 spacecraft can be, "explained, at least in part, by non-isotropic radiative cooling of the spacecraft [113]." So, the question is, does "at least in part" mean this effect comes near to explaining the anomaly? We argue it does not [114].

Consider radiation of the main-bus electrical systems power from the spacecraft rear. For the Pioneers, the aft has a louver system, and "the louver system acts to control the heat rejection of the radiating platform. A bimetallic spring, thermally coupled radiatively to the platform, provides the motive force for altering the angle of each blade. In a closed position (below 40 F) the heat rejection of the platform is minimized by virtue of the blockage of the blades while open fin louvers provide the platform with a nearly unobstructed view of space [4]."

If these louvers were open (above ~ 88 F) and all the diminishing electrical-power heat was radiated only out of the louvers, this mechanism could produce a significant effect. However, by nine AU the actuator spring temperature had already reached $\sim$40 F [4]. This means the louver doors were closed (i.e., the louver angle was zero) from where we obtained our data. Thus, from that time on of the radiation properties, the contribution of the thermal radiation to the Pioneer anomalous acceleration should be small. Although one might speculate that a louver stuck, there are 30 louvers on each craft. They clearly worked as designed, or else the temperature of the crafts' interiors would have fallen to disastrous levels.

As shown in Figure 16, in 1984 Pioneer 10 was at about 33 AU and the power was about 105 W. (Always reduce the total power numbers by 8 W to account for the radio beam power.) In (1987, 1992, 1996) the spacecraft was at $\sim$(41, 55, 65) AU and the power was $\sim$(95, 82, 73) W. The louvers were inactive, and no decrease in a_P was
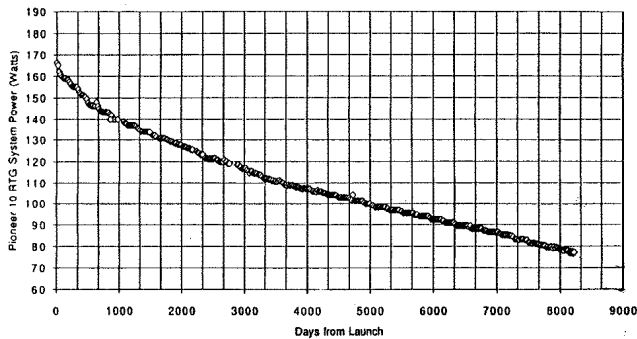
FIG. 16: The Pioneer 10 electrical power generated at the RTGs as a function of time from launch to near the end of 1994. By 1998.5, only ∼68 W was generated.

In fact, during the entire 11.5 year period from 1987 to 1998 the electrical power decreased from around 95 W to around 68 W, a change of 27 W. Since we already have noted that about ∼ 65 W is needed to cause our effect, such a large decrease in the "source" of the acceleration would have been seen. But as shown in Section VI, it was not. Even the small differences in the three intervals are most likely to be from gas leaks (as will be demonstrated in Section VIII F).

Later a double modification of this idea was given. It was first suggested that "most, if not all, of the unmodeled acceleration" of Pioneer 10 and 11 is due to an essentially constant supply of heat coming from the central compartment, directed out the front of the craft through the closed louvers [115]-(a). However, when one studies the electrical power history in both parts (instruments and experimental) of the central compartment, there is no constancy of heat. (See the details in [116].) Indeed during our data period the heat from this compartment decreased from about 73 W to about 57 Watts, or a factor of 1.26. This is inconsistent with the constancy of our result. Further, if one looks at the earlier, very roughly analyzed [117] data in Figure 7 one sees nothing close to the internal power change of 93 to 57 W (a factor of 1.6) [116].

To address this inconsistency a second modification [115]-b,c was made. It was arbitrarily argued that there was an incorrect determination of the reflection/absorption coefficients by a large factor. But these coefficients are known to 5%. If they were as poorly determined as speculated, the mission would have failed early on. (Further discussion is in [116].)

We conclude that neither the original proposal [113] nor the modification [115] can explain the anomalous Pioneer acceleration [114, 116]. A bound on the constancy of a_P comes from first noting the 11.5 year 1-day batch-sequential result, sensitive to time variation: $a_P = (7.77 \pm 0.16) \times 10^{-8}$ cm/s^2. Also given the constancy of the earlier imprecise date, it is conservative to take

three times this error to be our systematic uncertainty for radiative cooling of the craft, $\sigma_{\text{r.c.}} = \pm 0.48 \times 10^{-8}$ cm/s^2.

Although doubtful, one can also speculate that some mechanism like this might be involved with the baseline spin-rate change discussed in Section VIII B. In 1986-7, Pioneer 10 power was about 97 W, decreasing at about 2.5-3.0 W/yr. If you take a lever arm of 0.71 meters (the hexagonal bus size), this is more than enough to provide the 13 W-meters necessary to produce the baseline spin-rate change of Figure 11. Further for the first three years the decrease about matches the bus power loss rate. Then after the complex changes associated with the end of 1989 to 1990, there is a decrease in the base rate with a continued similar slope.

Perhaps the "baseline" rate is indeed from the heat of the bus being vented to the side. But the much larger gas leaks would be on top of the baseline.

E. Expelled Helium produced within the RTGs

Another possible on-board systematic is from the expulsion of the He being created in the RTGs from the α-decay of ^{238}Pu. To make this mechanism work, one would need that the He leakage from the RTGs be preferentially directed away from the Sun, with a velocity large enough to cause the acceleration.

The SNAP-19 Pioneer RTGs were designed in a such a way that the He pressure has not been totally contained within the Pioneer heat source over the life of RTGs [20]. Instead, the Pioneer heat source contains a pressure relief device which allows the generated He to vent out of the heat source and into the thermoelectric converter. (The strength member and the capsule clad contain small holes to permit He to escape into the thermoelectric converter.) The thermoelectric converter housing-to-power output receptacle interface is sealed with a viton O-ring. The O-ring allows the helium gas within the converter to be released by permeation to the space environment throughout the mission life of the Pioneer RTGs.

Information on the fuel pucks [118] shows that they each have heights of 0.212 inches with diameters of 2.145 inches. With 18 in each RTG and four RTGs per mission, this gives a total volume of fuel of about 904 cm^3. The fuel is PMC Pu conglomerate. The amount of ^{238}Pu in this fuel is about 5.8 kg. With a half life of 87.74 years, that means the rate of He production (from Pu decay) is about 0.77 gm/year, assuming it all leaves the cermet. Taking on operational temperature on the RTG surface of 320 F = 433 K, implies a $3kT/2$ helium velocity of 1.22 km/s. (The possible energy loss coming out of the viton is neglected for helium.) Using this in the rocket equation,

$$a(t) = -v(t)\frac{d}{dt}\Big[\ln M(t)\Big] \qquad (40)$$

with our nominal Pioneer mass with half the fuel gone

and the assumption that the gas is all unidirected, yields a maximal bound on the possible acceleration of 1.16×10^{-8} cm/s^2. So, we can rule out helium permeating through the O-rings as the cause of a_P although it is a systematic to be dealt with.

Of course, the gas is not totally unidirected. As one can see by looking at Figures 2 and III-2 of [20]: the connectors with the O-rings are on the RTG cylinder surfaces, on the ends of the cylinders where the fins are notched. They are equidistant (30 degrees) from two of the fins. The placement is exactly at the "rear" direction of the RTG cylinders, i.e., at the position closest to the Sun/Earth. The axis through the O-rings is parallel to the spin-axis. The O-rings, sandwiched by the receptacle and connector plates, "see" the outside world through an angle of about 90° in latitude [119]. (Overhead of the O-rings is towards the Sun.) In longitude the O-rings see the direction of the bus and space through about 90°, and "see" the fins through most of the rest of the longitudinal angle.

If one assumes a single elastic reflection, one can estimate the fraction of the bias away from the Sun. (Indeed, multiple and back reflections will produce an even greater bias. Therefore, we feel this approximation is justified.) This estimate is $(3/4)\sin 30°$ times the average of the heat momentum component parallel to the shortest distance to the RTG fin. Using this, we find the bias would be 0.31×10^{-8} cm/s^2. This bias effectively increases the value of our solution for a_P, which we hesitate to accept given all the true complications of the real system. Therefore we take the systematic expulsion to be $a_{\mathtt{He}} = (0.15 \pm 0.16) \times 10^{-8}$ cm/s^2.

F. Propulsive mass expulsion due to gas leakage

The effect of propulsive mass expulsion due to gas leakage has to be assessed. Although this effect is largely unpredictable, many spacecraft have experienced gas leaks producing accelerations on the order of 10^{-7} cm/s^2. [The reader will recall the even higher figure for Ulysses found in Section V D 2.] As noted previously, gas leaks generally behave differently after each maneuver. The leakage often decreases with time and becomes negligibly small.

Gas leaks can originate from Pioneer's propulsion system, which is used for mid-course trajectory maneuvers, for spinning-up or -down the spacecraft, and for orientation of the spinning spacecraft. The Pioneers are equipped with three pairs of hydrazine thrusters which are mounted on the circumference of the Earth-pointing high gain antenna. Each pair of thrusters forms a Thruster Cluster Assembly (TCA) with two nozzles aligned in opposition to each other. For attitude control, two pairs of thrusters can be fired forward or aft and are used to precess the spinning antenna (See Section II B.) The other pair of thrusters is aligned parallel to the rim of the antenna with nozzles oriented in co- and contra-rotation directions for spin/despin maneuvers.

During both observing intervals for the two Pioneers, there were no trajectory or spin/despin maneuvers. So, in this analysis we are mainly concerned with precession (i.e., orientation or attitude control) maneuvers only. (See Section II B.) Since the valve seals in the thrusters can never be perfect, one can ask if the leakages through the hydrazine thrusters could be the cause of the anomalous acceleration, a_P.

However, when we investigate the total computational accuracy of our solution in Section IX B, we will show that the currently implemented models of propulsion maneuvers may be responsible for an uncertainty in a_P only at the level of $\pm 0.01 \times 10^{-8}$ cm/s^2. Therefore, the maneuvers themselves are the main contributors neither to the total error budget nor to the gas leak uncertainty, as we now detail

The serious uncertainty comes from the possibility of undetected gas leaks. We will address this issue in some detail. First consider the possible action of gas leaks originating from the spin/despin TCA. Each nozzle from this pair of thrusters is subject to a certain amount of gas leakage. But only a differential leakage from the two nozzles would produce an observable effect causing the spacecraft to either spin-down or spin-up [120]. So, to obtain a gas leak uncertainty (and we emphasize "uncertainty" vs. "error" because we have no other evidence) let us ask how large a differential force is needed to cause the spin-down or spin-up effects observed?

Using the moment of inertia about the spin axis, $\mathcal{I}_\mathbf{z} = \sim 588.3$ kg·m^2 [17], and the antenna radius, $\mathcal{R} = 1.37$ m, as the lever arm, one can calculate that the differential force needed to torque the spin-rate change, $\ddot{\theta}_i$, in Intervals $i =$ I,II,III is

$$F_{\ddot{\theta}_i} = \frac{\mathcal{I}_\mathbf{z}\ddot{\theta}_i}{\mathcal{R}} = \left(2.57, \ 12.24, \ 1.03\right) \times 10^{-3} \ \text{dynes.} \quad (41)$$

It is possible that a similar mechanism of undetected gas leakage could be responsible for the net differential force acting in the direction along the line of sight. In other words, what if there were some undetected gas leakage from the thrusters oriented along the spin axis of the spacecraft that is causing a_P? How large would this have to be? A force of ($M = 241$ kg)

$$F_{a_P} = M a_P = 21.11 \times 10^{-3} \ \text{dynes} \quad (42)$$

would be needed to produce our final unbiased value of a_P. (See Section X. That is, one would need even more force than is needed to produce the anomalously high rotational gas leak of Interval II. Furthermore, the differential leakage to produce this a_P would have had to have been constant over many years and in the same direction for both spacecraft, without being detected as a spin-rate change. That is possible, but certainly not demonstrated. Furthermore if the gas leaks hypothesis were true, one would expect to see a dramatic difference in a_P during the three Intervals of Pioneer 10 data. Instead an almost 500 % spin-down rate change between

Intervals I and II resulted only in a less than 8% change in a_P.

Given the small amount of information, we propose to *conservatively* take as our gas leak uncertainties the acceleration values that would be produced by differential forces equal to

$$F_{a_{P(i)}\mathtt{g.l.}} \simeq \pm\sqrt{2}F_{\ddot{\theta}_i} = \qquad (43)$$
$$= \left(\pm 3.64, \ \pm 17.31, \ \pm 1.46\right) \times 10^{-3} \ \text{dynes}.$$

The argument for this is that, in the root sum of squares sense, one is accounting for the differential leakages from the two pairs of thrusters with their nozzles oriented along the line of sight direction. This directly translates into the acceleration errors introduced by the leakage during the three intervals of Pioneer 10 data,

$$\sigma(a_{P(i)\mathtt{g.l.}}) = \pm F_{a_{P(i)}\mathtt{g.l.}}/M = \qquad (44)$$
$$= \left(\pm 1.51, \ \pm 7.18, \ \pm 0.61\right) \times 10^{-8} \ \text{cm/s}^2.$$

Assuming that these errors are uncorrelated and are normally distributed around zero mean, we find the gas leak uncertainty for the entire Pioneer 10 data span to be

$$\sigma_{\mathtt{g.l.}} = \pm 0.56 \times 10^{-8} \ \text{cm/s}^2. \qquad (45)$$

This is one of our largest uncertainties.

The data set from Pioneer 11 is over a much smaller time span, taken when Pioneer 11 was much closer to the Sun (off the plane of the ecliptic), and during a maximum of solar activity. For Pioneer 11 the main effects of gas leaks occurred at the maneuvers, when there were impulsive lowerings of the spin-down rate. These dominated the over-all spin rate change of $\ddot{\theta}_{11} = -0.0234$ rpm/yr. (See Figure 12.) But in between maneuvers the spin rate was actually *increasing*. One can argue that this explains the higher value for $a_{P(11)}$ in Table I as compared to $a_{P(10)}$. Unfortunately, one has no *a priori* way of predicting the effect here. We do not know that the same specific gas leak mechanism applied here as did in the case of Pioneer 10 and there is no well-defined interval set as there is for Pioneer 10. Therefore, although we feel this "spin up" may be part of the explanation of the higher value of a_P for Pioneer 11, we leave the different numbers as a separate systematic for the next subsection.

At this point, we must conclude that the gas leak mechanism for explaining the anomalous acceleration seems very unlikely, because it is hard to understand why it would affect Pioneer 10 and 11 at the same level (given that both spacecraft had different quality of propulsion systems, see Section II B). One also expects a gas leak would obey the rules of a Poisson distribution. That clearly is not true. Instead, our analyses of different data sets indicate that a_P behaves as a constant bias rather than as a random variable. (This is clearly seen in the time history of a_P obtained with batch-sequential estimation.)

G. Variation between determinations from the two spacecraft

Finally there is the important point that we have two "experimental" results from the two spacecraft, given in Eqs. (23) and (24): 7.84 and 8.55, respectively, in units of 10^{-8} cm/s^2. If the Pioneer effect is real, and not a systematic, these numbers should be approximately equal.

The first number, 7.84, is for Pioneer 10. In Section VI D we obtained this number by correlating the values of a_P in the three data Intervals with the different spin-down rates in these Intervals. The weighted correlation between a shift in a_P and the spin-down rate is $\kappa_0 = (30.7 \pm 0.6)$ cm. (We argued in the previous Section VIII F that this correlation is the manifestation of the rotational gas leak systematic.) Therefore, this number represents the entire 11.5 year data arc of Pioneer 10. Similarly, Pioneer 11's number, 8.55, represents a $3\frac{3}{4}$ year data arc.

Even though the Pioneer 11 number may be less reliable since the craft was so much closer to the Sun, we calculate the time-weighted average of the experimental results from the two craft: $[(11.5)(7.84) + (3.75)(8.55)]/(15.25) = 8.01$ in units of 10^{-8} cm/s^2. This implies a bias of $b_{\mathtt{2\_craft}} = +0.17 \times 10^{-8}$ cm/s^2 with respect to the Pioneer 10 experimental result $a_{P(\mathtt{exper})}$. We also take this number to be our two spacecraft uncertainty. This means

$$a_{\mathtt{2-craft}} = b_{\mathtt{2-craft}} \pm \sigma_{\mathtt{2\_craft}} =$$
$$= (0.17 \pm 0.17) \times 10^{-8} \ \text{cm/s}^2. \qquad (46)$$

The difference between the two craft could be due to different gas leakage. But it also could be due to heat emitted from the RTGs. In particular, the two sets of RTGs have had different histories and so might have different emissivities. Pioneer 11 spent more time in the inner solar system (absorbing radiation). Pioneer 10 has swept out more dust in deep space. Further, Pioneer 11 experienced about twice as much Jupiter/Saturn radiation as Pioneer 10.

Further, note that $[a_{P(\mathtt{exper})}^{\mathtt{Pio11}} - a_{P(\mathtt{exper})}^{\mathtt{Pio10}}]$ and the uncertainty from differential emissivity of the RTGs, $\sigma_{\mathtt{d.e.}}$, are of the same size: 0.71 and 0.85 $\times 10^{-8}$ cm/s^2. It could therefore be argued that Pioneer 11's offset from Pioneer 10 comes from Pioneer 11 having obtained twice as large a differential emissivity bias as Pioneer 10. Then our final value of a_P, given in Section X, would be reduced by about 0.7 of our units since $\sigma_{\mathtt{d.e.}}$ would have become mainly a negative bias, $b_{\mathtt{d.e.}}$. This would make the final number closer to 8×10^{-8} cm/s^2. Because this model and our final number are consistent, we present this observation only for completeness and as a possible reason for the different results of the two spacecraft.

IX.   COMPUTATIONAL SYSTEMATICS

Given the very large number of observations for the same spacecraft, the error contribution from observational noise is very small and not a meaningful measure of uncertainty. It is therefore necessary to consider several other effects in order to assign realistic errors. Our first consideration is the statistical and numerical stability of of the calculations. We then go on to the cumulative influence of all modeling errors and editing decisions. Finally we discuss the reasons for and significance of the annual term.

Besides the factors mentioned above, we will discuss in this section errors that may be attributed to the specific hardware used to run the orbit determination computer codes, together with computational algorithms and statistical methods used to derive the solution.

A.   Numerical stability of least-squares estimation

Having presented estimated solutions along with their formal statistics, we should now attempt to characterize the true accuracy of these results. Of course, the significance of the results must be assessed on the basis of the expected measurement errors. These expected errors are used to weight a least-squares adjustment to parameters which describe the theoretical model. [Examination of experimental systematics from sources both external to and also internal to the spacecraft was covered in Sections VII-VIII.]

First we look at the numerical stability of the least squares estimation algorithm and the derived solution. The leading computational error source turns out to be subtraction of similar numbers. Due to the nature of floating point arithmetic, two numbers with high order digits the same are subtracted one from the other results in the low order digits being lost. This situation occurs with time tags on the data. Time tags are referenced to some epoch, such as say 1 January 1 1950 which is used by CHASMP. As more than one billion seconds have passed since 1950, time tags on the Doppler data have a start and end time that have five or six common leading digits. Doppler signal is computed by a differenced range formulation (see Section III B). This noise in the time tags causes noise in the computed Doppler at the 0.0006 Hz level for both Pioneers. This noise can be reduced by shifting the reference epoch closer to the data or increasing the word length of the computation, however, it is not a significant error source for this analysis.

In order to guard against possible computer compiler and/or hardware errors we ran orbit determination programs on different computer platforms. JPL's ODP resides on an HP workstation. The Aerospace Corporation ran the analysis on three different computer architectures: (i) Aerospace's DEC 64-bit RISC architecture workstation (Alphastation 500/266), (ii)

Aerospace's DEC 32-bit CISC architecture workstation (VAX 4000/60), and (iii) Pentium Pro PC. Comparisons of computations performed for CHASMP in the three machine show consistency to 15 digits which is just sufficient to represent the data. While this comparison does not eliminate the possibility of systematic errors that are common to both systems, it does test the numerical stability of the analysis on three very different computer architectures.

The results of the individual programs were given in Sections V and VI. In a test we took the JPL results for a batch-sequential *Sigma* run with 50-day averages of the anomalous acceleration of Pioneer 10, a_P. The data interval was from January 1987 to July 1998. We compared this to an Aerospace determination using CHASMP, where the was split into 200 day intervals, over a shorter data interval ending in 1994. As seen in Figure 14, the results basically agree.

Given the excellent agreement in these implementations of the modeling software, we conclude that differences in analyst choices (parameterization of clocks, data editing, modeling options, etc.) give rise to coordinate discrepancies only at the level of 0.3 cm. This number corresponds to an uncertainty in estimating the anomalous acceleration on the order of 8×10^{-12} cm/s^2.

But there is a slightly larger error to contend with. In principle the STRIPPER can give output to 16 significant figures. From the beginning the output was-rounded off to 15 and later to 14 significant figures. When Block 5 came on near the beginning of 1995, the output was rounded off to 13 significant figures. Since the Doppler residuals are 1.12 mm/s this last truncation means an error of order 0.01 mm/s. If we divide this number by 2 for an average round off, this translates to $\pm 0.04 \times 10^{-8}$ cm/s^2. The roundoff occurred in approximately all the data we added for this paper. This is the cleanest 1/3 of the Pioneer 10 data. Considering this we take the uncertainty to be

$$\sigma_{\texttt{num}} \pm 0.02 \times 10^{-8} \quad \text{cm/s}^2. \tag{47}$$

It needs to be stressed that such tests examine only the accuracy of implementing a given set of model codes, without consideration of the inherent accuracy of the models themselves. Numerous external tests, which we have been discussing in the previous three sections, are possible for assessing the accuracy of the solutions. Comparisons between the two software packages enabled us to evaluate the implementations of the theoretical models within a particular software. Likewise, the results of independent radio tracking observations obtained for the different spacecraft and analysis programs have enabled us to compare our results to infer realistic error levels from differences in data sets and analysis methods. Our analysis of the Galileo and Ulysses missions (reported in Sections V C and V D) was done partially for this purpose.

B. Accuracy of consistency/model tests

a. Consistency of solutions: A code that models the motion of solar system bodies and spacecraft includes numerous lengthy calculations. Therefore, the software used to obtain solutions from the Doppler data is, of necessity, very complex. To guard against potential errors in the implementation of these models, we used two software packages; JPL's ODP/*Sigma* modeling software [41, 54] and The Aerospace Corporation's POEAS/CHASMP software package [77, 78]. The differences between the JPL and Aerospace orbit determination program results are now examined.

As discussed in Section IV F, in estimating parameters the CHASMP code uses a standard variation of parameters method whereas ODP uses the Cowell method to integrate the equations of motion and the variational equations. In other words, CHASMP integrates six first-order differential equation, using the Adams-Moulton predictor-corrector method in the orbital elements. Contrariwise, ODP integrates three second-order differential equations for the accelerations using the Gauss-Jackson method. (For more details on these methods see Ref. [121].)

As seen in our results of Sections V and VI, agreement was good; especially considering that each program uses independent methods, models, and constants. Internal consistency tests indicate that a solution is consistent at the level of one part in 10^{15}. This implies an acceleration error on the order of no more then one part in 10^4 in a_P.

b. Earth orientation parameters: In order to check for possible problems with Earth orientation, CHASMP was modified to accept Earth orientation information from three different sources. (1) JPL's STOIC program that outputs `UT1R-UTC`, (2) JPL's Earth Orientation Parameter files (`UT1-UTC`), and (3) The International Earth Rotation Service's Earth Orientation Parameter file (`UT1-UTC`). We found that all three sources gave virtually identical results and changed the value of a_P only in the 4th digit [122].

c. Planetary ephemeris: Another possible source of problems is the planetary ephemeris. To explore this a fit was first done with CHASMP that used DE200. The solution of that fit was then used in a fit where DE405 was substituted for DE200. The result produced a small annual signature before the fit. After the fit, the maneuver solutions changed a small amount (less then 10%) but the value of the anomalous acceleration remained the same to seven digits. The post-fit residuals to DE405 were virtually unchanged from those using DE200. This showed that the anomalous acceleration was unaffected by changes in the planetary ephemeris.

This is pertinent to note for the following subsection. To reemphasize the above, a small "annual term" can be introduced by changing the planetary ephemerides. This annual term can then be totally taken up by changing the maneuver estimations. Therefore, in principle, any possible mismodeling in the planetary ephemeris could be at least partially masked by the maneuver estimations.

d. Differences in the codes' model implementations: The impact of an analyst's choices is difficult to address, largely because of the time and expense required to process a large data set using complex models. This is especially important when it comes to data editing. It should be understood that small differences are to be expected as models differ in levels of detail and accuracy. The analysts' methods, experience, and judgment differ. The independence of the analysis of JPL and Aerospace has been consistently and strictly maintained in order to provide confidence on the validity of the analyses. Acknowledging such difficulties, we still feel that using the very limited tests given above is preferable to an implicit assumption that all analysts' choices were optimally made.

Another source for differences in the results presented in Table I is the two codes' modeling of spacecraft reorientation maneuvers. ODP uses a model that solves for the resulted change in the Doppler observable Δv (instantaneous burn model). This is a more convenient model for Doppler velocity measurements. CHASMP models the change in acceleration, solves for Δa (finite burn model), and only then produces a solution for Δv. Historically, this was done in order to incorporate range observations (for Galileo and Ulysses) into the analysis.

Our best handle on this is the no-corona results, especially given that the two critical Pioneer 10 Interval III results differed by very little, 0.02×10^{-8} cm/s^2. This data is least affected by maneuver modeling, data editing, corona modeling, and spin calibration. Contrariwise, for the other data, the differences were larger. The Pioneer Interval I and II results and the Pioneer 11 results differed, respectively, by (0.21, 0.23, 0.25) in units of 10^{-8} cm/s^2. In these intervals models of maneuvers and data editing were crucial. Assuming that these errors are uncorrelated, we compute their combined effect on anomalous acceleration a_P as

$$\sigma_{\texttt{consist/model}} = \pm 0.13 \times 10^{-8} \text{ cm/s}^2. \qquad (48)$$

e. Mismodeling of maneuvers: A small contribution to the error comes from a possible mismodeling of the propulsion maneuvers. In Section IV E we found that for a typical maneuver the standard error in the residuals is $\sigma_0 \sim 0.095$ mm/s.

Then we would expect that in the period between two maneuvers, which on average is $\tau = 11.5/28$ year, the effect of the mismodeling would produce a contribution to the acceleration solution with a magnitude on the order of $\delta a_{\texttt{man}} = \sigma_0/\tau = 0.07 \times 10^{-8}$ cm/s^2. Now let us assume that the errors in the Pioneer Doppler residuals are normally distributed around zero mean with the standard deviation of $\delta a_{\texttt{man}}$ that constitute a single measurement accuracy. Then, since there are $N = 28$ maneuvers in the data set, the total error due to maneuver mismodeling is

$$\sigma_{\texttt{man}} = \frac{\delta a_{\texttt{man}}}{\sqrt{N}} = 0.01 \times 10^{-8} \text{ cm/s}^2. \qquad (49)$$

f. Mismodeling of the solar corona: Finally, recall that our number for mismodeling of the solar corona, $\pm 0.02 \times 10^{-8}$ cm/s^2, was already explained in Section VII C.

C. Apparent annual/diurnal periodicities in the solution

In Ref. [13] we reported, in addition to the constant anomalous acceleration term, a possible annual sinusoid. If approximated by a simple sine wave, the amplitude of this oscillatory term is about 1.6×10^{-8} cm/s^2. The integral of a sine wave in the acceleration, a_P, with angular velocity ω and amplitude A_0 yields the following first-order Doppler amplitude in two-way fractional frequency:

$$\frac{\Delta \nu}{\nu} = \frac{2 A_0}{c \, \omega}. \qquad (50)$$

The resulting Doppler amplitude for the annual angular velocity $\sim 2 \times 10^{-7}$ rad/s is $\Delta \nu / \nu = 5.3 \times 10^{-12}$. At the Pioneer downlink S-band carrier frequency of ~ 2.29 GHz, the corresponding Doppler amplitude is 0.012 Hz (i.e. 0.795 mm/s).

This term was first seen in ODP using the BSF method. As we discussed in Section IV G, treating a_P as a stochastic parameter in JPL's batch–sequential analysis allows one to search for a possible temporal variation in this parameter. Moreover, when many short interval times were used with least-squares CHASMP, the effect was also observed. (See Figure 14 in Section VI.)

The residuals obtained from both programs are of the same magnitude. In particular, the Doppler residuals are distributed about zero Doppler velocity with a systematic variation ~ 3.0 mm/s on a time scale of ~ 3 months. More precisely, the least-squares estimation residuals from both ODP/*Sigma* and CHASMP are distributed well within a half-width taken to be 0.012 Hz. (See, for example, Figure 9.) Even the general structures of the two sets of residuals are similar. The fact that both programs independently were able to produce similar post-fit residuals gives us confidence in the solutions.

With this confidence, we next looked in greater detail at the acceleration residuals from solutions for a_P. Consider Figure 17, which shows the a_P residuals from a value for a_P of $(7.77 \pm 0.16) \times 10^{-8}$ cm/s^2. The data was processed using ODP/*Sigma* with a batch-sequential filter and smoothing algorithm. The solution for a_P was obtained using 1-day batch sizes. Also shown are the maneuver times. At early times the annual term is largest. During Interval II, the interval of the large spin-rate change anomaly, coherent oscillation is lost. During Interval III the oscillation is smaller and begins to die out.

In attempts to understand the nature of this annual term, we first examined a number of possible sources, including effects introduced by imprecise modeling of maneuvers, the solar corona, and the Earth's troposphere.
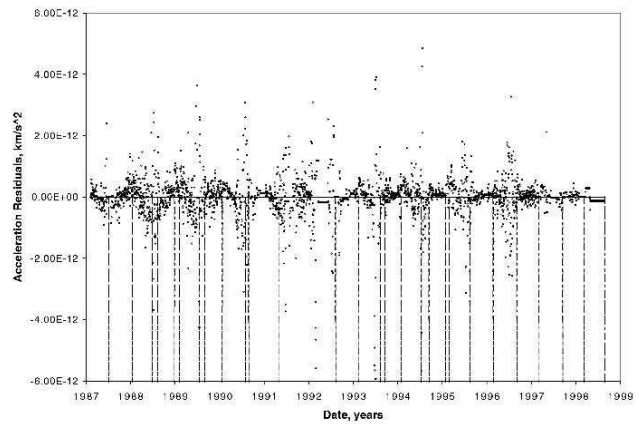

FIG. 17: ODP 1-day batch-sequential acceleration residuals using the entire Pioneer 10 data set. Maneuver times are indicated by the vertical dashed lines.

We also looked at the influence of the data editing strategies that were used. We concluded that these effects could not account for the annual term.

Then, given that the effect is particularly large in the out-of-the-ecliptic voyage of Pioneer 11 [13], we focused on the possibility that inaccuracies in solar system modeling are the cause of the annual term in the Pioneer solutions. In particular, we looked at the modeling of the Earth orbital orientation and the accuracy of the planetary ephemeris.

g. Earth's orientation: We specifically modeled the Earth orbital elements Δp and Δq as stochastic parameters. (Δp and Δq are two of the Set III elements defined by Brouwer and Clemence [123].) *Sigma* was applied to the entire Pioneer 10 data set with a_P, Δp, and Δq determined as stochastic parameters sampled at an interval of five days and exponentially correlated with a correlation time of 200 days. Each interval was fit independently, but with information on the spacecraft state (position and velocity) carried forward from one interval to the next. Various correlation times, 0-day, 30-day, 200-day, and 400-day, were investigated. The *a priori* error and process noise on Δp and Δq were set equal to 0, 5, and 10 μrad in separate runs, but only the 10 μrad case removed the annual term. This value is at least three orders of magnitude too large a deviation when compared to the present accuracy of the Earth orbital elements. It is most unlikely that such a deviation is causing the annual term. Furthermore, changing to the latest set of EOP has very little effect on the residuals. [We also looked at variations of the other four Set III orbital elements, essentially defining the Earth's orbital shape, size, and longitudinal phase angle. They had little or no effect on the annual term.]

h. Solar system modeling: We concentrated on Interval III, where the spin anomaly is at a minimum and where a_P is presumably best determined. Further, this data was partially taken after the DSN's Block 5 hard-

ware implementation from September 1994 to August 1995. As a result of this implementation the data is less noisy than before. Over Interval III the annual term is roughly in the form of a sine wave. (In fact, the modeling error is not strictly a sine wave. But it is close enough to a sine wave for purposes of our error analysis.) The peaks of the sinusoid are centered on conjunction, where the Doppler noise is at a maximum. Looking at a CHASMP set of residuals for Interval III, we found a 4-parameter, nonlinear, weighted, least-squares fit to an annual sine wave with the parameters amplitude $v_{\text{a.t.}} = (0.1053 \pm 0.0107)$ mm/s, phase $(-5.3° \pm 7.2°)$, angular velocity $\omega_{\text{a.t}} = (0.0177 \pm 0.0001)$ rad/day, and bias (0.0720 ± 0.0082) mm/s. The weights eliminate data taken inside of solar quadrature, and also account for different Doppler integration times T_c according to $\sigma = (0.765$ mm/s$) [(60$ s$)/T_c]^{1/2}$. This rule yields post-fit weighted RMS residuals of 0.1 mm/s.

The amplitude, $v_{\text{a.t.}}$, and angular velocity, $\omega_{\text{a.t.}}$, of the annual term results in a small acceleration amplitude of $a_{\text{a.t.}} = v_{\text{a.t.}}\omega_{\text{a.t.}} = (0.215 \pm 0.022) \times 10^{-8}$ cm/s^2. We will argue below that the cause is most likely due to errors in the navigation programs' determinations of the direction of the spacecraft's orbital inclination to the ecliptic.

A similar troubling modeling error exists on a much shorter time scale that is most likely an error in the spacecraft's orbital inclination to the Earth's equator. We looked at CHASMP acceleration residuals over a limited data interval, from 23 November 1996 to 23 December 1996, centered on opposition where the data is least affected by solar plasma. As seen in Figure 18, there is a significant diurnal term in the Doppler residuals, with period approximately equal to the Earth's sidereal rotation period ($23^h56^m04^s.0989$ mean solar time).
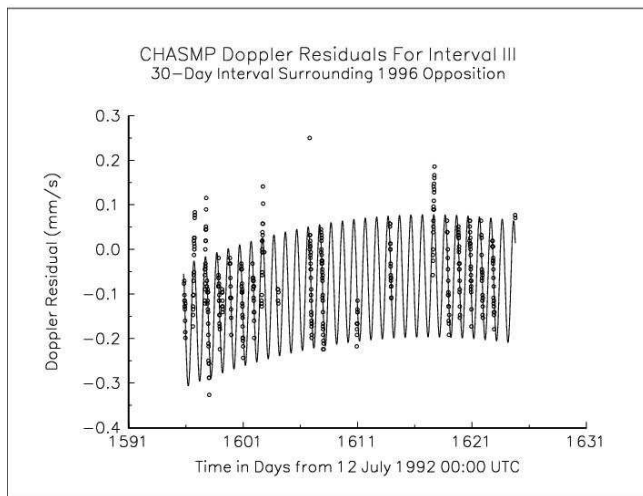
FIG. 18: CHASMP acceleration residuals from 23 November 1996 to 23 December 1996. A clear modeling error is represented by the solid diurnal curve. (An annual term maximum is also seen as a background.)

After the removal of this diurnal term, the RMS

Doppler residuals are reduced to amplitude 0.054 mm/s for $T_c = 660$ s ($\sigma_\nu/\nu = 2.9 \times 10^{-13}$ at $T_c = 1000$ s). The amplitude of the diurnal oscillation in the fundamental Doppler observable, $v_{\text{d.t.}}$, is comparable to that in the annual oscillation, $v_{\text{a.t.}}$, but the angular velocity, $\omega_{\text{d.t.}}$, is much larger than $\omega_{\text{a.t.}}$. This means the magnitude of the apparent angular acceleration, $a_{\text{d.t.}} = v_{\text{d.t.}}\omega_{\text{d.t.}} = (100.1 \pm 7.9) \times 10^{-8}$ cm/s^2, is large compared to a_P. Because of the short integration times, $T_c = 660$ s, and long observing intervals, $T \sim 1$ yr, the high frequency, diurnal, oscillation signal averages out to less than 0.03×10^{-8} cm/s^2 over a year. This intuitively helps to explain why the apparently noisy acceleration residuals still yield a precise value of a_P.

Further, all the residuals from CHASMP and ODP/*Sigma* are essentially the same. Since ODP and CHASMP both use the same Earth ephemeris and the same Earth orientation models, this is not surprising. This is another check that neither program introduces serious modeling errors of its own making.

Due to the long distances from the Sun, the spin-stabilized attitude control, the long continuous Doppler data history, and the fact that the spacecraft communication systems utilize coherent radio-tracking, the Pioneers allow for a very sensitive and precise positioning on the sky. For some cases, the Pioneer 10 coherent Doppler data provides accuracy which is even better than that achieved with VLBI observing natural sources. In summary, the Pioneers are simply much more sensitive detectors of a number of solar system modeling errors than other spacecraft.

The annual and diurnal terms are very likely different manifestations of the same modeling problem. The magnitude of the Pioneer 10 post-fit weighted RMS residuals of ≈ 0.1 mm/s, implies that the spacecraft angular position on the sky is known to ≤ 1.0 milliarcseconds (mas). (Pioneer 11, with ≈ 0.18 mm/s, yields the result ≈ 1.75 mas.) At their great distances, the trajectories of the Pioneers are not gravitationally affected by the Earth. (The round-trip light time is now ~ 24 hours for Pioneer 10.) This suggests that the sources of the annual and diurnal terms are both Earth related.

Such a modeling problem arises when there are errors in any of the parameters of the spacecraft orientation with respect to the chosen reference frame. Because of these errors, the system of equations that describes the spacecraft's motion in this reference frame is under-determined and its solution requires non-linear estimation techniques. In addition, the whole estimation process is subject to Kalman filtering and smoothing methods. Therefore, if there are modeling errors in the Earth's ephemeris, the orientation of the Earth's spin axis (precession and nutation), or in the station coordinates (polar motion and length of day variations), the least-squares process (which determines best-fit values of the three direction cosines) will leave small diurnal and annual components in the Doppler residuals, like those seen in Figures 17-18.

Orbit determination programs are particularly sensitive to an error in a poorly observed direction [124]. If not corrected for, such an error could in principle significantly affect the overall navigational accuracy. In the case of the Pioneer spacecraft, navigation was performed using only Doppler tracking, or line-of-sight observations. The other directions, perpendicular to the line-of-sight or in the plane of the sky, are poorly constrained by the data available. At present, it is infeasible to precisely parameterize the systematic errors with a physical model. That would have allowed one to reduce the errors to a level below those from the best available ephemeris and Earth orientation models. A local empirical parameterization is possible, but not a parameterization over many months.

We conclude that for both Pioneer 10 and 11, there are small periodic errors in solar system modeling that are largely masked by maneuvers and by the overall plasma noise. But because these sinusoids are essentially uncorrelated with the constant a_P, they do not present important sources of systematic error. The characteristic signature of a_P is a linear drift in the Doppler, not annual/diurnal signatures [125].

i. Annual/diurnal mismodeling uncertainty: We now estimate the annual term contribution to the error budget for a_P. First observe that the standard errors for radial velocity, v_r, and acceleration, a_r, are essentially what one would expect for a linear regression. The caveat is that they are scaled by the root sum of squares (RSS) of the Doppler error and unmodeled sinusoidal errors, rather than just the Doppler error. Further, because the error is systematic, it is unrealistic to assume that the errors for v_r and a_r can be reduced by a factor $1/\sqrt{N}$, where N is the number of data points. Instead, averaging their correlation matrix over the data interval, T, results in the estimated systematic error of

$$\sigma_{a_r}^2 = \frac{12}{T^2} \, \sigma_{v_r}^2 = \frac{12}{T^2} \left(\sigma_T^2 + \sigma_{v_{\text{a.t.}}}^2 + \sigma_{v_{\text{d.t.}}}^2 \right). \qquad (51)$$

$\sigma_T = 0.1$ mm/s is the Doppler error averaged over T (not the standard error on a single Doppler measurement). $\sigma_{v_{\text{a.t.}}}$ and $\sigma_{v_{\text{d.t.}}}$ are equal to the amplitudes of corresponding unmodeled annual and diurnal sine waves divided by $\sqrt{2}$. The resulting RSS error in radial velocity determination is about $\sigma_{v_r} = (\sigma_T^2 + \sigma_{v_{\text{a.t.}}}^2 + \sigma_{v_{\text{d.t.}}}^2)^{1/2} = 0.15$ mm/s for both Pioneer 10 and 11. Our four interval values of a_P were determined over time intervals of longer than a year. At the same time, to detect an annual signature in the residuals, one needs at least half of the Earth's orbit complete. Therefore, with $T = 1/2$ yr, Eq. (51) results in an acceleration error of

$$\sigma_{\text{a/d}} = \frac{0.50 \ \text{mm/s}}{T} = 0.32 \ \times 10^{-8} \ \text{cm/s}^2. \qquad (52)$$

We use this number for the systematic error from the annual/diurnal term.

X. ERROR BUDGET AND FINAL RESULT

It is important to realize that our experimental observable is a Doppler frequency shift, i.e., $\Delta\nu(t)$. [See Figure 8 and Eq. (15).] In actual fact it is a cycle count. We *interpret* this as an apparent acceleration experienced by the spacecraft. However, it is possible that the Pioneer effect is not due to a real acceleration. (See Section XI.) Therefore, the question arises "In what units should we report our errors?" The best choice is not clear at this point. For reasons of clarity we chose units of acceleration.

The tests documented in the preceding sections have considered various potential sources of systematic error. The results of these tests are summarized in Table II, which serves as a systematic "error budget." This budget is useful both for evaluating the accuracy of our solution for a_P and also for guiding possible future efforts with other spacecraft. In our case it actually is hard to totally distinguish "experimental" error from "systematic error." (What should a drift in the atomic clocks be called?) Further, there is the intractable mathematical problem of how to handle combined experimental and systematic errors. In the end we have decided to treat them all in a least squares *uncorrelated* manner.

The results of our analyses are summarized in Table II. There are two columns of results. The first gives a bias, b_P, and the second gives an uncertainty, $\pm\sigma_P$. The constituents of the error budget are listed separately in three different categories: 1) systematics generated external to the spacecraft; 2) on-board generated systematics, and 3) computational systematics. Our final result then will become some average

$$a_P = a_{P(\text{exper})} + b_P \pm \sigma_P, \qquad (53)$$

where, from Eq. (23), $a_{P(\text{exper})} = (7.84 \pm 0.01) \times 10^{-8}$ cm/s^2.

The least significant factors of our error budget are in the first group of effects, those external to the spacecraft. From the table one sees that some are near the limit of contributing. But in totality, they are insignificant.

As was expected, the on-board generated systematics are the largest contributors to our total error budget. All the important constituents are listed in the second group of effects in Table II. Among these effects, the radio beam reaction force produces the largest bias to our result, 1.10×10^{-8} cm/s^2. It makes the Pioneer effect larger. The largest bias/uncertainty is from RTG heat reflecting off the spacecraft. We argued for an effect as large as $(-0.55 \pm 0.55) \times 10^{-8}$ cm/s^2. Large uncertainties also come from differential emissivity of the RTGs, radiative cooling, and gas leaks, ± 0.85, ± 0.48, and ± 0.56, respectively, $\times 10^{-8}$ cm/s^2. The computational systematics are listed in the third group of Table II.

Therefore, our final value for a_P is

$$\begin{aligned} a_P &= (8.74 \pm 1.33) \times 10^{-8} \ \text{cm/s}^2 \\ &\sim (8.7 \pm 1.3) \times 10^{-8} \ \text{cm/s}^2. \end{aligned} \qquad (54)$$

TABLE II: Error Budget: A Summary of Biases and Uncertainties.

Item	Description of error budget constituents	Bias 10^{-8} cm/s^2	Uncertainty 10^{-8} cm/s^2
1	Systematics generated external to the spacecraft:		
	a) Solar radiation pressure and mass	+0.03	±0.01
	b) Solar wind		$\pm < 10^{-5}$
	c) Solar corona		±0.02
	d) Electro-magnetic Lorentz forces		$\pm < 10^{-4}$
	e) Influence of the Kuiper belt's gravity		±0.03
	f) Influence of the Earth orientation		±0.001
	g) Mechanical and phase stability of DSN antennae		± < 0.001
	h) Phase stability and clocks		± < 0.001
	i) DSN station location		$\pm < 10^{-5}$
	j) Troposphere and ionosphere		± < 0.001
2	On-board generated systematics:		
	a) Radio beam reaction force	+1.10	±0.11
	b) RTG heat reflected off the craft	−0.55	±0.55
	c) Differential emissivity of the RTGs		±0.85
	d) Non-isotropic radiative cooling of the spacecraft		±0.48
	e) Expelled Helium produced within the RTGs	+0.15	±0.16
	f) Gas leakage		±0.56
	g) Variation between spacecraft determinations	+0.17	±0.17
3	Computational systematics:		
	a) Numerical stability of least-squares estimation		±0.02
	b) Accuracy of consistency/model tests		±0.13
	c) Mismodeling of maneuvers		±0.01
	d) Mismodeling of the solar corona		±0.02
	e) Annual/diurnal terms		±0.32
	Estimate of total bias/error	+0.90	±1.33

The effect is clearly significant and remains to be explained.

XI. POSSIBLE PHYSICAL ORIGINS OF THE SIGNAL

A. A new manifestation of known physics?

With the anomaly still not accounted for, possible effects from applications of known physics have been advanced. In particular, Crawford [126] suggested a novel new effect: a gravitational frequency shift of the radio signals that is proportional to the distance to the spacecraft and the density of dust in the intermediate medium. In particular, he has argued that the gravitational interaction of the S-band radio signals with the interplanetary dust may be responsible for producing an anomalous acceleration similar to that seen by the Pioneer spacecraft. The effect of this interaction is a frequency shift that is proportional to the distance and the square root of the density of the medium in which it travels. Similarly, Didon, Perchoux, and Courtens [127] proposed that the effect comes from resistance of the spacecraft antennae as they transverse the interplanetary dust. This is related to more general ideas that an asteroid or comet belt, with its associated dust, might cause the effect by gravitational interactions (see Section VII E) or resistance to dust particles.

However, these ideas have problems with known properties of the interplanetary medium that were outlined in Section VII E. In particular, infrared observations rule out more than 0.3 Earth mass from Kuiper Belt dust in the trans-Neptunian region [98, 99]. Ulysses and Galileo measurements in the inner solar system find very few dust grains in the $10^{-18} - 10^{-12}$ kg range [128]. The density varies greatly, up and down, within the belt (which precludes a constant force) and, in any event, the density is not large enough to produce a gravitational acceleration on the order of a_P [95]-[97].

One can also speculate that there is some unknown interaction of the radio signals with the solar wind. An experimental answer could be given with two different transmission frequencies. Although the main communication link on the Ulysses mission is S-up/X-down mode, a small fraction of the data is S-up/S-down. We had hoped to utilize this option in further analysis. However, using them in our attempt to study a possible frequency dependent nature of the anomaly, did not provide any useful results. This was in part due to the fact that X-band data (about 1.5 % of the whole data available) were taken only in the close proximity to the Sun, thus prohibiting the study of a possible frequency dependence of the anomalous acceleration.

B. Dark matter or modified gravity?

It is interesting to speculate on the unlikely possibility that the origin of the anomalous signal is new physics [129]. This is true even though the probability is that some "standard physics" or some as-yet-unknown systematic will be found to explain this "acceleration." The first paradigm is obvious. "Is it dark matter or a modification of gravity?" Unfortunately, neither easily works.

If the cause is dark matter, it is hard to understand. A spherically-symmetric distribution of matter which goes as $\rho \sim r^{-1}$ produces a constant acceleration *inside* the distribution. To produce our anomalous acceleration even only out to 50 AU would require the total dark matter to be greater than $3 \times 10^{-4} M_\odot$. But this is in conflict with the accuracy of the ephemeris, which allows only of order a few times $10^{-6} M_\odot$ of dark matter even within the orbit of Uranus [8]. (A 3-cloud neutrino model also did not solve the problem [130].)

Contrariwise, the most commonly studied possible modification of gravity (at various scales) is an added Yukawa force [131]. Then the gravitational potential is

$$V(r) = -\frac{GMm}{(1+\alpha)r}\left[1 + \alpha e^{-r/\lambda}\right], \qquad (55)$$

where α is the new coupling strength relative to Newtonian gravity, and λ is the new force's range. Since the radial force is $F_r = -d_r V(r) = ma$, the power series for the acceleration yields an inverse-square term, no inverse-r term, then a constant term. Identifying this last term as the Pioneer acceleration yields

$$a_P = -\frac{\alpha a_1}{2(1+\alpha)}\frac{r_1^2}{\lambda^2}, \qquad (56)$$

where a_1 is the Newtonian acceleration at distance $r_1 = 1$ AU. (Out to 65 AU there is no observational evidence of an r term in the acceleration.) Eq. (56) is the solution curve; for example, $\alpha = -1 \times 10^{-3}$ for $\lambda = 200$ AU.

It is also of interest to consider some of the recent proposals to modify gravity, as alternatives to dark matter [132]-[135]. Consider Milgrom's proposed modification

of gravity [135], where the gravitational acceleration of a massive body is $a \propto 1/r^2$ for some constant $a_0 \ll a$ and $a \propto 1/r$ for $a_0 \gg a$. Depending on the value of H, the Hubble constant, $a_0 \approx a_P$! Indeed, as a number of people have noted,

$$a_H = cH \rightarrow 8 \times 10^{-8} \text{ cm/s}^2, \qquad (57)$$

if $H = 82$ km/s/Mpc.

Of course, there are (fundamental and deep) theoretical problems if one has a new force of the phenomenological types of those above. Even so, the deep space data piques our curiosity. In fact, Capozziello et al. [136] note the Pioneer anomaly in their discussion of astrophysical structures as manifestations of Yukawa coupling scales. This ties into the above discussion.

However, any universal gravitational explanation for the Pioneer effect comes up against a hard experimental wall. The anomalous acceleration is too large to have gone undetected in planetary orbits, particularly for Earth and Mars. NASA's Viking mission provided radio-ranging measurements to an accuracy of about 12 m [137, 138]. If a planet experiences a small, anomalous, radial acceleration, a_A, its orbital radius r is perturbed by

$$\Delta r = -\frac{l^6 a_A}{(GM_\odot)^4} \rightarrow -\frac{r\,a_A}{a_N}, \qquad (58)$$

where l is the orbital angular momentum per unit mass and a_N is the Newtonian acceleration at r. (The right value in Eq. (58) holds in the circular orbit limit.)

For Earth and Mars, Δr is about -21 km and -76 km. However, the Viking data determines the difference between the Mars and Earth orbital radii to about a 100 m accuracy, and their sum to an accuracy of about 150 m. The Pioneer effect is not seen.

Further, a perturbation in r produces a perturbation to the orbital angular velocity of

$$\Delta \omega = \frac{2l a_A}{GM_\odot} \rightarrow \frac{2\dot{\theta}\,a_A}{a_N}. \qquad (59)$$

The determination of the synodic angular velocity ($\omega_E - \omega_M$) is accurate to 7 parts in 10^{11}, or to about 5 ms accuracy in synodic period. The only parameter that could possibly mask the spacecraft-determined a_R is ($GM_\odot$). But a large error here would cause inconsistencies with the overall planetary ephemeris [8, 49]. [Also, there would be a problem with the advance of the perihelion of Icarus [139].]

We conclude that the Viking ranging data limit any unmodeled radial acceleration acting on Earth and Mars to no more than 0.1×10^{-8} cm/s^2. Consequently, if the anomalous radial acceleration acting on spinning spacecraft is gravitational in origin, it is *not* universal. That is, it must affect bodies in the 1000 kg range more than bodies of planetary size by a factor of 100 or more. This

would be a strange violation of the Principle of Equivalence [140]. (Similarly, the $\Delta\omega$ results rule out the universality of the a_t time-acceleration model. In the age of the universe, T, one would have $a_t T^2/2 \sim 0.7\ T$.)

A new dark matter model was recently proposed by Munyaneza and Viollier [141] to explain the Pioneer anomaly. The dark matter is assumed to be gravitationally clustered around the Sun in the form of a spherical halo of a degenerate gas of heavy neutrinos. However, although the resulting mass distribution is consistent with constraints on the mass excess within the orbits of the outer planets previously mentioned, it turns out that the model fails to produce a viable mechanism for the detected anomalous acceleration.

C. New suggestions stimulated by the Pioneer effect

Due to the fact that the size of the anomalous acceleration is of order cH, where H is the Hubble constant (see Eq. (57)), the Pioneer results have stimulated a number of new physics suggestions. For example, Rosales and Sánchez-Gomez [142] propose that a_P is due to a local curvature in light geodesics in the expanding spacetime universe. They argue that the Pioneer effect represents a new cosmological Foucault experiment, since the solar system coordinates are not true inertial coordinates with respect to the expansion of the universe. Therefore, the Pioneers are mimicking the role that the rotating Earth plays in Foucault's experiment. Therefore, in this picture the effect is not a "true physical effect" and a coordinate transformation to the co-moving cosmological coordinate frame would entirely remove the Pioneer effect.

From a similar viewpoint, Guruprasad [143] finds accommodation for the constant term while trying to explain the annual term as a tidal effect on the physical structure of the spacecraft itself. In particular, he suggests that the deformations of the physical structure of the spacecraft (due to external factors such as the effective solar and galactic tidal forces) combined with the spin of the spacecraft are directly responsible for the detected annual anomaly. Moreover, he proposes a hypothesis of the planetary Hubble's flow and suggests that Pioneer's anomaly does not contradict the existing planetary data, but supports his new theory of relativistically elastic space-time.

Østvang [144] further exploits the fact that the gravitational field of the solar system is not static with respect to the cosmic expansion. He does note, however, that in order to be acceptable, any non-standard explanation of the effect should follow from a general theoretical framework. Even so, Østvang still presents quite a radical model. This model advocates the use of an expanded PPN-framework that includes a direct effect on local scales due to the cosmic space-time expansion.

Belayev [145] considers a Kaluza-Klein model in 5 dimensions with a time-varying scale factor for the compactified fifth dimension. His comprehensive analysis led to the conclusion that a variation of the physical constants on a cosmic time scale is responsible for the appearance of the anomalous acceleration observed in the Pioneer 10/11 tracking data.

Modanese [146] considers the effect of a scale-dependent cosmological term in the gravitational action. It turns out that, even in the case of a static spherically-symmetric source, the external solution of his modified gravitational field equations contains a non-Schwartzschild-like component that depends on the size of the test particles. He argues that this additional term may be relevant to the observed anomaly.

Mansouri, Nasseri and Khorrami [147] argue that there is an effective time variation in the Newtonian gravitational constant that in turn may be related to the anomaly. In particular, they consider the time evolution of G in a model universe with variable space dimensions. When analyzed in the low energy limit, this theory produces a result that may be relevant to the long-range acceleration discussed here. A similar analysis was performed by Sidharth [148], who also discussed cosmological models with a time-varying Newtonian gravitational constant.

Inavov [149] suggests that the Pioneer anomaly is possibly the manifestation of a superstrong interaction of photons with single gravitons that form a dynamical background in the solar system. Every gravitating body would experience a deceleration effect from such a background with a magnitude proportional to Hubble's constant. Such a deceleration would produce an observable effect on a solar system scale.

All these ideas produce predictions that are close to Eq. (57), but they certainly must be judged against discussions in the following two subsections.

In a different framework, Foot and Volkas [150], suggest the anomaly can be explained if there is mirror matter of mirror dust in the solar system. this could produce a drag force and not violate solar-system mass constraints.

Several scalar-field ideas have also appeared. Mbelek and Lachièze-Rey [151] have a model based on a long-range scalar field, which also predicts an oscillatory decline in a_P beyond about 100 AU. This model does explain the fact that a_P stays approximately constant for a long period (recall that Pioneer 10 is now past 70 AU). From a similar standpoint Calchi Novati et al. [152] discuss a weak-limit, scalar-tensor extension to the standard gravitational model. However, before any of these proposals can be seriously considered they must explain the precise timing data for millisecond binary pulsars, i.e., the gravitational radiation indirectly observed in PSR 1913+16 by Hulse and Taylor [153]. Furthermore, there should be evidence of a distance-dependent scalar field if it is uniformly coupled to ordinary matter.

Consoli and Siringo [154] and Consoli [155] consider the Newtonian regime of gravity to be the long wavelength excitation of a scalar condensate from electroweak sym-

metry breaking. They speculate that the self-interactions of the condensate could be the origins of both Milgrom's inertia modification [132, 135] and also of the Pioneer effect.

Capozziello and Lambiase [156] argue that flavor oscillations of neutrinos in the Brans-Dicke theory of gravity may produce a quantum mechanical phase shift of neutrinos. Such a shift would produce observable effects on astrophysical/cosmological length and time scales. In particular, it results in a variation of the Newtonian gravitational constant and, in the low energy limit, might be relevant to our study.

Motivated by the work of Mannheim [133, 157], Wood and Moreau [158] investigated the theory of conformal gravity with dynamical mass generation. They argue that the Higgs scalar is a feature of the theory that cannot be ignored. In particular, within this framework they find one can reproduce the standard gravitational dynamics and tests within the solar system, and yet the Higgs fields may leave room for the Pioneer effect on small bodies.

In summary, as highly speculative as all these ideas are, it can be seen that at the least the Pioneer anomaly is influencing the phenomenological discussion of modern gravitational physics and quantum cosmology [159].

D. Phenomenological time models

Having noted the relationships $a_P = c\, a_t$ of Eq. (16) and that of Eq. (57), we were motivated to try to think of any (purely phenomenological) "time" distortions that might fortuitously fit the CHASMP Pioneer results shown in Figure 8. In other words, are Eqs. (57) and/or (16) indicating something? Is there any evidence that some kind of "time acceleration" is being seen?

The Galileo and Ulysses spacecraft radio tracking data was especially useful. We examined numerous "time" models searching for any (possibly radical) solution. It was thought that these models would contribute to the definition of the different time scales constructed on the basis of Eq. (6) and discussed in the Section IV B. The nomenclature of the standard time scales [54]-[55] was phenomenologically extended in our hope to find a desirable quality of the trajectory solution for the Pioneers.

In particular we considered:

i) **Drifting Clocks**. This model adds a constant acceleration term to the Station Time (ST) clocks, i.e., in the ST−UTC (Universal Time Coordinates) time transformation. The model may be given as follows:

$$\Delta \texttt{ST} = \texttt{ST}_{\texttt{received}} - \texttt{ST}_{\texttt{sent}} \quad \rightarrow \quad \Delta \texttt{ST} + \frac{1}{2} a_{\texttt{clocks}} \cdot \Delta \texttt{ST}^2 \tag{60}$$

where $\texttt{ST}_{\texttt{received}}$ and $\texttt{ST}_{\texttt{sent}}$ are the atomic proper times of sending and receiving the signal by a DSN antenna. The model fit Doppler well for Pioneer 10, Galileo, and Ulysses but failed to model range data for Galileo and Ulysses.

ii) **Quadratic Time Augmentation**. This model adds a quadratic-in-time augmentation to the TAI−ET (International Atomic Time – Ephemeris Time) time transformation, as follows

$$\texttt{ET} \quad \rightarrow \quad \texttt{ET} + \frac{1}{2} a_{\texttt{ET}} \cdot \texttt{ET}^2. \tag{61}$$

The model fits Doppler fairly well but range very badly.

iii) **Frequency Drift**. This model adds a constant frequency drift to the reference S-band carrier frequency:

$$\nu_{\texttt{S-band}}(t) = \nu_0 \Big(1 + \frac{a_{\texttt{fr.drift}} \cdot \texttt{TAI}}{c} \Big). \tag{62}$$

The model also fits Doppler well but again fits range poorly.

iv) **Speed of Gravity**. This model adds a "light time" delay to the actions of the Sun and planets upon the spacecraft:

$$v_{\texttt{grav}} = c \Big(1 + \frac{a_{\texttt{sp.grav}} \cdot |\vec{r}_{\texttt{body}} - \vec{r}_{\texttt{Pioneer}}|}{c^2} \Big). \tag{63}$$

The model fits Pioneer 10 and Ulysses well. But the Earth flyby of Galileo fit was terrible, with Doppler residuals as high as 20 Hz.

All these models were rejected due either to poor fits or to inconsistent solutions among spacecraft.

E. Quadratic in time model

There was one model of the above type that was especially fascinating. This model adds a quadratic in time term to the light time as seen by the DSN station. Take any labeled time $\texttt{T}_a$ to be

$$\texttt{T}_a = t_a - t_0 \rightarrow t_a - t_0 + \frac{1}{2} a_t \left(t_a^2 - t_0^2 \right). \tag{64}$$

Then the light time is

$$\Delta \texttt{TAI} = \texttt{TAI}_{\texttt{received}} - \texttt{TAI}_{\texttt{sent}} \quad \rightarrow$$
$$\rightarrow \quad \Delta \texttt{TAI} + \frac{1}{2} a_{\texttt{quad}} \cdot \left(\texttt{TAI}_{\texttt{received}}^2 - \texttt{TAI}_{\texttt{sent}}^2 \right). \tag{65}$$

It mimics a line of sight acceleration of the spacecraft, and could be thought of as an *expanding space* model. Note that $a_{\texttt{quad}}$ affects only the data. This is in contrast to the a_t of Eq. (16) that affects both the data and the trajectory.

This model fit both Doppler and range very well. Pioneers 10 and 11, and Galileo have similar solutions although Galileo solution is highly correlated with solar pressure; however, the range coefficient of the quadratic is negative for the Pioneers and Galileo while positive for Ulysses. Therefore we originally rejected the model because of the opposite signs of the coefficients. But when we later appreciated that the Ulysses anomalous acceleration is dominated by gas leaks (see Section V D 2), which

makes the different-sign coefficient of Ulysses meaningless, we reconsidered it.

The fact that the Pioneer 10 and 11, Galileo, and Ulysses are spinning spacecraft whose spin axis are periodically adjusted so as to point towards Earth turns out to make the quadratic in time model and the constant spacecraft acceleration model highly correlated and therefore very difficult to separate. The quadratic in time model produces residuals only slightly ($\sim 20\%$) larger than the constant spacecraft acceleration model. However, when estimated together with no *a priori* input i.e., based only the tracking data, even though the correlation between the two models is 0.97, the value a_{quad} determined for the quadratic in time model is zero while the value for the constant acceleration model a_P remains the same as before.

The orbit determination process clearly prefers the constant acceleration model, a_P, over that the quadratic in time model, a_{quad} of Eq. (65). This implies that a real acceleration is being observed and not a pseudo acceleration. We have not rejected this model as it may be too simple in that the motions of the spacecraft and the Earth may need to be included to produce a true expanding space model. Even so, the numerical relationship between the Hubble constant and a_P, which many people have observed (cf. Section XI C), remains an interesting conjecture.

XII. CONCLUSIONS

In this paper we have discussed the equipment, theoretical models, and data analysis techniques involved in obtaining the anomalous Pioneer acceleration a_P. We have also reviewed the possible systematic errors that could explain this effect. These included computational errors as well as experimental systematics, from systems both external to and internal to the spacecraft. Thus, based on further data for the Pioneer 10 orbit determination (the extended data spans 3 January 1987 to 22 July 1998) and more detailed studies of all the systematics, we can now give a total error budget for our analysis and a latest result of $a_P = (8.74 \pm 1.33) \times 10^{-8}$ cm/s^2.

This investigation was possible because modern radio tracking techniques have provided us with the means to investigate gravitational interactions to an accuracy never before possible. With these techniques, relativistic solar-system celestial mechanical experiments using the planets and interplanetary spacecraft provide critical new information.

Our investigation has emphasized that effects that previously thought to be insignificant, such as rejected thermal radiation or mass expulsion, are now within (or near) one order of magnitude of possible mission requirements. This has unexpectedly emphasized the need to carefully understand all systematics to this level.

In projects proposed for the near future, such as a Doppler measurement of the solar gravitational deflection using the Cassini spacecraft [160] and the Space Interferometry Mission [161], navigation requirements are more stringent than those for current spacecraft. Therefore, all the effects we have discussed will have to be well-modeled in order to obtain sufficiently good trajectory solutions. That is, a better understanding of the nature of these extra small forces will be needed to achieve the stringent navigation requirements for these missions.

Currently, we find no mechanism or theory that explains the anomalous acceleration. What we can say with some confidence is that the anomalous acceleration is a line of sight constant acceleration of the spacecraft toward the Sun [73]. Even though fits to the Pioneers appear to match the noise level of the data, in reality the fit levels are as much as 50 times above the fundamental noise limit of the data. Until more is known, we must admit that the most likely cause of this effect is an unknown systematic. (We ourselves are divided as to whether "gas leaks" or "heat" is this "most likely cause.")

The arguments for "gas leaks" are: i) All spacecraft experience a gas leakage at some level. ii) There is enough gas available to cause the effect. iii) Gas leaks require no new physics. However, iv) it is unlikely that the two Pioneer spacecraft would have gas leaks at similar rates, over the entire data interval, especially when the valves have been used for so many maneuvers. [Recall also that one of the Pioneer 11 thrusters became inoperative soon after launch. (See Section II B.)] v) Most importantly, it would require that these gas leaks be precisely pointed towards the front [19] of the spacecraft so as not to cause a large spin-rate changes. But vi) it could still be true anyway.

The main arguments for "heat" are: i) There is so much heat available that a small amount of the total could cause the effect. ii) In deep space the spacecraft will be in approximate thermal equilibrium. The heat should then be emitted at an approximately constant rate, deviating from a constant only because of the slow exponential decay of the Plutonium heat source. It is hard to resist the notion that this heat somehow must be the origin of the effect. However, iii) there is no solid explanation in hand as to how a specific heat mechanism could work. Further, iv) the decrease in the heat supply over time should have been seen by now.

Further experiment and analysis is obviously needed to resolve this problem.

On the Pioneer 10 experimental front, there now exists data up to July 2000. Further, there exists archived high-rate data from 1978 to the beginning of our data arc in Jan 1987 that was not used in this analysis. Because this early data originated when the Pioneers were much closer in to the Sun, greater effort would be needed to perform the data analyses and to model the systematics.

As Pioneer 10 continues to recede into interstellar space, its signal is becoming dimmer. Even now, the return signal is hard to detect with the largest DSN antenna. However, with appropriate instrumentation, the 305-meter antenna of the Arecibo Observatory in Puerto

Rico will be able to detect Pioneer's signal for a longer time. If contact with Pioneer 10 can be maintained with conscan maneuvers, such further extended data would be very useful, since the spacecraft is now so far from the Sun.

Other spacecraft can also be used in the study of a_P. The radio Doppler and range data from the Cassini mission could offer a potential contribution. This mission was launched on 15 October 1997. The potential data arc will be the cruise phase from after the Jupiter flyby (30 December 2000) to the vicinity of Saturn (just before the Huygens probe release) in July 2004. Even though the Cassini spacecraft is in three-axis-stabilization mode, using on-board active thrusters, it was built with very sophisticated radio-tracking capabilities, with X-band being the main navigation frequency. (There will also be S- and K-band links.) Further, during much of the cruise phase, reaction wheels will be used for stabilization instead of thrusters. Their use will aid relativity experiments at solar conjunction and gravitational wave experiments at solar opposition. (Observe, however, that the relatively large systematic from the close in Cassini RTGs will have to be accounted for.)

Therefore, Cassini could yield important orbit data, independent of the Pioneer hyperbolic-orbit data. A similar opportunity may exist, out of the plane of the ecliptic, from the proposed Solar Probe mission. Under consideration is a low-mass module to be ejected during solar flyby. On a longer time scale, the reconsidered Pluto/Kuiper mission (with arrival at Pluto around 2029) could eventually provide high-quality data from very deep space.

All these missions might help test our current models of precision navigation and also provide a new test for the anomalous a_P. In particular, we anticipate that, given our analysis of the Pioneers, in the future precision orbital analysis may concentrate more on systematics. That is, data/systematic modeling analysis may be assigned more importance relative to the astronomical modeling techniques people have concentrated on for the past 40 years [162]-[164].

Finally, we observe that if no convincing explanation is to be obtained, the possibility remains that the effect is real. It could even be related to cosmological quantities, as ha]s been intimated. [See Eq. (16) and Sec. XI, especially the text around Eq. (57).] This possibility necessitates a cautionary note on phenomenology: At this point in time, with the limited results available, there is a phenomenological equivalence between the a_P and a_t points of view. But somehow, the choice one makes affects one's outlook and direction of attack. If one has to consider new physics one should be open to both points of view. In the unlikely event that there is new physics, one does not want to miss it because one had the wrong mind set.

APPENDIX A: APPENDIX

In Table III we give the hyperbolic orbital parameters for Pioneer 10 and Pioneer 11 at epoch 1 January 1987, 01:00:00 UTC. The semi-major axis is a, e is the eccentricity, I is the inclination, Ω is the longitude of the ascending node, ω is the argument of the perihelion, M_0 is the mean anomaly, f_0 is the true anomaly at epoch, and r_0 is the heliocentric radius at the epoch. The direction cosines of the spacecraft position for the axes used are (α, β, γ). These direction cosines and angles are referred to the mean equator and equinox of J2000. The ecliptic longitude ℓ_0 and latitude b_0 are also listed for an obliquity of $23°26'21.''4119$. The numbers in parentheses denote realistic standard errors in the last digits.

TABLE III: Orbital parameters for Pioneer 10 and Pioneer 11 at epoch 1 January 1987, 01:00:00 UTC.

Parameter	Pioneer 10	Pioneer 11
a [km]	$-1033394633(4)$	$-1218489295(133)$
e	$1.733593601(88)$	$2.147933251(282)$
I [Deg]	$26.2488696(24)$	$9.4685573(140)$
Ω [Deg]	$-3.3757430(256)$	$35.5703012(799)$
ω [Deg]	$-38.1163776(231)$	$-221.2840619(773)$
M_0 [Deg]	$259.2519477(12)$	$109.8717438(231)$
f_0 [Deg]	$112.1548376(3)$	$81.5877236(50)$
r_0 [km]	$5985144906(22)$	$3350363070(598)$
α	$0.3252905546(4)$	$-0.2491819783(41)$
β	$0.8446147582(66)$	$-0.9625930916(22)$
γ	$0.4252199023(133)$	$-0.1064090300(223)$
ℓ_0 [Deg]	$70.98784378(2)$	$-105.06917250(31)$
b_0 [Deg]	$3.10485024(85)$	$16.57492890(127)$

[1] See the special issue of Science **183**, No. 4122, 25 January 1974; specifically, J. D. Anderson, G. W. Null, and S. K. Wong, Science **183**, 322 (1974).

[2] R. O. Fimmel, W. Swindell, and E. Burgess, *Pioneer Odyssey: Encounter with a Giant*, NASA document No. SP-349 (NASA, Washington D.C., 1974).

[3] R. O. Fimmel, J. Van Allen, and E. Burgess, *Pioneer: First to Jupiter, Saturn, and beyond*, NASA report NASA–SP-446 (NASA, Washington D.C., 1980).

[4] *Pioneer F/G Project: Spacecraft Operational Characteristics*, Pioneer Project NASA/ARC document No. PC-202 (NASA, Washington, D.C., 1971).

[5] *Pioneer Extended Mission Plan*, Revised, NASA/ARC document No. PC-1001 (NASA, Washington, D.C., 1994).

[6] For web summaries of Pioneer, go to: http://quest.arc.nasa.gov/pioneer10, http://spaceprojects.arc.nasa.gov/ Space_Projects/ pioneer/PNhome.html

[7] J. D. Anderson, E. L. Lau, K. Scherer, D. C. Rosenbaum, and V. L. Teplitz, Icarus **131**, 167 (1998).

[8] J. D. Anderson, E. L. Lau, T. P. Krisher, D. A. Dicus, D. C. Rosenbaum, and V. L. Teplitz, Astrophys. J. **448**, 885 (1995).

[9] K. Scherer, H. Fichtner, J. D. Anderson, and E. L. Lau, Science **278**, 1919 (1997).

[10] J. D. Anderson and B. Mashoon, Astrophys. J. **290**, 445 (1985).

[11] J. D. Anderson, J. W. Armstrong, and E. L.Lau, Astrophys. J. **408**, 287 (1993).

[12] J. D. Anderson, P. A. Laing, E. L. Lau, A. S. Liu, M. M. Nieto, and S. G. Turyshev, Phys. Rev. Lett. **81**, 2858 (1998). Eprint gr-qc/9808081.

[13] S. G. Turyshev, J. D. Anderson, P. A. Laing, E. L. Lau, A. S. Liu, and M. M. Nieto, in: *Gravitational Waves and Experimental Gravity, Proceedings of the XVIIIth Moriond Workshop of the Rencontres de Moriond*, ed. by J. Dumarchez and J. Tran Thanh Van (World Pub., Hanoi, 2000), pp. 481-486. Eprint gr-qc/9903024.

[14] There were four Pioneers built of this particular design. After testing, the best components were placed in Pioneer 10. (This is probably why Pioneer 10 has lasted so long.) The next best were placed in Pioneer 11. The third best were placed in the "proof test model." Until recently, the structure and many components of this model were included in an exhibit at the National Air and Space Museum. The other model eventually was dismantled. We thank Robert Ryan of JPL for telling us this.

[15] Figures given for the mass of the entire Pioneer package range from under 250 kg to over 315 kg. However, we eventually found that the total ("wet") weight at launch was 259 kg (571 lbs), including 36 kg of hydrazine (79.4 lbs). Credit and thanks for these numbers are due to Randall Rathbun, Allen Parker, and Bruce A. Giles of TRW, who checked and rechecked for us including going to their launch logs. Consistent total mass with lower fuel (27 kg) numbers were given by Larry Kellogg of NASA/Ames. (We also thank V. J. Slabinski of USNO who first asked us about the mass.)

[16] Information about the gas usage is by this time difficult to find or lost. During the Extended Mission the collaboration was most concerned with power to the craft. The folklore is that most of Pioneer 11's propellant was used up going to Saturn and used very little for Pioneer 10. In particular, a Pioneer 10 nominal input mass of 251.883 kg and a Pioneer 11 mass of 239.73 kg were used by the JPL program and the Aerospace program used 251.883 for both. The 251 number approximates the mass lost during spin down, and the 239 number models the greater fuel usage. These numbers were not changed in the programs. For reference, we will use 241 kg, the mass with half the fuel used, as our number with which to calibrate systematics.

[17] We take this number from Ref. [4], where the design, boom-deployed moment of inertia is given as 433.9 slug (ft)^2 (= 588.3 kg m^2). This should be a little low since we know a small amount of mass was added later in the

development. A much later order-of-magnitude number 770 kg m^2 was obtained with a too large mass [15, 16]. See J. A. Van Allen, *Episodic Rate of Change in Spin Rate of Pioneer 10,* Pioneer Project Memoranda, 20 March 1991 and 5 April 1991. Both numbers are dominated by the RTGs and magnetometer at the ends of long booms.

[18] Conscan stands for conical scan. The receiving antenna is moved in circles of angular size corresponding to one half of the beam-width of the incoming signal. This procedure, possibly iterated, allows the correct pointing direction of the antenna to be found. When coupled with a maneuver, it can also be used to find the correct pointing direction for the spacecraft antenna. The precession maneuvers can be open-loop, for orientation towards or away from Earth-pointing, or closed-loop, for homing on the uplink radio-frequency transmission from the Earth.

[19] When a Pioneer antenna points toward the Earth, this defines the "rear" direction on the spacecraft. The equipment compartment placed on the other side of of the antenna defines the "front" direction on the spacecraft. (See Figure 2.)

[20] *SNAP 19 Pioneer F & G Final Report*, Teledyne report IESD 2873-172, June, 1973, tech. report No. DOE/ET/13512-T1; DE85017964, gov. doc. # E 1.9, and S. T. Christenbury, private communications.

[21] F. A. Russo, in: *Proceedings of the 3rd RTG Working Group Meeting* (Atomic Energy Commission, Washington, DC, 1972), ed. by P. A. O'Rieordan, papers # 15 and 16.

[22] L. Lasher, Pioneer Project Manager, recently reminded us (March 2000) that not long after launch, the electrical power had decreased to about 155 W, and degraded from there. [Plots of the available power with time are available.]

[23] This is a "theoretical value," which does not account for inverter losses, line losses, and such. It is interesting to note that at mission acceptance, the total "theoretical" power was 175 Watts.

[24] We take the S-band to be defined by the frequencies 1.55-5.20 GHz. We take the X-band to be defined by the frequencies 5.20-10.90 GHz. It turns out there is no consistent international definition of these bands. The definitions vary from field to field, with geography, and over time. The above definitions are those used by radio engineers and are consistent with the DSN usage. (Some detailed band definitions can be found at `http://www.eecs.wsu.edu/~hudson/Teaching/ee432/spectrum.htm`.) [We especially thank Ralph McConahy of DSN Goldstone on this point.]

[25] dBm is used by radio engineers as a measure of received power. It stands for decibels in milliwatts.

[26] For a description of the Galileo mission see T. V. Johnson, C. M. Yeats, and R. Young, Space Sci. Rev. **60**, 3–21 (1992). For a description of the trajectory design see L. A. D'Amario, L. E. Bright, and A. A. Wolf, Space Sci. Rev. **60**, 22–78 (1992).

[27] The LGA was originally supposed to "trickle" down low-rate engineering data. It was also to be utilized in case a fault resulted in the spacecraft "safing" and shifting to a Sun-pointed attitude, resulting in loss of signal from the HGA. ["Safing" refers to a spacecraft entering the so called "safe mode." This happens in case of an emergency when systems are shut down.]

[28] J. D. Anderson, P. B. Esposito, W. Martin, C. L. Thornton, and D. O. Muhleman, Astrophys. J. **200**, 221 (1975).

[29] P. W. Kinman, IEEE Transactions on Microwave Theory and Techniques **40**, 1199 (1992).

[30] For descriptions of the Ulysses mission see E. J. Smith and R. G. Marsden, Sci. Am. **278**, No. 1, 74 (1998); B. M. Bonnet, Alexander von Humboldt Magazin, No. 72, 27 (1998).

[31] A technical description, with a history and photographs, of the Deep Space Network can be found at `http://deepspace.jpl.nasa.gov/dsn/`. The document describing the radio science system is at `http://deepspace.jpl.nasa.gov/dsndocs/810-5/810-5.html`.

[32] N. A. Renzetti, J. F. Jordan, A. L. Berman, J. A. Wackley, T. P. Yunck, *The Deep Space Network – An Instrument for Radio Navigation of Deep Space Probes*, Jet Propulsion Laboratory Technical Report 82-102 (1982).

[33] J. A. Barnes, A. R. Chi, L. S. Cutler, D. J. Healey, D. B. Leeson, T. E. McGunigal, J. A. Mullen, Jr., W. L. Smith, R. L. Sydnor, R. F. C. Vessot, and G. M. R. Winkler, IEEE Transactions on Instrumentation and Measurement **20**, 105 (1971).

[34] R. F. C. Vessot, in: *Experimental Gravitation*, ed. B. Bertotti, (Academic Press, New York and London, 1974), p.111.

[35] O. J. Sovers, J. L. Fanselow, and C. S. Jacobs, Rev. Mod. Phys., **70**, 1393 (1998).

[36] One-way data refers to a transmission and reception, only. Two-way data is a transmission and reception, followed by a retransmission and reception at the original transmission site. This would be, for example, a transmission from a radio antenna on Earth to a spacecraft and then a retransmission back from the spacecraft to the same antenna. Three-way refers to the same as two-way, except the final receiving antenna is different from the original transmitting antenna.

[37] Much, but not all, of the data we used has been archived. Since the Extended Pioneer Mission is complete, the resources have not been available to properly convert the entire data set to easily accessible format.

[38] The JPL and DSN convention for Doppler frequency shift is $(\Delta\nu)_{\rm DSN} = \nu_0 - \nu$, where ν is the measured frequency and ν_0 is the reference frequency. It is positive for a spacecraft receding from the tracking station (red shift), and negative for a spacecraft approaching the station (blue shift), just the opposite of the usual convention, $(\Delta\nu)_{\rm usual} = \nu - \nu_0$. In consequence, the velocity shift, $\Delta v = v - v_0$, has the same sign as $(\Delta\nu)_{\rm DSN}$ but the opposite sign to $(\Delta\nu)_{\rm usual}$. Unless otherwise stated, we will use the DSN frequency shift convention in this paper. We thank Matthew Edwards for asking us about this.

[39] As we will come to in Section XI D, this property allowed us to test and reject several phenomenological models of the anomalous acceleration that fit Doppler data well but failed to fit the range data.

[40] D. L. Cain, JPL Technical Report (1966).

[41] T. D. Moyer, *Mathematical Formulation of the Double Precision Orbit Determination Program (DPODP)*, Jet Propulsion Laboratory Technical Report 32-1527 (1971).

[42] T. D. Moyer, *Formulation for Observed and Computed*

Values of Deep Space Network (DSN) Data Types for Navigation, JPL Publication 00-7 (October 2000).

[43] A. Gelb, ed. *Applied Optimal Estimation* (M.I.T. Press, Cambridge, MA, 1974).

[44] D. O. Muhleman and J. D. Anderson, Astrophys. J. **247**, 1093 (1981).

[45] Once in deep space, all major forces on the spacecraft are gravitational. The Principle of Equivalence holds that the inertial mass (m_I) and the gravitational mass (m_G) are equal. This means the mass of the craft should cancel out in the dynamical gravitational equations. As a result, the people who designed early deep-space programs were not as worried as we are about having the correct mass. When non-gravitational forces were modeled, an incorrect mass could be accounted for by modifying other constants. For example, in the solar radiation pressure force the effective sizes of the antenna and the albedo could take care of mass inaccuracies.

[46] J. D. Anderson, in: *Experimental Gravitation,* ed. B. Bertotti (New York and London, Academic Press, 1974), p.163.

[47] J. D. Anderson, G. S. Levy, and N. A. Renzetti, "Application of the Deep Space Network (DSN) to the testing of general relativity," in *Relativity in Celestial Mechanics and Astrometry*, eds. J. Kovalevsky and V. A. Brumberg. (Kluwer Academic, Dordrecht, Boston, 1986), p. 329.

[48] X X Newhall, E. M. Standish, and J. G. Williams, Astron. Astrophys. **125**, 150 (1983).

[49] E. M. Standish, Jr., X X Newhall, J. G. Williams, and D. K. Yeomans, "Orbital ephemeris of the Sun, Moon, and Planets," in: Ref. [55], p. 279. Also see E. M. Standish, Jr. and R. W. Hellings, Icarus **80**, 326 (1989).

[50] E. M. Standish, Jr., X X Newhall, J. G. Williams, and W. M. Folkner, *JPL Planetary and Lunar Ephemeris, DE403/LE403,* Jet Propulsion Laboratory Internal IOM No. 314.10-127 (1995).

[51] C. M. Will, *Theory and Experiment in Gravitational Physics,* (Rev. Ed.) (Cambridge University Press, Cambridge, 1993).

[52] C. M. Will and K. Nordtvedt, Jr, Astrophys. J. **177**, 757 (1972).

[53] F. E. Estabrook, Astrophys. J. **158**, 81 (1969).

[54] T. D. Moyer, Parts. 1 and 2, Celest. Mech. **23**, 33, 57 (1981).

[55] P. K. Seidelmann, ed., *Explanatory Supplement to the Astronomical Almanac* (University Science Books, Mill Valley, CA, 1992).

[56] C. Ma, E. F. Arias, T. M. Eubanks, A. L. Fey, A.-M. Gontier, C. S. Jacobs, O. J. Sovers, B. A. Archinal, and P. Charlot, Astron. J. **116**, 516 (1998).

[57] A. Milani, A. M. Nobili, and P. Farinella, *Non-Gravitational Perturbations and Satellite Geodesy,* (Adam Hilger, Bristol, 1987). See, especially, p. 125.

[58] J. M. Longuski, R. E. Todd, and W. W. König, J. Guidance, Control, and Dynamics, **15**, 545 (1992).

[59] D.O. Muhleman, P.B. Esposito, and J. D. Anderson, Astrophys. J. **211**, 943 (1977).

[60] The propagation speed for the Doppler signal is the phase velocity, which is greater than c. Hence, the negative sign in Eq. (8) applies. The ranging signal propagates at the group velocity, which is less than c. Hence, there the positive sign applies.

[61] B.-G. Anderssen and S. G. Turyshev, JPL Internal IOM 1998-0625, and references therein.

[62] M. K. Bird, H. Volland, M. Pätzold, P. Edenhofer , S. W. Asmar and J. P. Brenkle, Astrophys. J. **426**, 373 (1994).

[63] The units conversion factor for A, B, C from m to cm^{-3} is $2N_c(S)/R_\odot = 0.01877$, where $N_c(S) = 1.240 \times 10^4 \nu^2$ is the S band (in MHz) critical plasma density, and $R_\odot$ is the radius of the Sun.

[64] These values of parameters A, B, C were kindly provided to us by John E. Ekelund of JPL. They represent the best solution for the solar corona parameters obtained during his simulations of the solar conjunction experiments that will be performed with the Cassini mission spacecraft in 2001 and 2002.

[65] This model is explained and described at
http://science.msfc.nasa.gov/ssl/pad/solar/
predict.htm

[66] These come from the adjustment in the system of data weights (inverse of the variance on each measurement) for Mariner 6/7 range measurements. Private communication by Inter-office Memorandum from D. O. Muhleman of Caltech to P. B. Esposito of JPL, dated 7 July 1971.

[67] G. W. Null, E. L. Lau, E. D. Biller, and J. D. Anderson, Astron. J. **86**, 456 (1981).

[68] P. A. Laing, "Implementation of J2000.0 reference frame in CHASMP," The Aerospace Corporation's Internal Memorandum # 91(6703)-1. January 28, 1991.

[69] J. H. Lieske, Astron. Astrophys. **73**, 282 (1979). Also, see *FK5/J2000.0 for DSM Applications,* Applied Technology Associates, 6 June 1985.

[70] E. M. Standish, Astron. Astrophys. **114**, 297 (1982)

[71] J. Sherman and W. Morrison. Ann. Math. Stat. **21**, 124 (1949)

[72] J. D. Anderson, Quarterly Report to NASA/Ames Research Center, *Celestial Mechanics Experiment, Pioneer 10/11,* 22 July 1992. Also see the later quarterly report for the period 1 Oct. 1992 to 31 Dec. 1992, dated 17 Dec. 1992, Letter of Agreement ARC/PP017. This last, specifically, contains the present Figure 7.

[73] We only measure Earth-spacecraft Doppler frequency and, as we will discuss in Sec. VIII A, the down link antenna yields a conical beam of width 3.6 degrees at half-maximum power. Therefore, between Pioneer 10's past and present (May 2001) distances of 20 to 78 AU, the Earth-spacecraft line and Sun-spacecraft line are so close that one can not resolve whether the force direction is towards the Sun or if the force direction is towards the Earth. If we could have used a longer arc fit that started earlier and hence closer, we might have able to separate the Sun direction from the Earth direction.

[74] A preliminary discussion of these results appeared in M. M. Nieto, T. Goldman, J. D. Anderson, E. L. Lau, and J. Pérez-Mercader, in: *Proc. Third Biennial Conference on Low-Energy Antiproton Physics, LEAP'94,* ed. by G. Kernel, P. Krizan, and M. Mikuz (World Scientific, Singapore, 1995), p. 606. Eprint hep-ph/9412234.

[75] Since both the gravitational and radiation pressure forces become so large close to the Sun, the anomalous contribution close to the Sun in Figures 6 and 7 is meant to represent only what anomaly can be gleaned from the data, not a measurement.

[76] B. D. Tapley, in *Recent Advances in Dynamical Astronomy*, eds. B. D. Tapley and V. Szebehely (Reidel,

Boston, 1973), p.396.

[77] P. A. Laing, *Thirty Years of CHASMP*, Aerospace report (in preparation).

[78] P. A. Laing, *Software Specification Document, Radio Science Subsystem, Planetary Orbiter Error Analysis Study Program (POEAS)*, Jet Propulsion Laboratory Technical Report DUK-5127-OP-D, 19 February 1981. POEAS was originally developed to support the Mariner Mars program.

[79] P. A. Laing and A. S. Liu. NASA Interim Technical Report, Grant NAGW-4968, 4 October 1996.

[80] Galileo is less sensitive to either an a_P- or an $a_t = a_P/c$-model effect than the Pioneers. Pioneers have a smaller solar pressure and a longer light travel time. Sensitivity to a clock acceleration is proportional to the light travel time squared.

[81] T. McElrath, private communication.

[82] T. P. McElrath, S. W. Thurman, and K. E. Criddle, in *Astrodynamics 1993*, edited by A. K. Misra, V. J. Modi,R. Holdaway, and P. M. Bainum (Univelt, San Diego CA, 1994), Ad. Astodynamical Sci. **85**, Part II, p. 1635, paper No. AAS 93-687.

[83] The gas leaks found in the Pioneers are about an order of magnitude too small to explain a_P. Even so, we feel that some systematic or combination of systematics (such as heat or gas leaks) will likely explain the anomaly. However, such an explanation has yet to be demonstrated. We will discuss his point further in Sections VI and VIII.

[84] More information on the "Heliocentric Trajectories for Selected Spacecraft, Planets, and Comets," can be found at `http://nssdc.gsfc.nasa.gov/space/helios/heli.html`.

[85] ODP/*Sigma* took the Interval I/II boundary as 22 July 1990, the date of a maneuver. CHASMP took this boundary date as 31 August 1990, when a clear anomaly in the spin data was seen. We have checked, and these choices produce less than one percent differences in the results.

[86] J. A. Estefan, L. R. Stavert, F. M. Stienon, A. H. Taylor, T. M. Wang, and P. J. Wolff, *Sigma User's Guide. Navigation Filtering/Mapping Program*, JPL document 699-FSOUG/NAV-601 (Revised: 14 Dec. 1998).

[87] G. W. Null, Astron. J. **81**, 1153 (1976).

[88] R. M. Georgevic, *Mathematical model of the solar radiation force and torques acting on the components of a spacecraft,* JPL Technical Memorandum 33-494 (1971).

[89] Data is available at `http://www.ngdc.noaa.gov/stp/SOLAR/IRRADIANCE/irrad.html`

[90] For an ideal flat surface facing the Sun, $\mathcal{K} = (\alpha + 2\epsilon) = (1 + 2\mu + 2\nu)$. α and ϵ are, respectively, the absorption and reflection coefficients of the spacecraft's surface. ODP uses the second formulation in terms of reflectivity coefficients, ODP's input μ and ν for Pioneer 10, are obtained from design information and early fits to the data. (See the following paragraph.) These numbers by themselves yield $\mathcal{K}_l = 1.71$. When a first (negative) correction is made for the antenna's parabolic surface, $\mathcal{K} \to 1.66$.

[91] There are complicating effects that modify the ideal antenna. The craft actually has multiple different-shaped surfaces (such as the RTGs), that are composed of different materials oriented at different angles to the spin axis, and which degrade with time. But far from the Sun, and given M and A, the sum of all such corrections can be subsumed, for our purposes, in an *effective* $\mathcal{K}$. It is still expected to be of order 1.7.

[92] Eq. (25) is combined with information on the spacecraft surface geometry and it's local orientation to determine the magnitude of its solar radiation acceleration as it faces the Sun. As with other non-gravitational forces, an incorrect mass in modeling the solar radiation pressure force can be accounted for by modifying other constants such as the effective sizes of the antenna and the albedo.

[93] E. J. Smith, L. Davis, Jr., D. E. Jones, D. S. Colburn, P. J. Coleman, Jr., P. Dyal, and C. P. Sonnett, Science **183**, 306 (1974); *ibid.* **188**, 451 (1975).

[94] This result was obtained from a limit for positive charge on the spacecraft [87]. No measurement dealt with negative charge, but such a charge would have to be proportionally larger to have a significant effect.

[95] R. Malhotra, Astron. J. **110**, 420 (1995); *ibid.* **111**, 504 (1996).

[96] A. P. Boss and S. J. Peale, Icarus **27**, 119 (1976).

[97] A. S. Liu, J. D. Anderson, and E. Lau, Proc. AGU (Fall Meeting, San Francisco, 16-18 December 1996), paper # SH22B-05.

[98] G. E. Backman, A. Dasgupta, and R. E. Stencel, Astrophys. J. **450**, L35 (1995). Also see S. A. Stern, Astron. Astrophys. **310**, 999 (1996).

[99] V. L. Teplitz, S. A. Stern, J. D. Anderson, D. Rosenbaum, R. J. Scalise, and P. Wentzler, Astrophys. J. **516**, 425 (1999).

[100] J. D. Anderson, G. Giampieri, P. A. Laing, and E. L. Lau, work in progress.

[101] R. F. C. Vessot, "Space experiments with high stability clocks," in proceedings of the "Workshop on the Scientific Applications of Clocks in Space," (November 7-8, 1996. Pasadena, CA). Edited by L. Maleki. JPL Publication 97-15 (JPL, Pasadena, CA, 1997), p. 67.

[102] O. J. Sovers and C. S. Jacobs, *Observational Model and Parameter Partials for the JPL VLBI Parameter Estimation Software "MODEST" - 1996*, Jet Propulsion Laboratory Technical Report 83-39, Rev. 6 (1996).

[103] J. I. Katz, Phys. Rev. Lett. **83**, 1892 (1999).

[104] There is an intuitive way to understand this. Set up a coordinate system at the closest axial point of an RTG pair. Have the antenna be in the (+z,-x) direction, and the RTG pair in the positive x direction. Then from the RTGs the antenna is in 1/4 of a sphere (positive z and negative x). The 'antenna occupies about 1/3 of 180 degrees in azimuthal angle. Its form is the base part of the parabola. Thus, it resembles a "flat" triangle of the same width, producing another factor of $\sim (1/2 - 2/3)$ compared to the angular size of a rectangle. It occupies of order $(1/4-1/3)$ of the latitudinal-angle phase space angle of 90°. This yields a total reduction factor of $\sim (1/96 - 2/108)$, or about 1 to 2 %.

[105] The value of 1.5% is obtained by doing an explicit calculation of the solid angle subtended by the antenna from the middle of the RTG modules using the Pioneer's physical dimensions. V. J. Slabinski of USNO independently obtained a figure of 1.6%.

[106] Our high estimate of 40 W is not compromised by imprecise geometry. If the RTGs were completely in the plane of the top of the dish, then the maximum factor multiplying the 40 W directed power would be $\kappa_z = 1$. This would presume all the energy was reflected and/or

absorbed and re-emitted towards the rear of the craft. (If the RTGs were underneath the antenna, then the total factor could ideally go as high as "2", from adding the RTG heat going out the opposite direction.) The real situation is that the average sine of the latitudinal angle up to the antenna from the RTGs is about 0.3. This means that the heat gong out the opposite direction might cause an effective factor κ_z to go as high as 1.3. However, the real reflection off of the antenna is not straight backwards. It is closer to 45°. The absorbed and re-emitted radiation is also at an angle to the rotation axis, although smaller. (This does not even consider reflected/reemitted heat that does not go directly backwards but rather bounces off of the central compartment.) So, the original estimate of $\kappa = 1$ is a good bound.

[107] J. D. Anderson, P. A. Laing, E. L. Lau, A. S. Liu, M. M. Nieto, and S. G. Turyshev, Phys. Rev. Lett. **83**, 1893 (1999).

[108] We acknowledge R. E. Slusher of Bell Labs for raising this possibility.

[109] B. A. Smith, G. A. Briggs, G. E. Danielson, A. F. Cook, II, M. E. Davies, G. E. Hunt, H. Masursky, L. A. Soderblom, T. C. Owen, C. Sagan, and V. E. Suomi, Space Sci. Rev. **21**, 103 (1977).

[110] C. E. Kohlhase and P. A. Penzo, Space Sci. Rev. **21**, 77 (1977).

[111] We are grateful to C. J. Hansen of JPL, who kindly provided us with operational information on the Voyager video cameras.

[112] B. A. Smith, L. A. Soderblom, D. Banfield, C. Barnet, T. Basilevsky, R. F. Beebe, K. Bollinger, J. M. Boyce, A. Brahic, G. A. Briggs, R. H. Brown, C. Chyba, S. A. Collins, T. Colvin, A. F. Cook, II, D. Crisp, S. K. Croft, D. Cruikshank, J. N. Cuzzi, G. E. Danielson, M. E. Davies, E. De Jong, L. Dones, D. Godfrey, J. Goguen, I. Grenier, V. R. Haemmerle, H. Hammel, C. J. Hansen, C. P. Helfenstein, C. Howell, G. E. Hunt, A. P. Ingersoll, T. V. Johnson, J. Kargel, R. Kirk, D. I. Kuehn, S. Limaye, H. Masursky, A. McEwen, D. Morrison, T. Owen, W. Owen, J. B. Pollack, C. C. Porco, K. Rages, P. Rogers, D. Rudy, C. Sagan, J. Schwartz, E. M. Shoemaker, M. Showalter, B. Sicardy, D. Simonelli, J. Spencer, L. A. Sromovsky, C. Stoker, R. G. Strom, V. E. Suomi, S. P. Synott, R. J. Terrile, P. Thomas, W. R. Thompson, A. Verbiscer, and J. Veverka, Science **246**, 1432 1989.

[113] E. M. Murphy, Phys. Rev. Lett. **83**, 1890 (1999).

[114] J. D. Anderson, P. A. Laing, E. L. Lau, A. S. Liu, M. M. Nieto, and S. G. Turyshev, Phys. Rev. Lett. **83**, 1891 (1999).

[115] L. K. Scheffer, (a) eprint gr-qc/0106010, the original modification; (b) eprint gr-qc/0107092; (c) eprint gr-qc/0108054.

[116] J. D. Anderson, P. A. Laing, E. L. Lau, M. M. Nieto, and S. G. Turyshev, eprint gr-qc/0107022.

[117] These results were not treated for systematics, used different time-evolving estimation procedures, were done by three separate JPL navigation specialists, separated and smoothed by one of us [72], and definitely not analyzed with the care of our recent run (1987.0 to 1998.5). In particular, the first two Pioneer 11 points, included in the early memos [72], were after Pioneer 11 encountered Jupiter and then was going back across the central

[118] T. K. Keenan, R. A. Kent, and R. N. R. Milford, *Data Sheets for PMC Radioisotopic Fuel*, Los Alamos Report LA-4976-MS (1972), available from NTIS. We thank Gary Reinhart for finding this data for us.

[119] Diagrams showing the receptacle and the bayonet coupling connector were made by the Deutsch Company of Banning, CA. (The O-ring was originally planned to be silicon.) Diagrams of the receptacle as mounted on the RTGs were made by Teledyne Isotopes (now Teledyne Brown Engineering). Once again we gratefully acknowledge Ted Christenbury for obtaining these documents for us.

[120] In principle, many things could be the origin of some spin down: structural deformations due to adjustments or aging, thermal radiation, leakage of the helium from the RTGs, etc. But in the case of Pioneer spacecraft none of these provide an explanation for the spin history exhibited by the Pioneer 10, especially the large unexpected changes among the Intervals I, II, and III.

[121] S. Herrick, *Astodynamics* (Van Nostrand Reinhold Co., London, New York, 1971-72). Vols. 1-2,

[122] We thank William Folkner of JPL for his assistance in producing several test files and invaluable advice.

[123] D. Brouwer and G. M. Clemence, *Methods of Celestial Mechanics* (Academic Press, New York, 1961).

[124] W.G. Melbourne, Scientific American **234**, No. 6, 58 (1976).

[125] We thank E. Myles Standish of JPL, who encouraged us to address in greater detail the nature of the annual/diurnal terms seen in the Pioneer Doppler residuals. (This work is currently under way.) He also kindly provided us with the accuracies from his internal JPL solar system ephemeris, which is continually under development.
new, soon to be published, solar system ephemeris.

[126] D. F. Crawford, eprint astro-ph/9904150.

[127] N. Didon, J. Perchoux, and E. Courtens, Université de Montpellier preprint (1999).

[128] D. A. Gurnett, J. A. Ansher, W. S. Kurth, and L. J. Granroth, Geophys. Res. Lett. **24**, 3125 (1997); M. Landgraf, K. Augustsson, E. Grün, and A. S. Gustafson, Science **286**, 239 (1999).

[129] Pioneer 10 data yielded another fundamental physics result, a limit on the rest mass of the photon. See L. Davis, Jr., A. S. Goldhaber, and M. M. Nieto, Phys. Rev. Lett. **35**, 1402 (1975).

[130] G. J. Stephenson, Jr., T. Goldman, and B. H. J. McKellar, Int. J. Mod. Phys. A **13**, 2765 (1998), hep-ph/9603392.

[131] M. M. Nieto and T. Goldman, Phys. Rep. **205**, 221 (1991); **216**, 343 (1992), and references therein.

[132] J. Bekenstein and M. Milgrom, Astrophys. J. **286**, 7 (1984); M. Milgrom and J. Bekenstein, in: *Dark Matter in the Universe*, eds. J. Kormendy and G. R. Knapp (Kluwer Academic, Dordrecht, Boston, 1987), p. 319; M. Milgrom, La Recherche **19**, 182 (1988).

[133] P. D. Mannheim, Astrophys. J. **419**, 150 (1993). Also see K. S. Wood and R. J. Nemiroff, Astrophys. J. **369**, 54 (1991).

[134] K. G. Begeman, A. H. Broeils, and R. H. Sanders, Mon. Not. R. Astron. Soc. **249**, 523 (1991); T. G. Breimer and R. H. Sanders, Astron. Astrophys. **274**, 96 (1993).

[135] M. Milgrom, Ann. Phys. (NY) **229**, 384 (1994). Also see

astro-ph/0112069.

[136] S. Capozziello, S. De Martino, S. De Siena, and F. Illuminati, Mod. Phys. Lett. A **16**, 693 (2001). Eprint gr-qc/0104052. Also see eprint gr-qc/9901042.

[137] R. D. Reasenberg, I. I. Shapiro, P. E. MacNeil, R. B. Goldstein, J. C. Breidenthal, J. P. Brenkle, D. L. Cain, T. M. Kaufman, T. A. Komarek, and A. I. Zygielbaum, Astrophys. J. **234**, L219 (1979).

[138] J. D. Anderson, J. K. Campbell, R. F. Jurgens, E. L. Lau, X X Newhall, M. A. Slade III, and E. M. Standish, Jr., in: *Proceedings of the Sixth Marcel Grossmann Meeting on General Relativity*, Part A, ed. H. Sato and T. Nakamura, (World Scientific, Singapore, 1992), p. 353.

[139] R. H. Sanders, private communication to M. Milgrom (1998).

[140] The Principle of Equivalence figure of merit is a_P/a_N. This is worse than for laboratory experiments (comparing small objects) or for the Nordtvedt Effect (large objects of planetary size) [51]. It again emphasizes that the Earth and Mars do not change positions due to a_P.

[141] F. Munyaneza and R. D. Viollier, eprint astro-ph/9910566.

[142] J. L. Rosales and J. L. Sánchez-Gomez, eprint gr-qc/9810085.

[143] V. Guruprasad, eprints astro-ph/9907363, gr-qc/0005014, gr-qc/0005090.

[144] D. Østvang, eprint gr-qc/9910054.

[145] W. B. Belayev, eprint gr-qc/9903016.

[146] G. Modanese, Nucl. Phys. B **556**, 397 (1999). Eprint gr-qc/9903085.

[147] R. Mansouri, F. Nasseri and M. Khorrami, Phys. Lett. A **259**,194 (1999). Eprint gr-qc/9905052.

[148] B. G. Sidharth, Nuovo Cim. **B115**, 151 (2000). Eprint astro-ph/9904088.

[149] M. A. Ivanov, Gen. Rel. and Grav. **33**, 479 (2001). eprint astro-ph/0005084. Also see eprint gr-qc/0009043, a contribution to the SIGRAV/2000 Congress.

[150] R. Foot and R. R. Volkas, Phys. Lett. B **517**, 13 (2001). Eprint gr-qc/0108051.

[151] J. P. Mbelek and M. Lachièze-Rey, eprint gr-qc/9910105.

[152] S. Calchi Novati, S. Capozziello, and G. Lambiase, Grav. Cosmol. **6**, 173 (2000). Eprint astro-ph/0005104.

[153] R. A. Hulse and J. H. Taylor, Astrophys. J. **195**, L51 (1975); J. H. Taylor and J. M. Weisberg, Astrophys. J. **253**, 908 (1982).

[154] M. Consoli and F. Siringo, eprint hep-ph/9910372.

[155] M. Consoli, eprint hep-ph/0002098.

[156] S. Capozziello and G. Lambiase, Mod. Phys. Lett. A **14**, 2193 (1999). Eprint gr-qc/9910026.

[157] P. D. Mannheim and D. Kazanas, Astrophys. J. **342**, 635 (1989); P. D. Mannheim, Gen. Rel. Grav. **25**, 697 (1993); P. D. Mannheim, Astrophys. J. **479**, 659 (1997).

[158] J. Wood and W. Moreau, eprint gr-qc/0102056.

[159] O. Bertolami and F. M. Nunes, Phys. Lett. B **452**, 108 (1999). Eprint hep-ph/9902439.

[160] L. Iess, G Giampieri, J. D. Anderson, and B. Bertotti, Class. Quant. Grav. **16**, 1487 (1999).

[161] R. Danner and S. Unwin, eds., *SIM Interferometry Mission: Taking the Measure of the Universe*, NASA document JPL 400-811 (1999). Also see http://sim.jpl.nasa.gov/

[162] The situation may be analogous to what happened in the 1980's to geophysical exploration. Mine and tower gravity experiments seemed to indicate anomalous forces with ranges on the order of km [163]. But later analyses showed that the experiments had been so precise that small inhomogeneities in the field surveys had introduced anomalies in the results at this newly precise level [164]. But the very important positive outcome was that geophysicists realized the point had been reached where more precise studies of systematics were necessary.

[163] F. D. Stacey, G. J. Tuck, G. J. Moore, S. C. Holding, B. D. Goodwin, and R. Zhou, Rev. Mod. Phys. **59**, 157 (1987); D. H. Eckhardt, C. Jekeli, A. R. Lazarewicz, A. J. Romaides, and R. W. Sands, Phys. Rev. Lett. **60**, 2567 (1988).

[164] Measurements were more often taken at easily accessible sites, such as roads, rather than at more inaccessible cites at different heights, such as mountain sides or marshes. See D. F. Bartlett and W. L. Tew, Phys. Rev. D **40**, 673 (1989); . *ibid.*, J. Geophys. Res. [Solid Earth Planet] **95**, 17363 (1990); C. Jekeli, D. H. Eckhardt, and A. J. Romaides, Phys. Rev. Lett. **64**, 1204 (1990). For a review, see Section 4 of Ref. [131].

Study of the anomalous acceleration of Pioneer 10 and 11: Errata

John D. Anderson,[a] Philip A. Laing,[b] Eunice L. Lau,[a] Anthony S. Liu, Michael Martin Nieto,[d] and Slava G. Turyshev[a]

[a] *Jet Propulsion Laboratory, California Institute of Technology, Pasadena, CA 91109*
[b] *The Aerospace Corporation, 2350 E. El Segundo Blvd., El Segundo, CA 90245-4691*
[c] *Astrodynamic Sciences, 2393 Silver Ridge Ave., Los Angeles, CA 90039*
[d] *Theoretical Division (MS-B285), Los Alamos National Laboratory,*
University of California, Los Alamos, NM 87545
Electronic addresses: john.d.anderson@jpl.nasa.gov, Philip.A.Laing@aero.org,
Eunice.L.Lau@jpl.nasa.gov, mmn@lanl.gov, turyshev@jpl.nasa.gov
(Dated: February 1, 2022)

We give the errata for this paper in both the arXiv [gr-qc/0104064, version 4] and published [Phys. Rev. D **65**, 082004 (2002)] formats.

PACS numbers: 04.80.-y, 95.10.Eg, 95.55.Pe

Sec. I-C, p. (4), para. 4, line 6 (published version only):
Delete "load sharing."

Sec. IV-F, 3rd para. from end, p. (16), lines 3-4 (published version only)
Delete "the" in front of "JPL's" and one of the two successive "from"s.

Sec. VII-B, p. 28 (26), 4 lines below Eq. (25):
1.73 should be 1.37.

Sec. VII-B, p. 29 (27):
Line 2: Change $f_\odot$ to $f_\odot/c$ and v^3 to v^2.
Eq. (29): Change v^3/c to v^2.

Eq. (29): Change 1.24×10^{-13} to 4.4×10^{-11}.
3 lines down: Change 10^{-5} to 10^{-3}.

Table II, p. 43 (40), item 1. (b):
10^{-5} should be 10^{-3}.

Sec. XI-C, p. 44 (41), 4 lines below Eq. (57):
10^{-3} should be 10^{-2}.

Sec. XI-C, p. 45 (42), para. 7, line 1:
"Inavov" should be "Ivanov."

Ref. [20], p. 49 (45):
"Mashoon" should be "Mashhoon."